NOTICE

The quality of this microfiche is heavily dependent upon the quality of the original thesis submitted for microfilming. Every effort has been made to ensure the highest quality of reproduction possible.

If pages are missing, contact the university which granted the degree.

Some pages may have indistinct print especially if the original pages were typed with a poor typewriter ribbon or if the university sent us a poor photocopy.

Previously copyrighted materials (journal articles, published tests, etc.) are not filmed.

Reproduction in full or in part of this film is governed by the Canadian Copyright Act, R.S.C. 1970, c. C-30. Please read the authorization forms which accompany this thesis.

THIS DISSERTATION
HAS BEEN MICROFILMED
EXACTLY AS RECEIVED

AVIS

La qualité de cette microfiche dépend grandement de la qualité de la thèse soumise au microfilmage. Nous avons tout fait pour assurer une qualité supérieure de reproduction.

S'il manque des pages, veuillez communiquer avec l'université qui a conféré le grade.

La qualité d'impression de certaines pages peut laisser à désirer, surtout si les pages originales ont été dactylographiées à l'aide d'un ruban usé ou si l'université nous a fait parvenir une photocopie de mauvaise qualité.

Les documents qui font déjà l'objet d'un droit d'auteur (articles de revue, examens publiés, etc.) ne sont pas microfilmés.

La reproduction, même partielle, de ce microfilm est soumise à la Loi canadienne sur le droit d'auteur, SRC 1970, c. C-30. Veuillez prendre connaissance des formules d'autorisation qui accompagnent cette thèse.

LA THÈSE A ÉTÉ
MICROFILMÉE TELLE QUE
NOUS L'AVONS REÇUE

ASYMMETRIC TURBULENT HEAT TRANSFER IN THE THERMAL ENTRANCE REGION

by

Reda M. Labib

A thesis submitted to the School of Graduate Studies in partial fulfillment of the requirements of the degree of

MASTER OF APPLIED SCIENCE

in the

Department of Mechanical Engineering
University of Ottawa
Ottawa, Canada

1979

ABSTRACT

In this study, the asymmetric turbulent fluid flow and heat transfer induced by square-rib roughness elements in parallel plates are analytically studied in an attempt to investigate the resultant effect of artificial roughness on the heat transfer and friction forces.

In the analysis, the fluid properties were assumed to be constant. The integral method together with a turbulence model based on modified Prandtl's mixing length theory for the rough surface was used to determine the velocity distribution and friction. The two velocity profiles in the problem were matched using an empirical correlation. The temperature distribution is then predicted and heat transfer coefficients are calculated.

The results of the velocity profiles and friction factors are in good agreement with the available experimental results. The heat transfer increases more than the fruction forces for a certain range of Reynold numbers, and Prandtl numbers for a given roughness structure.

Generally the results show the strong effect of asymmetry on engineering parameters. Furthermore, it is the roughness structure (including roughness geometry, relative roughness and roughness density) which influences the nature of asymmetry and heat transfer.

ACKNOWLEDGEMENT

The candidate is grateful to have had the opportunity to carry out this project under the guidance of Dr. Yung Lee, to whom special thanks are due for the encouragement, for his invaluable suggestions and for the countless hours he so willingly contributed. I am also grateful to him for the generaous financial support I received during the course of my work.

The candidate wishes to extend his gratitude to Dr. A.S. Krausz, Chairman, and other staff members of the Department of Mechanical Engineering, for their interest and encouragement for the duration of the project. The financial support in the form of a Scholarship, by the School of Graduate Studies of the University of Ottawa, is gratefully acknowledged.

Sincere thanks are also due to the staff of the computer laboratory at the University of Ottawa for their assistance and also to Mrs. D. Champion-Demers for her efforts in typing this thesis.

TABLE OF CONTENTS

LIST OF TABLES

LIST OF FIGURES

NOMENCLATURE

A	cross sectional area of the channel; constant
c	constant, Eq. (3.32)
D	diameter
F	body Force
F	f_r/f_s ratio
f	friction factor $\frac{2\,\tau_w}{\rho\,U_{av}^2}$
g	gravitational acceleration
H	Nu_r/Nu_s ratio
h	convective heat transfer coefficient
K	von Karman's constant, 0.4
K_s	sand roughness
l	mixing length
m	$\frac{Z_{or}}{\varepsilon}$
Nu	Nusselt number
n	constant
Q	flow rate
P	pressure
Pr	Prandtl number
p	pitch; distance between tips of roughness elements
q	heat flux
q'	heat generation
R	gas constant

r	radial distance
Re	Reynolds number, $\frac{U_{av} D_{hyd}}{\nu}$
St	Stanton number
S	distance between channel walls
T	temperature
t	time
u	velocity in x-direction
U_{av}	average velocity in the channel, $\frac{Q}{A}$
v	velocity in y-direction
w	velocity in Z-direction
x	coordinate in the axial direction
y,Y	coordinate perpendicular to the channel walls
Z	coordinate parallel to the channel walls, perpendicular to the axial direction
Z_{or}	parameter defined by (3.30), hydrodynamic roughness

Greek Symbols

σ	specific weight, ρg
δ	hydrodynamic boundary layer thickness
δ_{th}	thermal boundary layer thickness
ε	physical roughness height
ε_M	eddy diffusivity for momentum
ε_H	eddy diffusivity for heat
μ	absolute viscosity

ν kinematic viscosity

ρ density

τ shear stress

τ_w wall shear stress

Superscripts

$'$ fluctuating component

$-$ time averaged quantity

$+$ non-dimensionalized quantity,

in case of velocity $u^+ = \frac{u}{u_{\tau s}}$

in case of length $y^+ = \frac{y\, u_{\tau s}}{\nu}$

$++$ quantity non-dimensionalized,

in case of velocity $u^{++} = \frac{u}{u_{\tau r}}$

in case of length $y^{++} = \frac{y\, u_{\tau r}}{\nu}$

in case of temperature $T^{++} = \frac{(T_w - T)\, c\, \tau r}{q_w\, u_{\tau r}}$

Subscripts

b bulk

d fully developed

i	instantaneous
m	corresponding to the maximum velocity point
r	rough wall
s	smooth wall
t	turbulent
x	local
0(zero)	corresponding to the zero shear stress point
δ	corresponding to the conditions at δ, edge of the boundary layer
∞	corresponding to conditions outside the boundary, potential flow.

CHAPTER I

INTRODUCTION

Asymmetric turbulent flows are encountered in many practical situations where engineering requirements impose dissimilar boundary conditions such as in heat exchangers with enhanced heat transfer surfaces. Surfaces which are sufficiently rough will have increased heat transfer coefficients because the turbulence set up in the wakes of each roughness element will penetrate into the laminar sublayer. Therefore, it is generally expected that the effect would be greater for fluid flow with a higher Prandtl number.

In these fluid flows the form loss is dominant, and as for the completely rough region in duct flows with relatively coarse and tightly spaced roughness elements, the friction coefficient is shown to be independent of the Reynolds number [1].

Although the heat transfer coefficients increase with Reynolds number, the heat transfer per unit pumping power expended may not be improved by the roughened heat transfer surfaces. Certain roughness elements may, however, be used advantageously from the heat transfer point of view, but the analytical predictions in the literature are very limited |2|.

There are many possible shapes of heat transfer surfaces to which roughening may be applied. There are also many different shapes and sizes of roughness, so that the experimental investigation of combinations of heat transfer surface geometry and roughness is apt to become unwieldy.

One approach is to investigate the effect of roughness on one shape of system, and then to investigate, separately, the effect of shape, using smooth surface.

In this study, a semi-analytical investigation of the effect of a particular type of artificial roughness element on heat transfer in asymmetric conditions is presented.

The main research objectives were set as follows:

1. To correlate the locations of maximum velocity and zero shear stress, as a function of roughness structure and Reynolds number.
2. To predict the friction forces and velocity profiles across the channel flow and compare them with the experimental measurements [3].
3. To predict the local heat transfer charateristics and thermal entrance length for turbulent fluid flow, fully developed velocity profile, and uniform heat flux at the rough surface.
4. The resultant effect of additional roughness is found from a comparison of rough and smooth surfaces with respect to the heat transfer increase relative to the increase of drag forces. This relation is expressed in terms of the non-dimensional parameter, F/H

   where $$F/H = \left(\frac{f_r/f_s}{Nu_r/Nu_s} \right) .$$

CHAPTER II

LITERATURE SURVEY

Until recently, the studies of flow and heat transfer in noncircular and circular ducts have been primarily concerned with three groups of problems.

The first group dealt with the development of the velocity profile in the entrance region of a duct with no heat transfer. As the fluid moves down the duct, a boundary layer begins forming at the entrance and grows on the wall surface due to the fact that the fluid immediately adjacent to the wall has a velocity of zero.

The second group was concerned with flow in which the velocity profile of the fluid is already fully developed but enters a section of duct having a wall temperature different from the temperature of the entering fluid. This is the problem of a purely thermal entrance region.

The third group was concerned with the so-called fully developed problems in which the heat transfer and friction parameters do not change along the length of the duct. This is mainly to study the nature of turbulent flow and heat transfer under the fully developed condition.

Some attention has been given to the effect of the surface roughness on the transport of momentum and heat. In the literature, it seems that very few dealt with the resultant effect of roughness on the heat transfer and drag forces.

2.1 FULLY DEVELOPED TURBULENT FLUID FLOW

As a fluid flows through a constant cross-sectional duct, its velocity profile undergoes a change from its initial entrance form to that of a fully developed profile at an axial location far downstream from the entrance. The fully developed flow cases, both laminar and turbulent, have been the subject of many analytical and experimental studies mainly because of their greater simplicity and wider engineering applications.

One of the most rigorous studies of turbulent flow in a circular pipe was carried out by Deissler [4]. An investigation by Laufer [5] covers the structure of turbulent pipe flow quite thoroughly. Cremers and Eckert [6] measured the turbulence correlations with hot-wire anemometer in a triangular duct, and recently Clark [7] used the hot-wire anemometer to study the turbulent boundary layers.

The problems of fully developed turbulent flow in concentric annulus have been studied experimentally and analytically by Barrow [8], Lee and Barrow [9], Brighton and Jones [10], Rothfus [11], Levy [12], and Quarmby [13].

A small amount of work has been done on the determination of velocity profiles in the boundary layer for air flowing over rough plates. Van der Heggezijnen [14], studied velocity profiles on a plate having small quadrilateral pyramids on its surface. The projections on the surface were described as quadrilateral pyramids arranged in vertical and horizontal rows. Velocity profiles were determined at different distances from leading edge. Van Der Heggezijnen investigated the possibility that the velocity in the boundary layer could be represented by the formula,

$$u = y^n \tag{2.1}$$

Hansen [15] also made a study of the velocity profiles over rough plates and determined the value of the exponent n. He reported that for plates having a wavy surface the value of n varied from 0.189 to 0.194, increasing slightly as the velocity of the main stream increased.

Some attempts have been made to set up models of turbulent exchange of flows over rough and smooth surfaces. Allan [16] proposed a description of the distribution of the mean-velocity in two-dimensional or axisymmetric turbulent flow which included the effects of pressure gradients and of the surface roughness. Allan's expression for the distribution of mean velocity is given by

$$u^+ = 2.5 \ln y^+ + 5.1 + K f_c + c\beta \tag{2.2}$$

where: K: pressure gradient

f_c: pressure gradient function

c: value of the surface roughness function for just fully turbulent flow

β: roughness function.

Allan and Sharma [17] used experimental data for two-dimensional, low speed, turbulent boundary layer to verify the description of the mean-velocity distributions proposed by Allan [16]. They concluded that the effects of pressure gradient and of surface roughness on the mean-velocity distribution in the turbulent boundary layer can be treated independently. Allan's velocity distribution [16], accurately represents the experimental velocity profiles in flows over both smooth and rough surfaces at constant pressure and in diffusion up to near separating conditions.

2.1.1 Drag forces

Drag forces on surfaces having very small roughness such as painted metal plates as well as smooth plates covered with single protuberances, such as rivet heads, welded seams, joints, etc., were measured by Grunow [18]. Additional comprehensive data on roughness occurring in shipbuilding can also be found in several papers by Kempf [19].

The effect of the artificial roughness on the frinctional properties of annuli shape have been studied by Wilkie [20] for various inner surfaces roughened by transverse square and rectangular ribs. Rib heights varied from 0.1% to 1.6% of the equivalent diameter and pitch to height ratio from 2.5 to 50. He concluded that, increasing rib width at constant P/ε and ε/D reduces, f. Also slight chamfering of very sharp ribs reduces, f, by between 6% and 8%. However, further chamfering or rounding has no effect.

2.1.2 Roughness function

A critical review was presented by Lewis [21] of the methods used to evaluate the thermohydraulic performance of rough surfaces. In this study, the fundamental importance of the roughness function is verified and optimization is discussed. Also, Halls [2], transformation, which is used to relate measurements in annuli to circular tube of rad-bundle flows, is re-examined.

Musker and Lewkowicz [22] proposed an integral method for predicting the development of two-dimensional turbulent boundary layers, which can include the effect of surface roughness. The method based

on the energy integral equation is found to give good agreement with experimental measurement for both smooth and rough surfaces, in an arbitrary pressure distribution. This method is used to investigate the effect of surface roughness on the separation of a two-dimensional turbulent boundary layer developing over a flat plate with an external pressure distribution.

For the case of non-circular ducts, no measurement on eddy diffusivity distribution and turbulence could be found in the published works.

2.2 ASYMMETRIC HEAT TRANSFER IN THERMAL ENTRANCE REGION

It is well-known fact that thermal, entrance effects are always present when a fluid flowing adiabatically into a duct enters a region having a wall temperature different from that of the fluid. On entering the heated section, a new temperature distribution will be set up within the fluid; this may take various forms depending upon the heat flux boundary conditions and past history of the fluid. At the cross-section where heating commences, the temperature gradient in the fluid near the wall is theoretically infinite and decreases in the direction of fluid flow until a constant value is reached if constant fluid properties are assumed.

The thermal entrance region has been defined, either as that distance required for the local heat transfer coefficient to approach that of the fully developed value or, as the distance from the entrance to the cross-section where the non-dimensionalized temperature profile becomes independent of the flow direction. Since the velocity profile of the fluid entering a heat transfer passage is already fully developed, it is often

called a "purely thermal entrance region" to distinguish it from a simultaneously developing fluid flow in entrance region.

Some of the theoretical and experimental studies on turbulent fluid flow and heat transfer of the entrance region of a circular tube can be found in the works cited in References 23 to 26. For the purely thermal entrance region problem in the entrance regions of concentric annuli, the available pertinent analytical studies are those of Lee [23], Kays and Leung [24], Guarmby and Anand [25], and Chen and Yu [26]. Some results of experimental works on the thermal entrance region heat transfer in annuli are reported by Farman and Beckmann [27].

Lee [23] studied the problems of thermal boundary-layer growth and heat transfer, for hydrodynamically fully developed turbulent flow in concentric annuli, by means of the momentum and heat transfer integral equations, along with a modified universal velocity profile. The investigation was conducted for a range of radius ratios from 1.01 to 5, Prandtl number from 0.01 to 30 and a Reynolds number range of from 10,000 to 200,000. The results indicate that, for the range of parameter studied, the heat transfer coefficient attains the fully developed value in less than thirty equivalent diameters. Also, the thermal entrance length is moderately dependent upon radius ratio, Reynolds number and Prandtl number.

Quarmby and Anand [25] have studied the problem of thermal entrance region with two boundary conditions, i.e., either one wall has a constant temperature while the other is insulated or there is uniform heat flux at one annular surface. For both of the sublayers, the momentum eddy diffusivity was evaluated from Deissler's expression [4]. However, for the core region of the outside sublayers, they used the modified eddy

diffusivity of Reichardt [28] which was used by Kays and Leung [24]. The eddy diffusivity of heat, ε_H, was obtained from, ε_M, through the Jenkin's expression of the ratio [29] the solution was given for four different radius ratios with Reynolds numbers from 20,000 to 40,000 and for $Pr = 0.07$ and 1000.

The nature of turbulent flow and heat transfer under fully developed conditions has been studied extensively by many investigators over the last three decades. Turbulent heat transfer in smooth circular tubes with variable fluid properties was studied by Deissler [30]. Corcoran et al. [31] measured experimental values of temperature and velocity gradients for the flow between parallel plates. Lawn [32] and Grown [70] reported the studies of fully developed turbulent heat transfer in pipe flow.

The effects of various factors on the turbulent heat transfer and friction in the entrance regions of smooth passages were investigated analytically by Deissler [33]. He used integral heat transfer and momentum equations for calculating the thickness of the thermal and velocity boundary layers. The influence of Reynolds number, Prandtl number, initial velocity distribution, wall-boundary conditions, and of variable fluid properties were studied. His results indicate that approximately fully developed heat transfer and friction are, in general, attained in an entrance length less than 10 diameters. The effect of initial velocity distribution on heat transfer in the entrance region was that the value of (Nu_x/Nu_d) for a uniform initial velocity distribution were higher than those for a fully developed velocity distribution. This result might be expected because of higher friction in the case of uniform initial velocity profile.

2.2.1 Effect of Roughness on the Ratio of Pressure Drop and Heat Transfer Rate

The role played by a rough surface in fluid mechanics and heat transfer has been of interest for a long time. This interest has been for practical reasons because of the increase in friction and heat transfer rate associated with rough surface. One variable of interest with roughness is obviously the ratio of roughness height, ε, to tube diameter. Edwards and Sheriff [34] have noted that, to be effective, a roughness element must penetrate the laminar sublayer ($y^+ \approx 5$), and for full effectiveness roughness height should be larger than the combined laminar and buffer layer thickness ($y^+ \approx 30$). They found that there is no increase in the heat transfer for greater heights, but the friction factor continues to increase. Kaul and Von Kiss [35] found that, the pitch-to-height ratio of the roughness elements, appears to be particularly important in annuli with only the inner surface roughened.

Experimental data for rough pipe have been obtained by Nunner [36]. The rough pipes he used have higher friction factors and heat transfer coefficients than the smooth tubes. Nunner correlated these data with respect to the smooth pipes and he suggested the following equation

$$\frac{Nu_r}{Nu_{smooth}} = \left(\frac{f_r}{f_{smooth}} \right)^{0.5} \qquad (2.3)$$

However, this type of roughness does not appear to be well enough defined or reproducible to permit application of these data in design.

Kolar [37] has achieved a correlation of roughness effects on heat transfer using the shear velocity u^+ in the Reynolds number. Kolar used 60^0 triangular roughness elements and correlated the data by

$$\frac{Nu}{Pr^{0.4}} = 0.102\ Re_t^{0.914} \tag{2.4}$$

where Re_t Turbulent Reynolds number given by u^+D/ν

D Volumetric diameter defined by $D = \sqrt{4\ \text{vol.}/\pi L}$

A second method of correlation for artificial roughness has been suggested by Dipprey and Sabersky [38]. This correlation is based on a "heat transfer similarity law". The experiments were run with water in a tube roughened by a granular material giving three-dimensional roughness. Dipprey and Sabersky correlate their data in the fully rough region by

$$\left[8.48 + \frac{f/(2St) - 1}{(f/2)^{0.5}}\right] Pr^{-0.44} = 5.19(e^*)^{0.2} \tag{2.5}$$

where $e^* = Re\sqrt{f/2}\ e_s/D$

D diameter which is defined as $D = \sqrt{4\ \text{vol.}/\pi L}$

e_s/D represents equivalent sand grain roughness.

It is apparent from the above review of studies that, the crucial question of having roughness will improve the heat transfer per unit pumping power expended or not, still unknown.

CHAPTER III

ANALYTICAL STUDIES

3.1 BASIC EQUATIONS

Navier-Stokes equations for conservation of mass and momentum of an incompressible fluid flow with constant viscosity could be expressed in the following form: [1]

$$\rho\left(\frac{\partial u}{\partial t} + u\frac{\partial u}{\partial x} + v\frac{\partial u}{\partial y} + w\frac{\partial u}{\partial z}\right) = -\frac{\partial P}{\partial x} + \mu\nabla^2 u + F_x \tag{3.1}$$

$$\rho\left(\frac{\partial v}{\partial t} + u\frac{\partial v}{\partial x} + v\frac{\partial v}{\partial y} + w\frac{\partial v}{\partial z}\right) = -\frac{\partial P}{\partial y} + \mu\nabla^2 v + F_y \tag{3.2}$$

$$\rho\left(\frac{\partial w}{\partial t} + u\frac{\partial w}{\partial x} + v\frac{\partial w}{\partial y} + w\frac{\partial w}{\partial z}\right) = -\frac{\partial P}{\partial z} + \mu\nabla^2 w + F_z \tag{3.3}$$

If properties such as specific heat, c_p, and thermal conductivity, k, can be assumed to be independent of temperature, the corresponding energy equation has the following form:

$$\rho\, c_p \frac{DT}{Dt} = k\,\nabla^2 T + \frac{Dp}{Dt} + q' + \mu\phi \tag{3.4}$$

where ϕ represents the dissipation function given by

$$\phi = 2\left\{\left(\frac{\partial u}{\partial x}\right)^2 + \left(\frac{\partial v}{\partial y}\right)^2 + \left(\frac{\partial w}{\partial z}\right)^2\right\} + \left(\frac{\partial v}{\partial x} + \frac{\partial u}{\partial y}\right)^2 + \left(\frac{\partial w}{\partial y} + \frac{\partial v}{\partial z}\right)^2 + \left(\frac{\partial u}{\partial z} + \frac{\partial w}{\partial x}\right)^2 - \frac{2}{3}\left(\frac{\partial u}{\partial x} + \frac{\partial v}{\partial y} + \frac{\partial w}{\partial z}\right)^2,$$

and

$$\nabla^2 = \frac{\partial^2}{\partial x^2} + \frac{\partial^2}{\partial y^2} + \frac{\partial^2}{\partial z^2},$$

$\frac{DT}{Dt}$ is the substantial derivative of T, and q' is heat generation.

The continuity equation for incompressible steady flow is:

$$\frac{\partial u}{\partial x} + \frac{\partial v}{\partial y} + \frac{\partial w}{\partial z} = 0 \tag{3.5}$$

Even though flow is turbulent, the momentum and energy equations are still applicable if instantaneous values for the velocity, pressure, and temperature are used. Since the fluctuations are random and chaotic, it is evident that the solution of the equations for turbulent flow is far beyond our present capabilities.

Reynolds [39] modified the momentum equation by introducing the mean fluctuating values of the flow quantities in place of the instantaneous values. Since the instantaneous velocity component is the sum of the mean component and fluctuating velocity in the same direction, the transformation of the above Navier-Stoke equation due to Reynolds [39] can be obtained by introducing

$$u_i = u + u', \; v_i = v + v', \; w_i = w + w' \quad \text{and} \quad p_i = p + p'$$

Now, Reynolds equation for incompressible steady flow in a straight duct of uniform cross-section neglecting body forces has the following form:

$$\rho\left(u\frac{\partial u}{\partial x} + v\frac{\partial u}{\partial y} + w\frac{\partial u}{\partial z}\right) = -\frac{\partial P}{\partial x} + \mu\nabla^2 u - \left[\frac{\partial}{\partial x}(\rho\overline{u'^2}) + \frac{\partial}{\partial y}(\rho\overline{u'v'}) + \frac{\partial}{\partial z}(\rho\overline{u'w'})\right] \tag{3.6}$$

$$\rho\left(u\frac{\partial v}{\partial x} + v\frac{\partial v}{\partial y} + w\frac{\partial v}{\partial z}\right) = -\frac{\partial P}{\partial y} + \mu\nabla^2 v - \left[\frac{\partial}{\partial x}(\rho\overline{u'v'}) + \frac{\partial}{\partial y}(\rho\overline{v'^2}) + \frac{\partial}{\partial z}(\rho\overline{v'w'})\right] \tag{3.7}$$

$$\rho\left(u\frac{\partial w}{\partial x} + v\frac{\partial w}{\partial y} + w\frac{\partial w}{\partial z}\right) = -\frac{\partial P}{\partial z} + \mu\nabla^2 w - \left[\frac{\partial}{\partial x}(\rho\overline{u'w'}) + \frac{\partial}{\partial y}(\rho\overline{v'w'}) + \frac{\partial}{\partial z}(\rho\overline{w'^2})\right] \tag{3.8}$$

The corresponding energy equation in turbulent flow is:

$$u \frac{\partial T}{\partial x} + v \frac{\partial T}{\partial y} + w \frac{\partial T}{\partial z} = k \nabla^2 T$$

$$- \left(\frac{\partial}{\partial x} \overline{u'T'} + \frac{\partial}{\partial y} \overline{v'T'} + \frac{\partial}{\partial z} \overline{w'T'} \right) \qquad (3.9)$$

In the above equations, the three normal stresses, $-\rho\overline{u'^2}$, $-\rho\overline{v'^2}$, and $-\rho\overline{w'^2}$ and the three shear stresses, $-\rho\overline{u'v'}$, $-\rho\overline{v'w'}$ and $-\rho\overline{u'w'}$ are called the Reynolds stresses or eddy stresses. The problem under consideration, is that of developing steady, incompressible, constant cross-sectional duct flow. Therefore, all of the derivatives with respect to time, t, and the body force are neglected.

In the absence of secondary flow Eq.(3.6) is sufficient to determine the axial velocity distribution. In most situations, axial thermal conduction, and eddy diffusion are either zero or negligibly small, and the terms $\frac{\partial^2 T}{\partial x^2} - \frac{\partial}{\partial x} \overline{u'T'}$ can be ignored. For further simplification of Eq. (3.6) the boundary layer approximation introduced by Prandtl [40] is applied so that terms $\frac{\partial^2 u}{\partial x^2}$, and $\frac{\partial \overline{u'^2}}{\partial x}$ are also ignored.

Now, for two dimensional axisymmetric flow the appropriate equation of momentum is:

$$u \frac{\partial u}{\partial x} + v \frac{\partial u}{\partial y} + \frac{1}{\rho} \frac{\partial P}{\partial x} = \nu \frac{\partial^2 u}{\partial y^2}$$

$$- \frac{\partial}{\partial y} (\overline{u'v'}) \qquad (3.10)$$

and the equation of energy is:

$$u \frac{\partial T}{\partial x} + v \frac{\partial T}{\partial y} = k \frac{\partial^2 T}{\partial y^2}$$

$$- \frac{\partial}{\partial y} (\overline{v'T'}) \qquad (3.11)$$

In Eq. (3.11) the last term represents the turbulent heat convection and it is analogous to the Reynolds stress. Using the concept of the eddy diffusivity, ε, the turbulence terms in the momentum equation $-\overline{v'u'}$ and in the energy equation $-\overline{v'T'}$ are often expressed as $\varepsilon_M(\partial u/\partial y)$, and $\varepsilon_H(\partial T/\partial y)$ respectively. However, the eddy diffusivity is not a fluid property because it is a function of position and flow conditions [1]. Now with

$$-\overline{u'v'} = \varepsilon_M\left(\frac{\partial u}{\partial y}\right)$$

and,

$$-\overline{v'T'} = \varepsilon_H\left(\frac{\partial T}{\partial y}\right)$$

equations (3.10) and (3.11) yield

$$u\frac{\partial u}{\partial x} + v\frac{\partial u}{\partial y} + \frac{1}{\rho}\frac{\partial P}{\partial x} = \frac{\partial}{\partial y}\left[(\nu + \varepsilon_M)\frac{\partial u}{\partial y}\right] \tag{3.12}$$

and

$$u\frac{\partial T}{\partial x} + v\frac{\partial T}{\partial y} = \frac{\partial}{\partial y}\left[(k + \varepsilon_H)\frac{\partial T}{\partial y}\right] \tag{3.13}$$

Corresponding equations for cylindrical coordinates are:

$$u\frac{\partial u}{\partial x} + v\frac{\partial u}{\partial r} + \frac{1}{\rho}\frac{\partial P}{\partial x} = \frac{1}{r}\frac{\partial}{\partial r}\left[r(\nu + \varepsilon_M)\frac{\partial u}{\partial r}\right] \tag{3.14}$$

and,

$$u\frac{\partial T}{\partial x} + v\frac{\partial T}{\partial r} = \frac{1}{r}\frac{\partial}{\partial r}\left[r(k + \varepsilon_H)\frac{\partial T}{\partial r}\right] \tag{3.15}$$

In the present study, we are concerned with the determination of the fully developed velocity profile and temperature profile in the developing region of a partially roughened rectangular duct.

In the calculation of fluid frictions, entrance length, and heat transfer, the velocity distribution must be determined from the momentum equation and used in the energy equation to solve the temperature profiles for the specified boundary conditions.

3.2 PHYSICAL MODEL

Depending upon the type of roughness on the rough wall, the local flow mechanism in the vicinity of that wall may not fully satisfy the boundary layer approximations. Large scale roughness may cause flow recirculation in the wake zone of the roughness elements, where some of the neglected terms in the momentum equations become important.

In the present study, asymmetric flow was introduced in a rectangular duct of large aspect ratios by roughening one of the wider sides with square ribs of different pitches.

The momentum integral equation was broken into smooth and rough side equations and to take care of the above mentioned complication, the parameter Z_{or} was introduced in the rough side equation. This will be further mentioned in section 3.3.2 where the velocity fields to be used in the present analysis are discussed.

The assumptions selected for the present study are as follows:

(1) The flow is steady, and turbulent at all points along the ducts,

(2) the flow is of an incompressible Newtonian fluid, and the fluid properties are constant,

(3) the temperature profiles are uniform across the entrance section, where the thermal boundary layer thickness is zero at the entrance,

(4) flow outside the boundary layer is potenial flow,

(5) the rough wall is heated and the smooth one is insulated,

(6) The usual boundary layer conceptions [1,41]

$$\frac{\partial u}{\partial y} >> \frac{\partial u}{\partial x} , \frac{\partial v}{\partial x} , \frac{\partial v}{\partial y}$$

$$\frac{\partial P}{\partial x} \simeq \frac{dP}{dx} , \frac{\partial P}{\partial y} \simeq 0 \quad \text{and}$$

$$\frac{\partial T}{\partial y} >> \frac{\partial T}{\partial x}$$

will be applied and also, it is assumed that the viscous dissipation and work of compression are negligible compared with heat conduction.

It must be pointed out that the point of zero shear stress is not necessarily coincident with the zero positions of viscous or turbulent shear stresses, nor with the position of maximum velocity. That was explained by Lee [9,42], and further discussed in section 3.3.1.

3.3 MOMENTUM EQUATION IN THE DEVELOPED REGION

In general, the problem of finding exact solutions of Navier-Stokes equations presents insurmountable mathematical difficulties. This is, primarily, a consequence of its being non-linear.

However, the momentum method for the boundary layer introduced by Van Karman [43] has been a powerful tool for the prediction of boundary layers so far. Together with an assumed velocity field, it forms the basis of many existing solutions of the boundary layer. It can, in fact, be derived through a partial integration of Eq. (3.10) [44].

The basic integral equations for conservation of mass and momentum of developing incompressible fluid flow in a duct can be written from the diagram describing the idealized model shown in Fig. (3.2·a).

Mass

$$\frac{d}{dx}\,(u_{av}\,S) = \frac{d}{dx}\int_{o}^{S} u\,dy = 0 \tag{3.16}$$

Momentum

middle portion (potential flow);

$$\frac{dP}{dx} = -\,\rho\,u_{\infty}\,\frac{du_{\infty}}{dx} \tag{3.17}$$

Rough side:

$$\tau_{wr} = -\,\delta_r\,\frac{dP}{dx} - \frac{d}{dx}\int_{Z_{or}}^{\delta_r} \rho\,u_r^2\,dy_r + \rho\,u_{\infty}\,\frac{d}{dx}\int_{Z_{or}}^{\delta_r} u_r\,dy_r \tag{3.18}$$

Smooth side;

$$\tau_{ws} = -\,\delta_s\,\frac{dP}{dx} - \frac{d}{dx}\int_{o}^{\delta_s} \rho\,u_s^2\,dy_s + \rho\,u_{\infty}\,\frac{d}{dx}\int_{o}^{\delta_s} u_s\,dy_s \tag{3.19}$$

The details of the derivation are presented in Appendix 1.

For fully developed flow sufficiently far from the entrance, the flow is essentially one-dimensional with the velocity field invariant in the streamwise (x) direction. When the conditions

$$\frac{\partial}{\partial x} = 0, \quad v = 0,$$

characterizing fully developed flow are imposed on Eq. (3.10), one obtains

$$\mu \frac{d^2u}{dy^2} - \rho \frac{d\,\overline{u'v'}}{dy} - \frac{dP}{dx} = 0 \tag{3.20}$$

with boundary conditions

$$\text{at} \quad y = 0; \quad u = 0, \quad \overline{u'v'} = 0, \quad \mu \frac{\partial u}{\partial y} = \tau_w$$

$$y = Z_{or}; \quad u = 0, \quad \overline{u'v'} = 0, \quad \mu \frac{\partial u}{\partial y} = \tau_w$$

$$\text{at} \quad y = y_o; \quad \tau = \mu \frac{du}{dx} - \rho\, \overline{u'v'} = 0$$

The momentum equations simplify to (see Appendix 2 for a derivation from Eq. (3.20))

Rough side;

$$\tau_{wr} = - y_{or} \frac{dP}{dx} \tag{3.21}$$

Smooth side;

$$\tau_{ws} = - y_{os} \frac{dP}{dx} \tag{3.23}$$

where $y_{os} + y_{or} = S$.

3.3.1 Eddy Diffusivity for Momentum

The turbulent mixing motion is responsible not only for an exchange of momentum, but also enhances the transfer of heat and mass in fields of flow associated with non uniform distributions of temperature or concentration. The methods for the calculation of the turbulent flow, temperature, and concentration fields developed so far are based on empirical hypotheses which endeavour to establish a relationship between the Reynolds stresses produced by the mixing motion, and the mean values of the velocity components together with a suitable hypothesis concerning heat and mass transfer.

The concept of eddy diffusivity, first initiated by Bussinesq [45] can be introduced into the analysis if we rewrite Eq. (3.20) as

$$\frac{d}{dy}\left(\mu \frac{du}{dy} - \rho \overline{u'v'}\right) - \frac{dP}{dx} = 0 \tag{3.23}$$

where the quantity in the parentheses corresponds to the shear stress τ in the channel

$$\tau = \mu \frac{\partial u}{\partial y} - \rho \overline{u'v'} \tag{3.24}$$

If we put

$$\tau_t = - \rho \overline{u'v'} = \rho \varepsilon_M \frac{\partial u}{\partial y} \tag{3.25}$$

we get

$$\frac{\tau}{\rho} = (\nu + \varepsilon_M) \frac{du}{dy} \tag{3.26}$$

This last equation, together with an eddy diffusivity model, has been extensively used to predict turbulent transport for a wide

variety of flow geometries [30,46]. However, in asymmetric flows, where the stationary values of the mean and fluctuating velocities do not coincide, the concept of eddy diffusivity as used above presents some difficulties. As discussed by Lee and Barrow [9], at points where the velocity gradient is zero, the shear stress is not necessarily zero, although Eq. (3.26) predicts it to be zero.

Newton's equation, after which the relation by Boussinesq [45] is patterned, is justified in connecting the laminar shear with the local derivative of the velocity because the mean-free-path length of the molecules is generally very small compared to the boundary layer thickness. As a consequence, the local shear is influenced by the velocity variation very close to the place where the shear occurs. In turbulent flow, on the other hand, one finds that in the turbulent mixing process, fluid particles are transported over distances which are of the same order of magnitude as the boundary layer thickness and one must, therefore, expect the turbulent shear to be influenced by the flow situation in a regime which cannot be considered as small.

It has been found experimentally that in certain flow situations that a finite shear occurs at a location where the transverse velocity variation is zero and vice-versa. This has been found, for instance, in a wall jet and in flow through a parallel-wall channel with a rough and a smooth wall (the case of this study). A partial explanation of this non-universality may be taken from Townsend's [47] suggestion that the fluctuating motion consists of an "active" component which interacts locally with the mean motion and, also of an "inactive"

component, governed by far-away conditions, and, therefore, not directly correlated with the mean motion. A discussion of why the zero shear and zero gradient points are not necessarily coincident in turbulent flows is given in reference [48] through an analysis of Navier-Stokes and Von Karman's momentum equations.

3.3.2 Velocity Profile

The simplified equations of motion presented in section (3.3), are not enough to predict the mean flow parameters which are sought in the present study. A turbulent model is necessary to give the velocity profiles encountered in the flow situations. In the present work, a model based on L. Prandtl's mixing length theory [40] is adopted. A physical interpretation of the mixing length can be given in the following way: the mixing length is that distance in the transverse direction which must be covered by an agglomeration of fluid particles travelling with its original mean velocity in order to make the difference between its velocity and the velocity in the new lamina equal to the mean transverse fluctuation in turbulent flow [1]. Using this concept of mixing length, an expression for turbulent shear stress can be reached:

$$\tau_t = \rho \, \ell^2 \left| \frac{du}{dy} \right| \frac{du}{dy} \tag{3.27}$$

Together with the assumptions that the mixing length is proportional to the wall distance through a constant K, and that shear stress does not change with wall distance, we get the following expression for the velocity profile in turbulent flow near a wall:

$$u = \frac{u_\tau}{K} \ln y + c_1 \tag{3.28}$$

Through dimensional considerations, it can be shown that Eq. (3.28) can be written for hydrodynamically smooth walls as

$$\frac{u_s}{u_{\tau s}} = \frac{1}{K} \ell n \frac{y_s u_{\tau s}}{\nu} + c \qquad (3.29)$$

and for rough walls as

$$\frac{u_r}{u_{\tau_r}} = \frac{1}{K} \ell n \frac{y_r}{Z_{or}} \qquad (3.30)$$

where $Z_{or} = m \varepsilon$, the hydrodynamic or characteristic roughness. Here, m is a constant which is supposed to incorporate roughness characteristics.

A number of expressions for the velocity profile near a smooth wall are available in literature [4, 49 - 53]. The expression for velocity profile due to Reichardt [28], among many others as shown in Table 3.1, was chosen to be used in the present study because of its simple, continuous form valid for $y > 0$ and including the so-called "Laminar sub-layer".

$$u_s^+ = \frac{1}{K} \ell n(1 + Ky^+) + 7.8[1 - \exp(-\frac{y^+}{11}) - \frac{y^+}{11} \exp(-\frac{y^+}{3})] \qquad (3.31)$$

where $K = 0.4$ Von Karman's constant.

The above profile simplifies to the following expression as conceived by Prandtl and Taylor [44] for large $y^+ (> \sim 100$, see Table 3.1)

$$u^+ = \frac{1}{K} \ell n\, y^+ + c \qquad (3.32)$$

with $K = 0.4$ again and the value of $c = 5.52$, adjusted to have numerical agreement with Eq. (3.31).

For the rough wall profile given by Eq. (3.30), a number of and varying values of m are reported in the literature for different shape and density of roughness, ranging from $\frac{1}{3.83}$ [54] to $\frac{1}{9400}$ [55].

In view of the widely varying values of m with no apparent correlation reported in the literature, it was obvious that further work was necessary to establish relations between roughness structures on walls and velocity profiles.

In the above equation (3.30), the parameter Z_{or} may be interpreted as a hypothetical distance from the wall where the velocity is assumed to be zero. This shift of the reference point for the rough wall velocity profile has been shown to depend on the roughness Reynold's number $\frac{\varepsilon u_\tau}{\nu}$ (which is measure of the roughness structure through the wall shear stress) by Clauser [56] on the basis of experiments conducted with two-dimensional roughness elements. Hama [57] has subsequently verified Clauser's generalization for three-dimensional roughness and Perry and Joubert [58] have extended pressure gradient. Wu [59] has reported a similar shift for rough surfaces with uniform spherical particles arranged in a random and compact form.

The reported data suggest that this point is somewhere between the root and the tip of the physical roughness height. Exactly where for a particular roughness structure is to be found through experiments.

3.3.3 Friction Factor

The friction losses occurring during turbulent flow are proportional to the kinetic energy of the fluid pen unit volume and the area of the solid surface in contact with the fluid. This is the basis of the definition of the friction factor. Viscosity has been found to have but slight effect during turbulent flow. The friction factor is generally defined as:

$$f = \frac{\tau}{\frac{1}{2} \rho \, u_w^2}$$

For rough side of the channel, it can be defined as:

$$f_r = \frac{2 \, \tau_{wr}}{\rho \, u_{av}^2} \tag{3.33}$$

Using equation (3.21)

$$f_r = \frac{2 \, y_{or}}{\rho \, u_{av}^2} \left(- \frac{dP}{dx} \right) \tag{3.34}$$

For smooth side;

$$f_s = \frac{2 \, \tau_{ws}}{\rho \, u_{av}^2} \tag{3.35}$$

using equation (3.22)

$$f_s = \frac{2 \, y_{os}}{\rho \, u_{av}^2} \left(- \frac{dP}{dx} \right) \tag{3.36}$$

making a fully developed momentum balance on a fluid element

$$\tau_{wr} + \tau_{ws} = S \left(- \frac{dP}{dx} \right) \tag{3.37}$$

Hence, the friction factor for the whole channel can be defined as,

$$f = \frac{\tau_{wr} + \tau_{ws}}{\rho \, u_{av}^2} \tag{3.38}$$

which becomes

$$f = \frac{S}{\rho u_{av}^2} \left(-\frac{dP}{dx} \right) \tag{3.39}$$

from Eqs. (3.37), (3.33) and (3.35) we get the average local friction factor,

$$f = \frac{f_r + f_s}{2} \tag{3.40}$$

3.4 * ENERGY EQUATION IN THE THERMAL ENTRANCE REGION

The solution of the energy equation in the developing region is essentially a problem of finding the temperature distribution. However, even though this equation (Eq. (3.11)) can be greatly simplified, it is still extremely difficult if not impossible to solve because of non-linearities involved in the equation.

Here, we are studying the problem of a rectangular duct where the thermal boundary layer is developed in the entrance region. The problem will be studied from an integral view point.

Two boundary conditions will be considered for the solution:

1. One wall has a constant heat flux while the other is insulated.
2. The distribution of the shear stress, τ, and heat flux, q, can be derived from the equation of momentum and energy.

Now the heat balance of a fluid element in the developing region, see (Fig. 3.2 b) gives,

$$- dy\, dx\, u\rho c_p \frac{\partial T}{\partial x} dx - dy\, dx\, v\rho c_p \frac{\partial T}{\partial y} dy$$

$$= dx\{(q + \frac{\partial q}{\partial y} dy) - q\} \tag{3.41}$$

Rearranging

$$u \frac{\partial T}{\partial x} + v \frac{\partial T}{\partial y} = - \frac{1}{\rho c_p} \frac{\partial}{\partial y} q \qquad (3.42)$$

Equation (3.42) in combination with equation (3.13) yields,

$$\frac{q}{\rho \varepsilon_p} = (K + \varepsilon_H) \frac{\partial T}{\partial y} \qquad (3.43)$$

The temperature distribution, T, for a given wall heat flux may be determined from Eq. (3.43).

3.4.1 Eddy Diffusivity for Heat

The ratio of eddy diffusivity of heat and momentum, $\varepsilon_H/\varepsilon_M$, which is often called the turbulent Prandtl number, plays an important role in most analytical studies to predict heat transfer coefficients in turbulent convective heat transfer [41]. To simplify the mathematical manipulation, Prandtl [60] assumed that the mixing length for heat transfer is the same as the mixing length for momentum transfer;

$$\varepsilon_H = \varepsilon_M = \ell^2 \frac{du}{dy} \qquad (3.44)$$

that means a particle of fluid travels the same distance before losing its identity and before attaining a different temperature. Under these conditions, a true analogy exists between momentum and heat transfer for turbulent flow. Many investigators assumed this ratio $\varepsilon_M/\varepsilon_H = 1$. As Prandtl did, however, recent experimental work has shown that they are not equal.

In the literature reviewed there are few models describing the relationship, ε_H and ε_M, i.e. turbulent Prandtl Number, like Jenkins model [29], which does not even show a good agreement with the experimental values.

In the present work, the turbulent Prandtl number has been assumed equal to 1, for the following reasons: firstly, a lack of an accurate correlation, and secondly for the reason of simplicity.

Consequently, it appears that the problem of turbulent Prandtl number is still subjected to further studies, both experimentally and analytically. A general relationship between ε_H and ε_M is needed so that the analogy between heat transfer and momentum transfer will become useful. The effects of turbulence structure, fluid properties, and wall characteristics on eddy motion must be taken into consideration.

3.4.2 Temperature Profile

The temperature profile can be derived from the energy equation (3.43), if the functions for the heat flux and eddy diffusivity for heat are known. Eq. (3.43) in non-dimensional parameters can be given as:

$$\frac{q}{q_w} = \left(\varepsilon_{H/\nu} + \frac{1}{Pr}\right) \frac{dT^{++}}{dy_r^{++}} \tag{3.44}$$

where

$$T^{++} = \frac{(T_w - T)c\ \tau_r}{q_w\ u_{\tau_r}}$$

In Eq. (3.44), q_w refers to the heat flux at the rough wall.

To solve Eq. (3.44) the distribution of heat flux across the flow section, $q(y_r^{++})$ must be known. Strictly speaking, in order to express the local heat flux, q, in terms of the known wall value, q_w, it is not necessary to make assumptions on the velocity distribution,

because the local mass flow rate at any point, y_r^{++}, in the cross-section can be calculated from Eqs. (3.30) and (3.31). However, the expression for q from this procedure is formidable with little improvement in the final calculation as has been shown by Barrow [61] and Lee [23].

Extending Lee's contention we can assume that the heat flux changing linearly across the channel

$$q\,(y_r^{++}) = q_w\left(1 - \frac{y_r^{++}}{\delta_{th}^{++}}\right) \tag{3.45}$$

Now the evaluation of, $\varepsilon_M(y_r^{++})$ from Eq. (3.25) requires a knowledge of, $\tau(y_r^{++})$ and, $u(y_r^{++})$. The shear stresses are assumed to be constant up to (y_{or}), along with the assumption that was made by Reitchardt [12] to obtain the velocity profile Eq. (3.31). With the Prandtl [60] assumption for, $\varepsilon_H/\varepsilon_M = 1$.

Therefore,

$$(\varepsilon_H/\nu)_r = \{1/(du_r^{++}/dy_r^{++})\} - 1 \tag{3.46}$$

$$\text{for } Z_{or}^{++} < y_r^{++} < y_{or}^{++}$$

and

$$(\varepsilon_H/\nu)_s = \{(1/d\,u_s^{++}/dy_r^{++})\} - 1 \tag{3.47}$$

$$\text{for } y_{or}^{++} < y_r^{++} < S^{++}$$

Now combination of Eq. (3.44) with Eqs. (3.45), (3.46) and (3.47) yields

$$T^{++} = \int_{Z_{or}^{++}}^{S^{++}} \frac{1}{(\varepsilon_H/\nu + 1./Pr)}\, dy_r^{++} - \frac{1}{S^{++}} \int_{Z_{or}^{++}}^{S^{++}} \frac{y_r^{++}}{(\varepsilon_H/\nu + 1/Pr)}\, dy_r^{++} \tag{3.48}$$

3.4.3 Thermal Entrance Length

The energy integral equation for the thermal boundary layer that builds up on the heated surface (rough surface) of the channel while the other surface is insulated, can be written from an idealized model illustrated in Fig. (3.2 b) as,

$$\int_{Z_{or}}^{\delta_{th}} uc\,\rho T dy)_1 + q_w\,\delta x + \{\int_{Z_{or}}^{\delta_{th}} uc\,\rho\,dy)_2 - \int_{Z_{or}}^{\delta_{th}} uc\,\rho\,dy)_1\} T_{\delta_{th}}$$

$$= \int_{Z_{or}}^{\delta_{th}} uc\,\rho T dy)_2 \qquad (3.49)$$

where the subscripts on the parentheses refer to plane 1. and 2. in the diagram.

For small heat fluxes, the properties, c and, ρ may be assumed to be constant, and an integration of Eq. (3.49) then reduces to

$$q_w\, x = \rho c \int_{Z_{or}}^{\delta_{th}} u(T - T_{\delta_{th}})\,dy \qquad (3.50)$$

On introduction of the non-dimensional quantities as defined in the "Nomenclature", Eq. (3.50) may be written as

$$\frac{x^{++}}{S^{++}} = \frac{1}{S^{++}} \int_{Z_{or}}^{\delta_{th}^{++}} u^{++} (T^{++}_{\delta_{th}} - T^{++})\,dy^{++}_r \qquad (3.51)$$

The details of the derivation are presented in Appendix 7. In the entry region, where $\delta_{th} < S$, so that provided u^{++} and T^{++} are known functions of y^{++}_r, the length x for a given thermal

boundary layer thickness δ_{th} may be determined. The calculation procedure is presented in Section 3.5.

3.4.4 Nusselt Number

The local heat transfer coefficient and Nusselt number are defined in the usual way, as:

$$h_x = \frac{q_w}{(T_w - T_b)_x} \tag{3.52}$$

$$Nu_x = \frac{h_x\ De}{k} \tag{3.53}$$

and Reynold's number as

$$Re = \frac{\rho\ u_b\ De}{\mu} \tag{3.54}$$

In dimensionless form, Eqs. (3.53) and (3.54) become:

$$Nu_x = \frac{De^{++}}{T_b^{++}}\ Pr \tag{3.55}$$

and

$$Re = 2S^{++}\ u_b^{++} \tag{3.56}$$

Now the bulk temperature, (T_b), is defined as:

$$T_b = \left(\frac{\int_{dA} Tu\ dA}{\int_{dA} u\ dA} \right)_x \tag{3.57}$$

and in terms of dimensionless parameters, as:

$$T_b^{++} = \frac{\int_{Z_{or}^{++}}^{y_{mr}^{++}} T^{++}\ U_r^{++}\ y_r^{++}\ dy_r^{++} + \int_{y_{mr}^{++}}^{S^{++}} T^{++}\ U_s^{++}\ y_r^{++}\ dy_r^{++}}{\int_{Z_{or}^{++}}^{y_{mr}^{++}} u_r^{++}\ y_r^{++}\ dy_r^{++} + \int_{y_{mr}^{++}}^{S^{++}} U_s^{++}\ y_r^{++}\ dy_r^{++}} \tag{3.58}$$

The bulk velocity, (U_b) is defined as:

$$U_b = \frac{\int_{dA} U \, dA}{\int_{dA} dA} \tag{3.59}$$

and in terms of dimensionless parameters, as,

$$U_b^{++} = \frac{1}{S^{++}} \left[\int_{Z_{or}^{++}}^{y_{mr}^{++}} U_r^{++} \, dy_r^{++} + \int_{y_{mr}^{++}}^{S^{++}} U_s^{++} \, dy_r^{++} \right] \tag{3.60}$$

3.5 METHOD OF SOLUTION

In order to predict the velocity distribution across the flow channel and the friction factor, f, the location of the maximum velocity point and zero shear stress point should be known.

Bhuiyan [3], did an intensive experiment studying the effects of the geometrical parameters (A, S, ε, p, D_{hyd}) and Reynolds number, on the locations of the zero shear stress and maximum velocity points. He used a double pitot tube to measure the location of maximum velocity, and a single channel hot wire probe to measure the location of zero shear stress. He assumed that,

$$\phi(y, S, \varepsilon, p, u, \rho, \mu) = 0 \tag{3.61}$$

which expressed in terms of dimensionless parameter as,

$$\phi\left(\frac{u\rho S}{\mu} , \frac{Y}{S} , \frac{S}{\varepsilon} , \frac{p}{s} \right) = 0 \tag{3.62}$$

and he obtained correlations for, y_{mr}, y_{or}, which were based on $\sqrt{\overline{U'^2}}$.

Harjalic and Launder [62] showed that the minimum values of the axial turbulence intensity occurs at approximately $0.8(S - y_{or})$.

Therefore, Bhuiyan's correlation for y_{or} and y_{mr} are correlated as [63]

$$\frac{y_{or}}{S} = 0.523\ Re^{0.033} \left(\frac{S}{\varepsilon}\right)^{0.157} \left(\frac{p}{\varepsilon}\right)^{0.158} - 0.25 \tag{3.63}$$

and

$$\frac{y_{mr}}{S} = 0.299\ Re^{0.066} \left(\frac{S}{\varepsilon}\right)^{0.140} \left(\frac{p}{\varepsilon}\right)^{0.201} \tag{3.64}$$

Having the values of, y_{mr} and y_{or}, Z_{or} can be calculated as

$$Z_{or}^{++} = y_{mr}^{++} \exp(-D\{\ell n\ [(S^{++} - y_{mr}^{++})D] + c.K\}) \tag{3.65}$$

where

$$D = \frac{U_{\tau_s}}{U_{\tau_r}} = \sqrt{\frac{S}{y_{mr} - 1}} \tag{3.66}$$

Knowing Z_{or}, we can predict the velocity distributions in the fully developed region using Eqs. (3.30) and (3.31)

The friction factors, f, are calculated using Eqs. (3.63), (3.63) and (3.64). The computation was carried out numerically on the University of Ottawa computer, IBM 65/60. A simplified flowchart of the program is given in Appendix (8).

The system of Eqs. (3.46), (3.47) and (3.48) can be solved to predict the temperature distribution in the fully developed region, where we used Runge-Kutta method for integrating Eq. (3.48).

The thermal entrance length and local Nusselt number are computed from the appropriate equations.

All of the calculations of the numerical integration were carried out through a CSMP program on the computer. A simplified flowchart of the program is given in Appendix (9).

CHAPTER IV

RESULTS AND DISCUSSION

4.1 VELOCITY PROFILE

The predicted velocity profiles for different Reynolds numbers are shown in Figs. 4.1 and 4.2. These analytical results are compared with the experimental velocity measurements [3]. In general, the logarithmic velocity profiles chosen for the present study represent the actual velocity fields encountered, except near the rough wall in a region of about 1.5ε from the roughness root. This deviation may be attributed to the vortex structures, which possibly prevail between the roughness elements. It is an indication of the failure of the mixing length hypothesis and the assumptions used in the derivation of the logarithmic law near the rough wall.

Between the sublayers near the walls and the maximum velocity point, the velocity profiles are in good agreement with the law-of-the-wall profiles. Thus, as far as the mean flow properties are concerned, the fluid particles within these regions are unaware of the nature of the opposite surface.

It is often assumed, without any justification, that the position of zero shear stress coincides with the maximum velocity point. The total shear stress for the fully developed flow is found in Eq. (3.24):

$$\tau = \mu \frac{du}{dy} - \rho \overline{u'v'} \qquad (4.1)$$

Thus, the assumption of zero shear stress where $\frac{du}{dy} = 0$ is based on the assumption that $\overline{u'v'} = 0$. This cannot be accepted immediately

for a general case, although it is true for some geometries for reasons of symmetry.

In this study, the locations of zero shear stress and maximum mean velocity points do not coincide as mentioned in section (3.3.2). The variation in the positions of these points indicates a strong dependence on Re, S/ε, and P/ε. They become proportionately closer to the smooth wall with increase of Reynolds number and decrease of S/ε. The latter result simply reflects a greater effect of physical roughness because it occupies a larger portion of the space between the walls. The variation with Reynolds number indicates stronger diffusion of turbulent eddies as the momentum exchange near the rough wall becomes more vigorous.

These points deviate more from the center-line of the channel towards the smooth wall with increase P/ε, i.e., for a lower roughness density at the same S/ε ratio. This may seem unexpected since a higher roughness density would imply a more vigorous momentun exchange than a lower roughness density, and hence a smaller y_{os}/S ratio. A closer examination of vortex patterns between roughness elements of different pitches [64,65] reveals the possibility that at a higher roughness the flow will tend to skip over the tips of the elements; however, at a lower density, the flow will find some time to re-attach, and when it faces a new element it will be thrown into the stream creating vigorous eddies. Thus the points under consideration are even further displaced from the rough wall. The non-coincidence of the two points and the larger displacement of the maximum velocity point than the zero-shear point simply indicate the stronger effect of dissimilar boundary

conditions on the turbulent flow field rather than the mean motion. To be able to say anything more about the functional relationship between roughness density and position of maximum velocity and zero shear in a channel, further studies of separation, re-attachment and vortex structures on roughened walls should be done.

4.2 FRICTION FACTOR

The friction factors, f, are calculated using Eq. (A.7.2) and are compared in Fig. 4.3 with the experimental values [3]. The agreement between the analysis and the experiment is good. In the same figure comparison was made with the friction factor taken from the classical Moody diagram corresponding to the same relative roughness. The differences, which might be significant between the values of the present study and the ones taken from the Moody diagram, are due to the following reasons:

1. The Moody diagram predicts a constant friction factor in the Reynolds number range considered for the rough side, since the flow is completely rough in this range [1,66]. The present study indicates a transition range type flow between the completely smooth and completely rough regimes. This is due to the asymmetry of the roughness distribution on the channel walls. The combination of completely rough flow on one side and smooth flow on the other produces this type of observed behaviour, namely the variation of total friction factor with both Re and S/ε (or ε/D).

2. The Moody diagram does not recognize the effect of roughness density on the friction factor as shown in Fig. 4.3. For different values of roughness density for a given S/ϵ, the friction factor is the same for a given Reynolds number.

   The effect of P/ϵ on the non-dimensional ratio f_r/f_s can be shown in Figs. 4.4, and 4.5. In general this ratio increases with increase of P/ϵ. This is possibly due to increase in momentun exchange at lower roughness density [64,65].

3. Also if the test channel had different shapes of roughness (i.e. rectangular ribs, triangular ribs, etc.) with the same height, one would still tend to use the same relative roughness value used above in order to calculate the friction factor from the Moody diagram. This in turn would predict exactly the same friction factor for all of the cases and obviously this cannot be the case. The problem arises because the Moody diagram was evalued for a particular type of roughness (i.e. sand roughness).

   To be able to use the Moody diagram an equivalent sand roughness should be defined for every particular roughness structure on a wall. This sand roughness should also be a function of Reynolds number in case of asymmetric roughness distribution. The use of the parameter Z_{or}, which is connected to be the equivalent sand roughness through the logarithmic rough wall profile, is introduced in the present study to provide a step in the theoretical analysis of the behaviour of the flow near a rough wall.

4.3 TEMPERATURE PROFILE

The dimensionless temperature profiles, T^{++}, predicted in the fully developed region, using Eq. (3.48),are plotted in Figs. 4.6 to 4.9. These calculations have been carried out for different Reynolds numbers Re, relative height of roughness, S/ε, and roughness density, P/ε.

For a given location in the channel, the dimensionless temperature increases with increase of Reynolds number. A similar trend was reported by Lee [23] for a case of concentric annuli.

It can be seen in Figs. 4.6 to 4.8 that for given Reynolds and Prandtl numbers the effect of the relative height of roughness is rather small on the bulk temperature.

Fig. 4.9 shows the effect of roughness density, P/ε, on the temperature profile for a given relative height of roughness and Reynolds number. The dimensionless temperature increases with decreasing roughness density, i.e. higher values of P/ε, (i.e. lower roughness density) the flow tends to re-attach, and in the face of a new element it will be ejected into the stream producing more turbulence.

The development of the temperature profile at the thermal entrance region has been predicted for different values of, δ_{th}^{++}, and is shown in Fig. 4.10. Further details of the thermal entrance length in which the development takes place will be discussed in section 4.4.

4.4 THERMAL ENTRANCE LENGTH

For the purely thermal entrance case where the velocity profile is already fully developed at the entrance, the thermal entrance length is usually defined [23] as the distance from the entrance to the cross section where the temperature profile has no straight line portion perpendicular to the fluid flow axis.

The predicted effect of Prandtl number on the thermal entrance length, x^{++}/S^{++}, as illustrated in Figs. 4.11 and 4.12 shows the same trend that Lee [23] observed in his work on the purely thermal entrance problem. It can be seen from Fig. 4.12 that the effect of Prandtl number on the thermal boundary layer thickness is considerable. The thermal entrance lengths for a smooth case [67] are compared with the results of this study for different Prandtl numbers. It may be seen from the graph that the thermal entrance length is greater than that found for the smooth case up to Re ≈ 30,000. The differences decrease and approach the values of the smooth case, after which further decrease is observed.

This is possibly due to the unsymmetric boundary condition, i.e. heated rough wall and insulated smooth wall.

It has been found that the thermal entrance length is affected by the relative height roughness and the roughness density.

Effect of S/ε.

A typical prediction of the effect of relative height of roughness

for a given roughness density and Prandtl number is presented in Fig. 4.13. For a given Reynolds number, the thermal entrance length increases with increase in S/ϵ. Since the laminar sublayer decreases with increase of Reynolds number, i.e. greater effect of roughness, one would expect that the thermal entrance length will decrease.

Effect of P/ϵ.

The effect of P/ϵ on the thermal entrance lengths can be seen in Fig. 4.14. The results are also compared with the smooth one. In general, the thermal entrance lengths decrease with decreasing roughness density. This possibly contributed to the decrease of P/ϵ as previously explained.

4.5 NUSSELT NUMBER

The predicted Nusselt number in the entrance region of a rectangular duct, as shown in Figs. 4.15 to 4.17, clearly indicates that the results of the present analysis are always greater than that of the channel with smooth surfaces. This trend was obvious from the fact that rough surface develop considerably larger values of heat transfer coefficient.

This increase in the heat transfer coefficient can also be deduced from other aspects of the turbulent flow in a rectangular duct. It can be shown for the present geometry by force balance

that the shear stress on the rough wall, τ_{wr}, is always greater than the shear stress on the smooth wall, τ_{ws}. This greater shear stress on the rough wall is understandable, because a part of the turbulent shearing stresses can be transmitted to the wall through pressure forces exerted on the roughness elements. The large value of shear means a larger value of ε_M. At the same time, the larger value of ε_M indicates vigorous thermal diffusion and hence higher rate of heat transfer. Therefore, it is not surprising to see from Figs. 4.15 to 4.17 the increase in heat transfer coefficient.

Fig. 4.16 shows the effect of relative height of roughness on the heat transfer coefficient. In general, the heat transfer decreases with the increase of S/ε. This is possibly due to the effect of roughness on the exchange mechanism and is confined to the regions located in the proximity of the wall [68]. When S/ε approaches infinity the heat transfer coefficient will have the value that associated with the smooth surface. Also the effect of relative height of roughness on the variation of Nusselt numbers and entrance lengths can be seen in Fig. 4.18. The values of (Nu_x/Nu_d) for smaller S/ε are higher than those for lager S/ε.

The predicted effect of roughness density can be seen from Fig. 4.17. Nusselt numbers increase with increase of P/ε. This is due to the vigorous eddies produced, as discussed in section 4.1. Since the Nusselt number should eventually have the smooth surface value as P/ε increases, one may expect that

it will reach to a maximum value at the optimum value of P/ε, beyond which it continues to decrease. No attempt was made here to find the optimum roughness density at this time, and it is recommended that a further study on this matter be made. Effect of P/ε on the variation of Nusselt numbers and entrance lengths can be seen in Fig. 4.19. For a given (x^{++}/S^{++}), the values of (Nu_x/Nu_d) for smaller P/ε are higher than those for larger P/ε.

The curves in Figs. 4.20 to 4.23 show the effect of Reynolds number on the values of the ratios (Nu_x/Nu_d) in the thermal entrance region of a rectangular duct at a given value of x^{++}/S^{++} and Prandtl number. It is seen that for a given Prandtl number, S/ε and P/ε, the Reynolds number seems to have a minor influence on entrance effects. Similar behaviour was observed by Lee [23] for smooth concentric annuli.

To illustrate the effect of Prandtl number, a comparison is made in Fig. 4.24 as a function of (x^{++}/S^{++}) for three values of Prandtl number of 0.1, 1 and 10. For a fixed Reynolds number, S/ε and P/ε, the entrance effects at a given distance, x^{++}/S^{++}, decrease with increasing Parndtl number, the same trends as observed in the pipe flow case [69]. Predicted Nusselt numbers for fully developed heat transfer, calculated from Eq. (3.55), are plotted against Reynolds number for various values of Prandtl number in Fig. 4.25. Nusselt numbers close to the entrance are, as expected, very large in comparison with the fully developed

values as seen in Fig. 4.26. At $x = 0$, the thickness of the thermal boundary layer is zero, and consequently, in theory, the heat transfer coefficient becomes infinite at the cross section.

4.6 F/H RATIO

It has been demonstrated in section (4.5) that the heat transfer coefficient increases with the introduction of roughness on the channel wall. On the other hand, as explained in section 4.2, rough surfaces develop considerably larger values of friction coefficient than a channel with smooth walls. To determine whether the percentage increase in the rate of heat transfer will be offset by the increase in the pressure losses, the non-dimensional ratio F/H has been used. If F/H is greater than 1, the increase in the rate of heat transfer will be offset by an increase in pressure losses, which requires higher pumping power. Conversely, if F/H is less than 1, then the heat transfer will increase more rapidly than the drag, resulting in a more effective system.

Nunner [36] obtained heat transfer data for air with $Pr = 0.72$, which can be approximately correlated with the friction coefficient as follows:

$$\frac{Nu}{Nu_{smooth}} = \left(\frac{f}{f_{smooth}}\right)^{0.5} \qquad (2.3)$$

This conclusion implies that $F/\sqrt{H}$ is constant. In this investigation it has been found that F/H ratio is affected by the parameters P/ε, S/ε, Pr and Re. A comparison of Nunner's data and this study is

presented in Figs. 4.27 and 4.28. It can be seen that the ratio $F/\sqrt{H}$ is not a constant, but is rather affected by different parameters. The parametric effect will be discussed in the following:

Effect of P/ε

Figs. 4.29 and 4.30 show the ratio F/H plotted vs. P/ε for Prandtl number = 0.72 and different values of relative height of roughness and Reynolds number from 10,000 to 100,000. As clearly indicated from the figues, the ratio F/H increases with increase of P/ε. This is expected, since a part of the turbulent shearing stresses can be transmitted to the wall through pressure forces exerted on protuberances. No analogue exists for this mechanism in heat trnasfer.

Effect of S/ε

The effect of S/ε is shown in Figs. 4.29 and 4.30. In general, a small increase in F/H with decrease in S/ε is noticed. This is due to the fact that the effect of roughness on the exchange mechanism is confined to the regions located in the proximity of the wall. Similar observations have been reported by Owen and Thomson [68], who made measurements of different values of Prandtl number in a rough tube.

Effect of Prandtl number

It is well known that at very low Prandtl numbers where the predominent mechanism is molecular diffusion roughness would be expected to have a lesser influence on the turbulent heat transfer

process. The heat transfer conductance increases substantially at high Prandtl numbers due to any small disturbance of the laminar sublayer which represents a high thermal resistance. This trend can be shown in Figs. 4.31 and 4.32 where the ratio F/H decreases with increase of Prandtl number from 0.72 to 10. However, for further increase of Prandtl number (Pr ≈ 30) it was found that the ratio F/H increases as shown in Figs. 4.23 to 4.35. A complete picture of the effect of different Prandtl numbers, (up to Pr = 100), on the ratio F/H is shown in Figs. 4.35 and 4.37. It is postulated that the ratio F/H has a minimum value beyond which friction forces may dominate. This may possibly be due to the assumption of $\varepsilon_H/\varepsilon_M = 1$, which was discussed in section (3.4.1).

Effect of Reynolds Number

As indicated in section (4.5), heat transfer increases with increase in Reynolds number. It was also shown in section (4.2) that friction forces increase with increase in Reynolds number. Since the friction forces increase more rapidly than heat transfer, one would expect that the ratio F/H will increase with increase of Reynolds number. A typical variation of F/H with Re is presented in Figs. 4.38 and 4.39. It should be noted that the effect of Reynolds number is significant at high values (Re > 30,000). At high Reynolds number, a great influence of roughness is expected due to the thinner laminar sublayer.

For the ranges of parameters used in this study, i.e. ($Re = 10{,}000$ to $100{,}000$, $Pr = 0.1$ to 100, $S/\varepsilon = 8.61$ to 29.45 and $P/\varepsilon = 2$ to 8) it can be concluded that, for an efficient system of heat transfer, one must

Decrease the relative height of roughness,

Increase the pitch between the roughness elements,

Decrease the Reynolds number.

CHAPTER V

CONCLUSION

The following conclusions were derived from the semi-analytical investigation of the drag; local heat transfer characteristics and entrance length for fluid flow flowing turbulently in a channel with a partially roughened surfaced, fully developed velocity profile, and a uniform heat flux at the rough surface:

1. A good agreement was obtained between the analytical results for velocity profiles and friction forces and the experimental results [3].
2. The fact that the locations of maximum velocity and zero shear stress are non-coincident for asymmetric turbulent flow was further established.
3. The friction forces decrease with an increase of S/ε and increase with an increase of P/ε.
4. The heat transfer coefficient increases with an increase of P/ε, and decreases with an increase of S/ε.
5. The effect of increasing P/ε was to decrease (Nu_x/Nu_d), for a given x^{++}/S^{++} and Reynolds number. Increase in P/ε also leads to a decrease in the thermal entrance length, and to an increase in the Nusselt number.

6. For low Prandtl number, an increase in Reynolds number leads to an increase in $(x^{++}/S^{++})_d$. At very high values of the Prandtl number, the variation of $(x^{++}/S^{++})_d$ with Reynolds number is more complex. The effect of Reynolds number has in general a minor influence on $(x^{++}/S^{++})_d$ for Prandtl numbers greater than unity.
7. With increase of P/ε, decrease of Reynolds number, and for a Prandtl number approximately between 6 and 12 there will be a subsequent decrease of F/H ratio.

REFERENCES

1. H.Schlichting, "Boundary Layer Theory", McGraw Hill Book Co., Inc. 6th Edition (1968).

2. W.B. Hall, "Heat Transfer in Channels Having Rough and Smooth Surfaces", J. of Mech.Eng. Science V. 4, No. 3, (1962).

3. A. Bhuiyan, "An Asymmetric Turbulent Fluid Flow Induced by Rectangular Ribbed Surface Roughness", Master of App. Sci., Dept. of Mech. Eng., Univ. of Ottawa, (1977).

4. R.G. Deissler, "Analytical Investigation of Turbulent Flow in Smooth Tubes with Heat Transfer with Variable Fluid Properties for Prandtl Number of 1", NACA TN 2242, (1950).

5. J. Laufer, "The Structure of Turbulence in Fully Developed Pipe Flow", NACA Rept. 1174 (1954).

6. C.J. Cremers and E.R.G. Eckert, "Hot-Wire Measurements of Turbulence Correlations in a Triangular Duct", J. of Applied Mech., 609-614 (1962).

7. J.A. Clark, "A Study of Incompressible Turbulent Boundary Layers in Channel Flow", J. of Basic Eng., Trans. ASME, 90, 455-468, Dec. (1968).

8. H. Barrow, "Fluid Flow and Heat Transfer in an Annulus With a Heated Core Tube", Proc. Inst. Mect. Eng. 56, 1113, (1955).

9. Y. Lee and H. Barrow, "Turbulent Flow and Heat Transfer in Concentric and Eccentric Annuli", Proceedings, I. Mech. E., 178, 1-16 (1964).

10. J.A. Brighton and J.B. Jones, "Fully Developed Turbulent Flow in Annuli", J. of Basic Eng., Trans. ASME, Sec. D, 86, 835-844, (1964).

11. R.R. Rothfus, W.K. Sartory and R.I. Kermode, "Flow in Concentric Annuli at High Reynolds Numbers", A.I.Ch.E. Journal, 12, 1086-1091, Nov. (1966).

12. S. Levy, "Turbulent Flow in an Annulus", J. of Heat Transfer, ASME, 89, 25-31 Feb. (1967).

13. A. Quarmby, "An Analysis of Turbulent Flow in Concentric Annuli", Appli. Sci. Res., 19, 205-273, (1968).

14. B.G. Van der Hegge-Zijnen, "Measurements of the Velocity Distribution in the Boundary Layer Along a Rough Surface", Verhandel Koninkl wetenschap Amsterdam 31, 499 (1928).

15. M. Hansen, "Study of the Velocity Profile Over Rough Plates", NACA TM 585, (1930).

16. W.K. Allan, "Velocity Distribution in Turbulent Flow", J. Mech. Engg. Sci. 12, No. 6, 391, (1970).

17. W.K. Allan and V. Sharma, "An Investigation of Low Turbulent Flows Over Smooth and Rough Surface", J. Mech. Engg. Sci. 16, 71-78 (1974).

18. F. Schultz-Grunow, "Der hydraulische Reibungswiderstand von Platten mit MaBig Rauher Oberflache" Insbesondere von Schiffsaberflachen, Jb. Schiffbautechen Ges. 39, 176-198 (1938).

19. G. Kempf, "The Effect of Roughness on the Resistance of Ships", Engg. London 143, 417 (1937).

20. D. Wilkie, "Forced Convection Heat Transfer from Surfaces Roughened by Transverse Ribs", Third International Heat Transfer Conference, Chicago, Illinois 1, 19 (1966).

21. M.J. Lewis, "Roughness Functions, the Thermohydraulic Performance of Rough Surfaces and the Hall Transformation -- an Overview", Int. J. Heat Mass Transfer V. 17, 809-814 (1974).

22. A.J. Musker and A.K. Lewkowicz, "The Effect of Ship Hull Roughness on the Development of Turbulent Boundary Layers", Int. Symposium on ship viscous resistance, SSPA, Goteborg (1978).

23. Y. Lee, "Turbulent Heat Transfer from the Core Tube in Thermal Entrance Region of Concentric Annuli", Int. J. Heat Mass Transfer, 11, 509-522, (1968).

24. W.M. Kays and E.Y. Leung, "Heat Transfer in Annular Passages Hydrodynamically Developed Turbulent Flow with Arbitrarily Prescribed Heat Flux", Int. J. Heat Mass Transfer, 6, 537-557 (1963).

25. A. Quarmby and R.K. Anand, "Turbulent Heat Transfer in Concentric Annuli with Constant Wall Temperatures", J. of Heat Transfer, Trans. ASME, 23-45, Feb. (1970).

26. J.C. Chen, and W.S. Yu, "Entrance Region and Variable Heat Flux Effects in Turbulent Heat Transfer to Liquid Metals Flowing in Concentric Annuli", Int. J. Heat Mass Transfer, 13, 667-680 (1970).

27. R.F. Farmanand, R.B. Beckmann, "Entrance Region Heat Transfer in An Annulus", American Inst. C. Engg., 63, (1967).

28. H. Reichardt, "Vollstandige Darstellung der Turbulenten Geschwindigkeitsverteilung in Glatten Leitungen", ZAMM 31, 208-219 (1951).

29. R. Jenkins, "Heat Transfer Fluid Mech.", Inst. Stanford University Press, Stanford, Calif., p. 147, (1951).

30. R.G. Deissler, "Investigation of Turbulent Flow and Heat Transfer in Smooth Tubes", Including the Effects of Variable Fluid Properties", Trans. ASME, 73, 101-107 (1951).

31. W. H. Corcoran, F. Page, Jr., W. G. Shlinger and B. H. Sage, "Temperature Gradients in Turbulent Gas Streams", Industrial and Eng. Chem., 44 (1952).

32. C.J. Lawn, "Turbulent Heat Transfer at Low Reynolds Numbers", J. of Heat Transfer, Trans. ASME, 532-536, Nov. (1969).

33. R.G. Deissler, "Turbulent Heat Transfer and Friction in the Entrance Regions of Smooth Passages", Trans. ASME, 88, 1221-1223 (1955).

34. F.J. Edwards and N. Sheriff, "International Developments in Heat Transfer", Conf. Int. Developments in Heat Transfer, Vol. 2, pp. 415-425, ASME, (1961).

35. V. Kaul and M. Von Kiss, "Forced Convection Heat Transfer and Pressure Drop in Artificially Roughened Flow Passages", Neue Technik 6:297. (1964).

36. W. Nunner, "Versuchsauswertung and Ergebnisse", VDI Forschungsheft 455, B22:5, (1956) (AERE Lib./Trans. 786).

37. V. Kolar, "Heat Transfer in Turbulent Flow of Fluids Through Smooth and Rough Tubes", Int. J. Heat Mass Transfer, V. 8 pp. 639-653, (1965).

38. D.F. Dipprey and R.H. Sabersky, "Heat and Momentum Transfer in Smooth and Rough Tubes at Various Prandtl Numbers", Int. J. Heat Mass Transfer, V. 6, pp. 329-353, (1963).

39. J. O. HInze, "Turbulence", McGraw-Hill, Chapter I, (1959).

40. L. Prandtl, "Uber Flussigkeitsbewegung bei Sehr Kleiner Reibung", Proc. of the Third Inter. Math. Congr., Heidelberg (1904).

41. W.M. Kays, "Convective Heat and Mass Transfer", McGraw-Hill, (1966).

42. Y. Lee, "Turbulent Flow and Heat Transfer in Concentric and Eccentric Annuli", Ph.D. Thesis, Univ. of Liverpool, (1964).

43. T. Von Karman, "Uber Laminer und Turbulente Reibung", ZAMM, pp. 233-253, (1912).

44. J. M. Kay, "Fluid Mechanics and Heat Transfer", Camb. Univ. Press, London, (1957).

45. J. Bussinesq, "Théorie de l'écoulement Tourbillant", MéM. Prés. Acad. Sci. XXIII, 46, Paris quoted from (1) Chapter 19, (1877).

46. S. D. Park and Y. Lee, "Diabatic Turbulent Flow in the Entrance Region of Concentric Annuli", EIC, V. 14, n. B-3, (1971).

47. A. A. Townsend, "Equilibrium Layers and Wall Turbulence", J. Fluid Mech., V. 11, pp. 97-120, (1961).

48. B. Kjellstrom and S. Hedberg, "On Shear Stress Distributions for Flow in Smooth and Partially Rough Annuli", Aktiebolaget Atomenergi AE-243, Sweden, (1966).

49. T. von Karman, "The Analogy Betweem Fluid Friction and Heat TRansfer", Trans. ASME 61, p. 705, (1939).

50 E. R. Van Driest, "On Turbulent Flow Near a Wall", J. of Aero. Sci., V. 23, p. 1007, (1956).

51. W. D. Rannie, "Heat Transfer in Turbulent Shear Flow", J. of Aero. Sci., V. 23, p. 485, (1956).

52. D. V. Spalding, "Single Formula for the Law of the Wall", J. of Appl. Mech., ASME, V. 28, pp. 455-458, (1961).

53. D. T. Wasan, C. L. Tien and C. R. Wilkie, "Theoretical Correlation of Velocity and Eddy Viscosity for Flow Close to a Pipe Wall", J. of A.I.ch. E., V.9, p. 567, (1963).

54. K. Hanjalic, "Two-Dimensional Asymmetric Turbulent Flow in Ducts", Ph.D. Thesis, Univ. of London (1970).

55. R. L. Simpson, "A Generalized Correlation of Roughness Density Effects on the Turbulent Boundary Layer", AIAA J., V.2, pp. 242-244, (1973).

56. F. H. Clauser, "Turbulent Boundary Layers in Adverse Pressure Gradients", J. of Aero. Sci. V.21, pp. 91-108, (1954).

57. F. R. Hama, "Boundary Layer Characteristics for Smooth and Rough Surface", Trans. of Soc. of Naval Arch. and Marine Eng., V.62, pp. 333-358, (1954).

58. A. F. Perry and P. N. Joubert, "Rough Wall Boundary Layer in Adverse Pressure Gradietns", J. of Fluid Mech., V.17, pp. 193-211, (1963).

59. J. Wu. "Flow in Turbulent Wall Layer Over Uniform Roughness", J. of Appl. Mech., V.40, pp. 863-867, (1973).

60. L. Prandtl: Z. Angew, Math. U. Mech. 5: 136 (1952); see also NACATM 1231, (1949).

61. H. Barrow, "Semi-Theoretical Solution of Asymmetric Heat Transfer in Annular Flow", J. of Mech. Eng. Sci., 2, pp. 331-336, (1960).

62. K. Hanjalic and B. E. Launder, "Fully Developed Asymmetric Flow in a Plane Channel", J. Fluid Mech., JI, pp. 301-335, (1972).

63. Y. Lee, M. A. Bhuiyan and R. M. Labib, "Asymmetric Turbulent Fluid Flow Induced by Square Ribbed Surface Roughness", 7th CANCAM Conf., Sherbrooke, (1979).

64. H. Famf amd G. Feurstein, "War,eibergamg amd Druckverlust an Ringspaltstromung", 4th Int. Heat Transfer Conf., FC5.3, Paris (1970).

65. F. Williams and J. Watts, "The Development of Rough Surface with Improved Heat Transfer Performance and a Study of the Mechanisms Involved", 4th Int. Heat Transfer Conf., FC5.5, Paris (1970).

66. M. Tenneks and J. L. Lumley, "A First Course in Turbulence", The M.I.T., Cambridge, Massachusetts, and London, England (1972).

67. H. Barrow and Y. Lee, "Heat Transfer with Unsymmetrical Thermal Boundary Conditions", Int. J. Heat Mass Transfer, 7, 580. (1964).

68. P. R. Owen and W. R. Thomson, "Heat Transfer Across Rough Surfaces", JFM. 15, pp. 321-334, (1943).

69. D. F. Dippery and R. H. Sabersky, "Heat and Momentum Transfer in Smooth and Rough Tubes at Various Prandtl Numbers", Int. J. Heat Mass Transfer, 6, pp. 329-35[illegible] (1963).

70. R. A. Gowen and J. W. Smith, "Turbulent Heat Transfer from Smooth and Rough Surfaces", Int. J. of Heat Mass Transfer, 11, pp. 1657-1674, (1969).

APPENDIX 1

Derivation of Integral Equation

A.1.1 Middle portion

continuity equation (from figure 3.1 a):

$$(S - \delta_r - \delta_s) \frac{du_\infty}{dx} = v_{\delta_r} + v_{\delta_s} \qquad \text{(A.1.1)}$$

Momentum equation:

$$(S - \delta_r - \delta_s)\, dp + d(\rho u_\infty^2)(S - \delta_r - \delta_s)$$

$$= \rho (u_\infty v_{\delta_r} dx + u_\infty v_{\delta_s} dx)$$

$$(S - \delta_r - \delta_s) \frac{d}{dx} (p + \rho u_\infty^2 = \rho u_\infty (v_{\delta_r} + v_{\delta_s})$$

Using continuity equation (A.1.1)

$$(S - \delta_r - \delta_s)\left[\frac{dp}{dx} + 2 \rho u_\infty \frac{du_\infty}{dx}\right]$$

$$= (S - \delta_r - \delta_s)\, \rho u_\infty \frac{du_\infty}{dx}$$

$$dp = - \rho u_\infty du_\infty \qquad \text{(A.1..2)}$$

A.1.2 Rough side

continuity equation

$$\frac{d}{dx} \int_{Z_{or}}^{\delta_r} \rho u_r \, dy_r = - \rho v_{\delta_r} \qquad \text{(A.1.3)}$$

Momentum equation:

$$\tau_w dx + (\delta_r - Z_{or})\, dP = - d \int_{Z_{or}}^{\delta_r} \rho u_r^2 \, dy_r - u_{\delta_r} \rho v_{\delta_r} dx$$

Using continuity equation (A.1.3) and

$$u_{\delta_r} = u_\infty$$

and also assuming $Z_{or} << \delta_r$

$$\tau_{wr} = - \delta_r \frac{dP}{dx} - \frac{d}{dx} \int_{Z_{or}}^{\delta_r} \rho u_r^2 \, dy_r + \rho u_\infty \frac{d}{dx} \int_{Z_{or}}^{\delta_r} u_r \, dy_r \qquad (A.1.4)$$

A.1.3 Smooth side:

continuity equation

$$\frac{d}{dx} \int_0^{\delta_s} \rho \, u_s \, dy_s = - \rho \, v_{\delta_s} \qquad (A.1.5)$$

Momentum equation:

$$\tau_{ws} \, dx + \delta_s \, dP = - d \int_0^{\delta_s} \rho \, u_s^2 \, dy_s - u_{\delta_s} \rho v_{\delta_s} \, dx$$

Using continuity equation A.1.5 and

$$u_{\delta_s} = u_\infty$$

$$\tau_{ws} = - \delta_s \frac{dP}{dx} - \frac{d}{dx} \int_0^{\delta_s} \rho \, u_s^2 \, dy_s + \rho u_\infty \frac{d}{dx} \int_0^{\delta_s} u_s \, dy_s \qquad (A.1.6)$$

A.1.4 Adding equations A.1.1, A.1.3 and A.1.5 the continuity equation for whole channel becomes

$$\frac{d}{dx} \int_0^S u \, dy = 0$$

with the understanding that u is in three portions with corresponding upper and lower limits of validity in the channel.

APPENDIX 2

Derivation of fully developed region momentum equation from equation (3.23)

$$\frac{d}{dy}\left(\mu \frac{du}{dy} - \rho \overline{u'v'}\right) = \frac{dP}{dx}$$

Integrating once

$$\mu \frac{du}{dy} - \rho \overline{u'v'} = y \frac{dP}{dx} + c$$

Using the boundary condition

$$\text{at } y = 0;\ \overline{u'v'} = 0,\ \mu \frac{du}{dy} = \tau_w$$

$$\mu \frac{du}{dy} - \rho \overline{u'v'} = y \frac{dP}{dx} + \tau_w \qquad \text{(A.2.1)}$$

and using the other boundary condition

$$\text{at } y = y_o;\ \tau = \mu \frac{du}{dy} - \rho \overline{u'v'} = 0$$

$$\tau_w = - y_o \frac{dP}{dx} \qquad \text{(A.2.2)}$$

APPENDIX 3

Fully developed shear stress distribution

Substituting equation (3.24) into equation (A.2.1)

$$\tau = y \frac{dP}{dx} + \tau_w \qquad (A.3.1)$$

dividing by τ_w

$$\frac{\tau}{\tau_w} = \frac{y}{\tau_w} \frac{dP}{dx} + 1$$

Substituting the result from equation (A.2.2) into the right hand side and simplifying

$$\frac{\tau}{\tau_w} = 1 - \frac{y}{y_o} \qquad (A.3.2)$$

The relations (A.3.1) and (A.3.2) can be directly written down by a force balance on an infinitesimal fluid element of thickness dx and height y and y_o, respectively.

APPENDIX 4

Summary of relations between mean flow parameters

$$u_{\tau r} = \sqrt{\frac{\tau_{wr}}{\rho}} \qquad \text{(Definition)}$$

$$u_{\tau s} = \sqrt{\frac{\tau_{ws}}{\rho}} \qquad \text{(Definition)}$$

$$f_s = \frac{2\,\tau_{ws}}{\rho\,u_{av}^2} \qquad \text{(Definition)}$$

$$f_r = \frac{2\,\tau_{wr}}{\rho\,u_{av}^2} \qquad \text{(Definition)}$$

$$f = \frac{f_s + f_r}{2}$$

$$\tau_{wr} = -\,y_{or}\,\frac{dP}{dx} \qquad \text{(Appendix 2)}$$

$$\tau_{ws} = -\,y_{os}\,\frac{dP}{dx} \qquad \text{(Appendix 2)}$$

$$\tau_{wr} + \tau_{ws} = -\,s\,\frac{dP}{dx} \qquad \text{(Eq. 3.37)}$$

$$\frac{\tau_r}{\tau_{wr}} = \left(1 - \frac{y_r}{y_{or}}\right) \qquad \text{(Appendix 3)}$$

$$\frac{\tau_s}{\tau_{ws}} = \left(1 - \frac{y_s}{y_{os}}\right) \qquad \text{(Appendix 3)}$$

$$Re = \frac{u_{av}\,D_{hyd}}{\nu} \qquad \text{(Definition)}$$

$$Z_{or} = y_{mr}\,\exp\left[-\frac{u_{\tau s}}{u_{\tau r}}\left\{\ln\left(\frac{u_{\tau s}\,S}{\nu} - \frac{u_{\tau s}\,y_{mr}}{\nu}\right) + C\,K\right\}\right] \qquad \text{(Eq. 3.65)}$$

$$u_{av} = \frac{Q}{A} \qquad \text{(Definition)}$$

$$S = y_{or} + y_{os} \qquad \text{(Definition)}$$

$$m = \frac{Z_{or}}{\epsilon} \qquad \text{(Definition)}$$

$$\frac{y_{or}}{S} = 0.523\ Re^{0.033}\ (S/\epsilon)^{0.157}\ (P/\epsilon)^{0.158} - 0.25 \qquad \text{(Eq. 3.63)}$$

$$\frac{y_{mr}}{S} = 0.299\ Re^{0.066}\ (S/\epsilon)^{0.140}\ (P/\epsilon)^{0.201} \qquad \text{(Eq. 3.64)}$$

APPENDIX 5

Reynolds number Re in terms of mean flow parameters

$$u_{av} = \frac{\int udA}{A} = \frac{\int_0^{y_{ms}} u_s \, dA + \int_{Z_{or}}^{y_{mr}} u_r \, dA}{A} \qquad (A.5.1)$$

$$u_s = u_{\tau s} \left\{ \frac{1}{k} \ln \left(1 + k \frac{y u_{\tau s}}{\nu}\right) + 7.8 \left[1 - \exp\left(-\frac{y u_{\tau s}}{11\,\nu}\right) - \frac{y u_{\tau s}}{11\,\nu} \exp\left(-\frac{y u_{\tau s}}{3\,\nu}\right)\right]\right\}$$

$$u_r = u_{\tau r} \left(\frac{1}{k} \ln \frac{y}{Z_{or}}\right)$$

$$dA = 1 \, . \, dy$$

$$A = 1 \, . \, S$$

Substitution of the above quantities into Eq. (A.6.1) and integration gives:

$$u_{av} = \frac{\nu}{S} \left\{ \frac{1 + k y_{ms}^+}{k^2} \left[\ln \left(1 + k y_{ms}^+\right) - 1\right] + 7.8 \left[y_{ms}^+ - 11 \left\{1 - \exp\left(-\frac{y_{ms}^+}{11}\right)\right\} + \frac{9}{11}\left(1 + \frac{y_{ms}^+}{3}\right) \exp\left(-\frac{y_{ms}^+}{3}\right) - \frac{9}{11}\right] + \frac{y_{mr}^+}{k} \left[\ln y_{ms}^+ + ck - \frac{u_{\tau r}}{u_{\tau s}}\right] + \frac{Z_{or}^+}{k} \frac{u_{\tau r}}{u_{\tau s}}\right\} \qquad (A.5.2)$$

$$Re = \frac{2\,(1 + k\,y_{ms}^{+})}{k^2}\left[\ell n\,(1 + k y_{ms}^{+}) - 1\right]$$

$$+ 15.6\left\{y_{ms}^{+} - 11\,(1 - \exp\,(\frac{y_{ms}^{+}}{11}))\right.$$

$$\left. + \frac{9}{11}\,(1 + \frac{y_{ms}^{+}}{3})\,\exp\,(-\frac{y_{ms}^{+}}{3}) - \frac{9}{11}\right\}$$

$$+ 2\,\frac{y_{mr}^{++}}{k}\left[\ell n\,y_{ms}^{+} + ck - \frac{u_{\tau r}}{u_{\tau s}}\right]$$

$$+ 2\,\frac{Z_{or}^{++}}{k}\,\frac{u_{\tau r}}{u_{\tau s}} \qquad \text{(A.5.3)}$$

APPENDIX 6

Friction factor f in terms of mean flow parameters

$$\frac{\tau_{wr}}{\tau_{ws}} = \frac{y_{or}}{y_{os}} = \frac{y_{or}}{S-y_{or}} = \frac{1}{\frac{S}{y_{or}} - 1}$$

$$\frac{u_{\tau r}}{u_{\tau s}} = \frac{1}{\sqrt{\frac{S}{y_{or}} - 1}} = \frac{1}{D} \qquad \text{(A.6.1)}$$

$$f_r = \frac{2\,\tau_{wr}}{\rho\, u_{av}^2}$$

$$= 2\,\left(\frac{u_{\tau r}}{u_{av}}\right)^2$$

$$= \frac{2}{D^2}\,\left(\frac{u_{\tau s}}{u_{av}}\right)^2$$

$$f_s = \frac{2\,\tau_{ws}}{\rho\, u_{av}^2}$$

$$= 2\,\left(\frac{u_{\tau s}}{u_{av}}\right)^2 ,$$

Let $\Omega = \frac{u_{\tau s}}{u_{av}}$, then using Eq. A.6.2, Ω becomes

$\Omega = \frac{S^+}{E}$, where

$$E = \frac{1 + k\, y_{ms}^{+}}{k^2}\left[\ell n\,(1 + k y_{ms}^{+}) - 1\right] + 7.8$$

$$\left\{y_{ms}^{+} - 11\,(1 - \exp\,(-\frac{y_{ms}^{+}}{11})) + \frac{9}{11}\,(1 + \frac{y_{ms}^{+}}{3})\right.$$

$$\left.\exp\,(-\frac{y_{ms}^{+}}{3}) - \frac{9}{11}\right\}$$

$$+ \frac{1}{k}\left[y_{mr}^{+}\,(\ell n\, y_{ms}^{+} + ck - \frac{1}{D}) + \frac{Z_{or}^{+}}{D}\right]$$

$$y_{ms}^{+} = S^{+} - y_{mr}^{+}$$

and

$$f = \Omega^2\,(1 + \frac{1}{D^2}) = \frac{\tau}{\frac{1}{2}\,\rho u_{av}^{2}} \qquad \text{(A.6.2)}$$

APPENDIX 7

Energy integral equation

Applying the energy equation for the idealised model (from figure 3.1.b)

$$\int_{Z_{or}}^{\delta_{th}} u\, c\, \rho\, T\, dy)_{(1)} + q_w\, \delta_{th}\, x + \left[\int_{Z_{or}}^{\delta_{th}} u\, c\, \rho\, dy)_{(2)} - \int_{Z_{or}}^{\delta_{th}} u\, c\, \rho\, dy)_{(1)}\right] T_{\delta_{th}}$$

$$= \int_{Z_{or}}^{\delta_{th}} u\, c\, \rho\, T\, dy)_{(2)}$$

for small heat fluxes, the properties, c and ρ may be assumed to be constant.

$$q_w\, \delta_x = \rho\, c \left[-\int_{Z_{or}}^{\delta_{th}} u\,(T - T_{\delta_{th}}) + \int_{Z_{or}}^{\delta_{th}} u\,(T - T_{\delta_{th}})\right] dy$$

$$\therefore\ q_w\, \delta_x = \rho\, c\, \frac{d}{dx} \int_{Z_{or}}^{\delta_{th}} u\,(T - T_{\delta_{th}})\, dy\, dx$$

integrating once

$$q_w\, x = \rho\, c \int_{Z_{or}}^{\delta_{th}} u\,(T - T_{\delta_{th}})\, dy$$

introducing the nondimensional quantities yields

$$q_w\, x = \rho\, c \int_{Z_{or}}^{\delta_{th}^{++}} u^{++}\, u_{\tau r}\, \frac{q}{c}\, \frac{u_{\tau r}}{\tau_r}\, (T_{\delta_{th}}^{++} - T^{++})$$

$$dy_r^{++} \quad \frac{\nu}{u_{\tau r}}$$

$$x = \int_{Z_{or}}^{\delta_{th}^{++}} u^{++} \left(T_{\delta_{th}}^{++} - T^{++}\right) dy_r^{++} \quad \frac{\nu}{u_{\tau r}}$$

Dividing by s^{++}

$$\frac{x^{++}}{S^{++}} = \frac{1}{S^{++}} \int_{Z_{or}}^{\delta_{th}^{++}} u^{++} \left(T_{\delta_{th}}^{++} - T^{++}\right) dy_r^{++}$$

APPENDIX 8

Flowchart of theoretical calculations of friction factor and velocity profile.

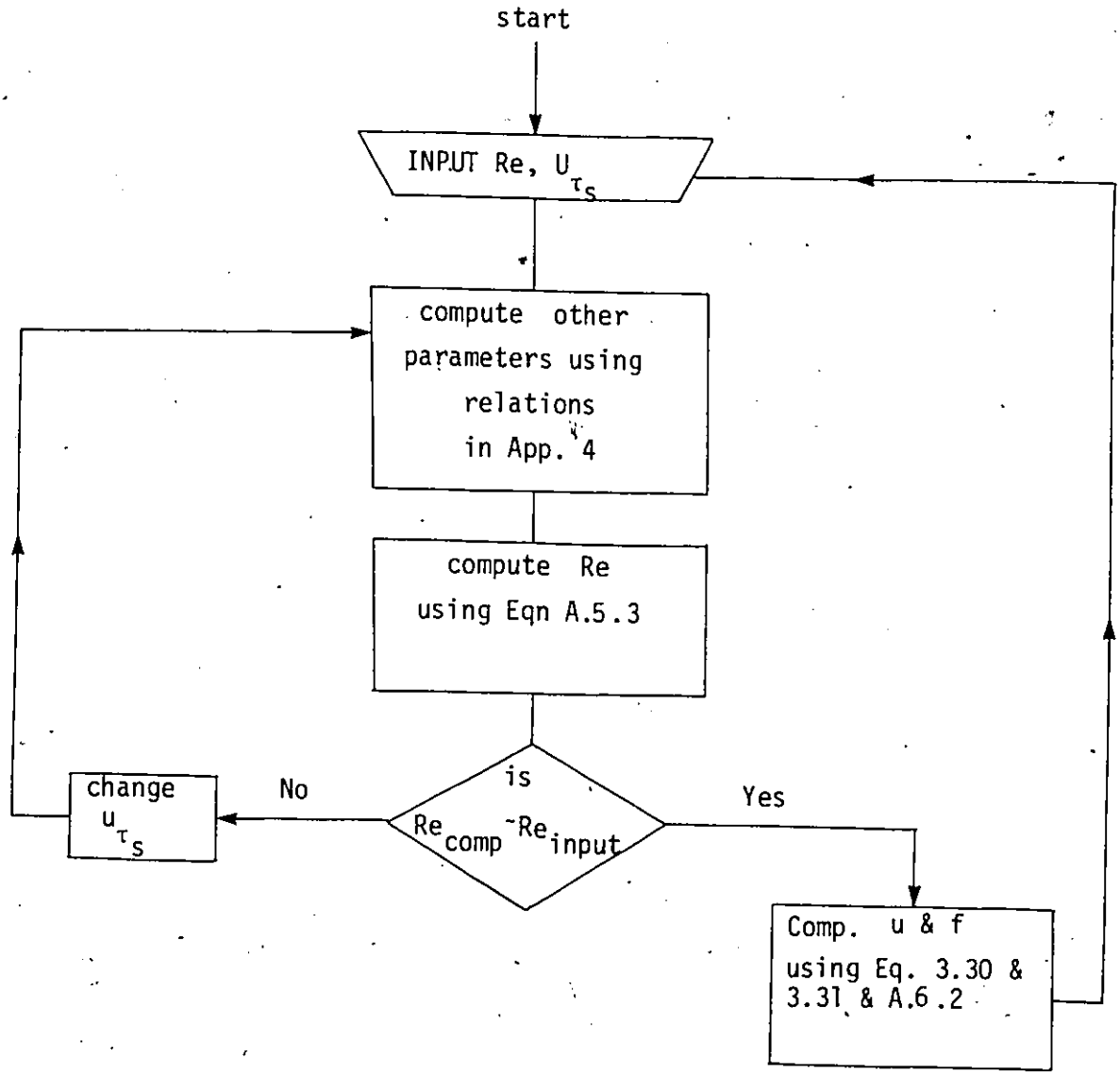

APPENDIX 9

Flowchart for calculation of temperature profile and Nusselt number.

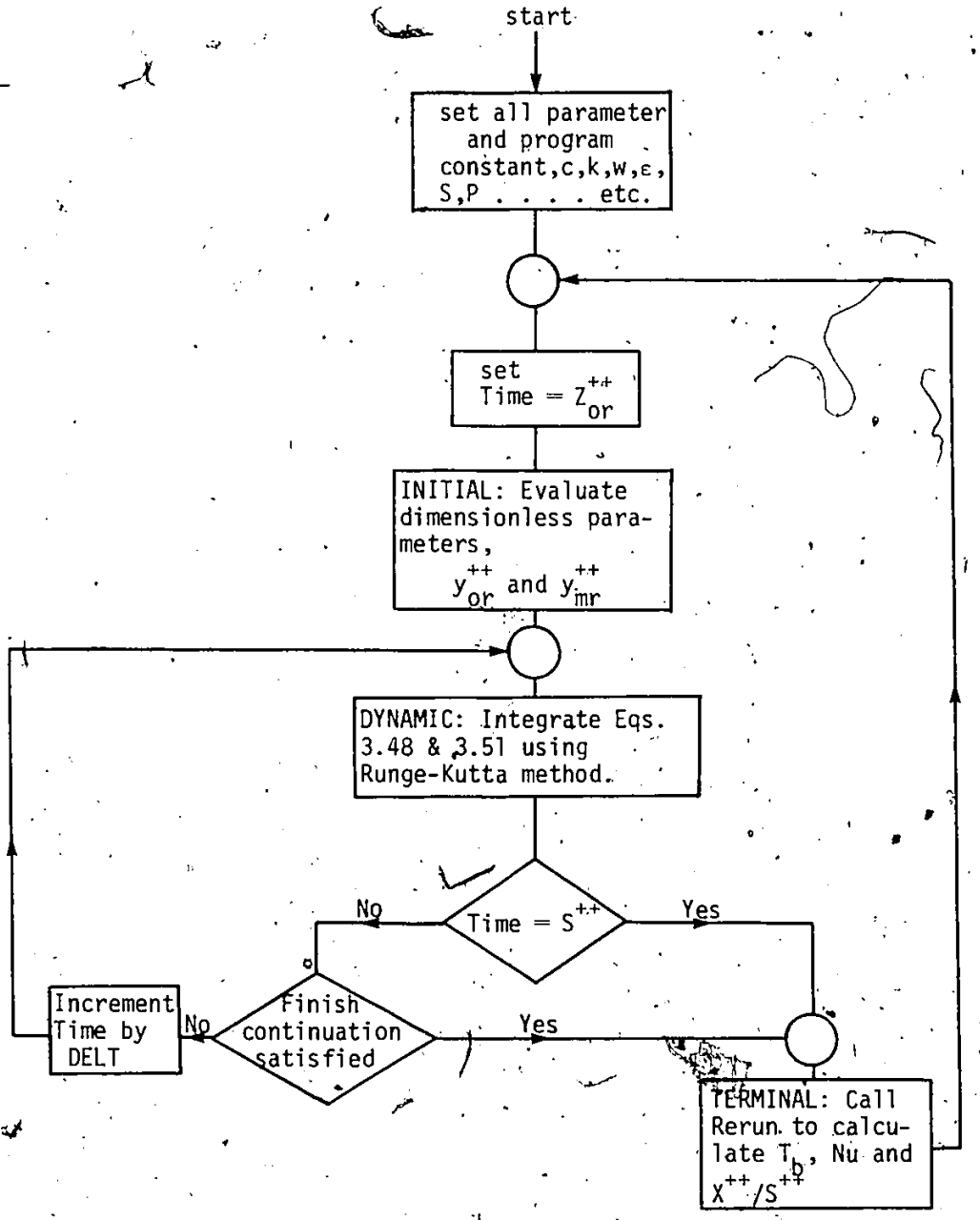

TABLE 3.1

Law of the Wall [3]

	Range	Equation
Prandtl & Taylor [40]	$0 < y^+ < 11.5$	$u^+ = y^+$
Von Karman [49]	$0 < y^+ < 5$	$u^+ = y^+$
	$5 < y^+ < 30$	$u^+ = 5 \ln y^+ - 3.05$
	$30 < y^+$	$u^+ = 2.5 \ln y^+ + 5.5$
Reichardt [28]	$0 < y^+$	$u^+ = 2.5 \ln(1 + 0.4 y^+) + 7.8[1-\exp(-y^+/11)-(y^+/11)\exp(-0.33y^+)]$
Deissler [4]	$0 < y^+ < 26$	$u^+ = \int_0^{y^+} \frac{dy^+}{1+(0.124)^2 u^+y^+[1-\exp(0.124)^2u^+y^+]}$
	$26 < y^+$	$u^+ = 2.78 \ln y^+ + 3.8$
Van Driest [50]	$0 < y^+$	$u^+ = \int_0^{y^+} \frac{2dy^+}{1+\{1+0.64\, y^{+2}[1-\exp(-y^+26)]^2\}^{1/2}}$
Ronnie [51]	$0 < y^+ < 27.5$	$u^+ = 14.54 \tanh(0.0688\, y^+)$
	$27.5 < y^+$	$u^+ = 2.5 \ln y^+ + 5.5$
Spalding [52]	$0 < y^+$	$y^+ = u^+ + 0.1108[\exp(0.4\, u^+) - 1 - 0.4\, u^+ - (0.4\, u^+)^2/2! - (0.4\, u^+)^3/3! - (0.4\, u^+)^4/4!]$
Wasan et al. [53]	$0 < y^+ < 20$	$u^+ = y^+ - 1.04\times10^{-4} (y^+)^4 + 3.03\times10^{-6} (y^+)^5$
	$80 < y^+$	$u^+ = 2.5 \ln y^+ + 5.5$

TABLE 3.2

Variation of C with y^+

y_s^+	C
1	1.01
4	0.55
9	2.35
15	4.00
25	4.94
35	5.38
54	5.58
81	5.58
100	5.57
121	5.55
144	5.55
195	5.54
255	5.53
324	5.53
361	5.52
400	5.52
484	5.52
576	5.52
676	5.52
900	5.52

TABLE 4.1 a

Fully Developed Nusselt Number and Thermal Entrance Length based on $(Nu_x/Nu_d) = 1.00$

$S/\varepsilon = 8.61$			$P/\varepsilon = 2.0$		$Re = 10.000$	
Pr	0.1		1.0		10.0	
δ_{th}^{++}	Nu_x	X^{++}/S^{++}	Nu_x	X^{++}/S^{++}	Nu_x	X^{++}/S^{++}
0.1	58.83	0.307	118.25	0.799	250.67	1.251
0.3	27.92	2.059	82.44	3.401	222.07	4.019
0.5	21.08	4.509	72.15	6.456	212.42	7.157
0.7	17.87	7.530	66.64	9.997	206.78	10.755
1.0	14.96	17.379	60.91	25.594	200.42	30.158

$S/\varepsilon = 8.61$			$P/\varepsilon = 2.0$		$Re = 50,000$	
Pr	0.1		1.0		10.0	
δ_{th}^{++}	Nu_x	x^{++}/S^{++}	Nu_x	x^{++}/S^{++}	Nu_x	x^{++}/S^{++}
0.1	100.02	0.637	340.49	0.922	1035.12	1.006
0.3	60.11	3.172	263.94	3.763	943.54	3.878
0.5	49.72	6.281	238.85	7.056	907.89	7.178
0.7	44.46	9.839	224.76	10.759	886.21	10.875
1.0	39.39	21.696	210.00	24.423	861.85	25.195

TABLE 4.1 a (continued)

$S/\varepsilon = 8.51$	$P/\varepsilon = 2.0$				$Re = 100.000$	
P_r	0.1		1.0		10.0	
δ_{th}^{++}	Nu_x	X^{++}/S^{++}	Nu_x	X^{++}/S^{++}	Nu_x	X^{++}/S^{++}
0.1	141.26	0.765	580.85	0.958	2115.68	0.994
0.3	92.21	3.505	462.91	3.872	1927.57	3.915
0.5	78.53	5.769	422.84	7.238	1852.97	7.265
0.7	71.38	10.430	400.02	10.975	1807.07	10.966
1.0	64.38	22.623	376.23	24.012	1756.24	24.360

$S/\varepsilon = 8.51$	$P/\varepsilon = 2.0$				$Pr = 0.72$	
Re	10,000		50,000		100,000	
δ_{th}^{++}	Nu_x	x^{++}/S^{++}	Nu_x	x^{++}/S^{++}	Nu_x	x^{++}/S^{++}
0.1	104.65	0.733	281.68	0.899	468.92	0.945
0.3	69.56	3.275	212.21	3.725	365.56	3.851
0.5	59.86	6.295	190.11	7.009	331.30	7.212
0.7	54.75	9.808	177.86	10.705	311.99	10.946
1.0	49.53	24.697	165.17	24.198	291.90	24.046

TABLE 4.1 b

Fully Developed Nusselt Number and Thermal Entrance Length Effect of Roughness Intensity (P/ε)

$S/\varepsilon = 8.51$	$Re = 50,000$				$Pr = 0.72$	
	$P/\varepsilon = 2$		$P/\varepsilon = 4$		$P/\varepsilon = 8$	
δ_{th}^{++}	Nu_x	x^{++}/S^{++}	Nu_x	x^{++}/S^{++}	Nu_x	x^{++}/S^{++}
0.1	281.68	0.899	480.91	0.455	1630.97	0.108
0.3	212.21	3.725	337.51	2.277	856.58	0.945
0.5	190.11	7.009	295.82	4.548	593.96	2.192
0.7	177.86	10.705	273.44	7.079	615.59	3.681
1.0	165.17	24.198	251.93	15.488	548.25	7.922

TABLE 4.1 c

Fully Developed Nusselt Number and Thermal Entrance Length Effect of Relative Height of Roughness (S/ε).

$P/\varepsilon = 2$	Re = 50,000						Pr = 0.72	
	$S/\varepsilon = 8.51$		$S/\varepsilon = 13.82$		$S/\varepsilon = 24.24$		$S/\varepsilon = 29.45$	
δ_{th}^{++}	Nu_x	x^{++}/S^{++}	Nu_x	x^{++}/S^{++}	Nu_x	x^{++}/S^{++}	Nu_x	x^{++}/S^{++}
0.1	281.68	0.899	277.40	0.925	270.43	0.960	267.38	0.974
0.3	212.21	3.725	209.21	3.806	204.49	3.915	202.47	3.957
0.5	190.11	7.009	187.52	7.146	183.44	7.329	181.72	7.400
0.7	177.86	10.705	176.50	10.754	171.77	11.161	170.21	11.263
1.0	165.17	24.198	163.00	24.559	159.66	25.033	158.25	25.215

TABLE 4.2

F/H Ratio Asymmetric Flow

$S/\epsilon = 8.61$ $Pr = 0.72$

Re	P/ε	Nu_r	Nu_s [67]	H (Nu_r/Nu_s)	f_r	f_s	F (f_r/f_s)	F/H
10,000	2	48.16	30.7	1.569	0.009304	0.0079	1.178	0.751
50,000	2	158.34	102	1.552	0.007026	0.0052804	1.330	0.857
100,000	2	276.82	175	1.582	0.006428	0.00421755	1.524	0.964
10,000	4	56.62	30.7	1.844	0.012825	0.0079	1.623	0.880
50,000	4	198.15	102	1.943	0.010267	0.0052804	1.944	1.001
100,000	4	352.65	175	2.015	0.009708	0.00421755	2.302	1.142
10,000	8	73.18	30.7	2.384	0.02104	0.0079	2.663	1.117
50,000	8	275.05	102	2.697	0.019299	0.0052804	3.655	1.355
100,000	8	511.30	175	2.922	0.01993	0.00421755	4.726	1.617

TABLE 4.2 (continued)

$S/\varepsilon = 13.82$ $Pr = 0.72$

Re	P/ε	Nu_r	Nu_s [67]	H (Nu_r/Nu_s)	f_r	f_s	F (f_r/f_s)	F/H
10,000	2	46.65	30.7	1.519	0.009122	0.0079	1.155	0.76
50,000	2	163.02	102	1.598	0.006892	0.0052804	1.304	0.816
100,000	2	273.20	175	1.561	0.0063020	0.00421755	1.494	0.957
10,000	4	55.67	30.7	1.814	0.0125	0.0079	1.582	0.872
50,000	4	194.91	102	1.911	0.0099870	0.0052804	1.891	0.989
100,000	4	346.64	175	1.981	0.009426	0.00421755	2.235	1.128
10,000	8	71.65	30.7	2.333	0.020241	0.0079	2.562	1.098
50,000	8	268.32	102	2.631	0.018395	0.0052804	3.484	1.324
100,000	8	494.96	175	2.840	0.018831	0.00421755	4.465	1.572

TABLE 4.2 (continued)

$S/\varepsilon = 24.24$ $Pr = 0.72$

Re	P/ε	Nu_r	Nu_s [67]	H (Nu_r/Nu_s)	f_r	f_s	F (f_r/f_s)	F/H
10,000	2	45.13	30.7	1.470	0.008868	0.0079	1.123	0.764
50,000	2	153.12	102	1.501	0.00671	0.0052804	1.270	0.846
100,000	2	267.88	175	1.531	0.006135	0.0042175	1.455	0.950
10,000	4	54.28	30.7	1.768	0.012065	0.0079	1.527	0.864
50,000	4	190.35	102	1.866	0.009636	0.0052804	1.825	0.978
100,000	4	338.55	175	1.934	0.009081	0.0042175	2.153	1.110
10,000	8	69.54	30.7	2.265	0.019267	0.0079	2.439	1.070
50,000	8	259.93	102	2.548	0.017389	0.0052804	3.293	1.290
100,000	8	479.96	175	2.743	0.017676	0.0042175	4.191	1.528

TABLE 4.2 (continued)

$S/\varepsilon = 29.45$ $Pr = 0.72$

Re	P/ε	Nu_r	Nu_s [67]	H (Nu_r/Nu_s)	f_r	f_s	F (f_r/f_s)	F/H
10,000	2	44.67	30.7	1.455	0.008763	0.0079	1.109	0.762
50,000	2	151.80	102	1.489	0.006638	0.0052804	1.256	0.844
100,000	2	265.63	175	1.518	0.00607	0.00421755	1.439	0.948
10,000	4	53.68	30.7	1.749	0.011895	0.0079	1.506	0.86
50,000	4	188.45	102	1.847	0.009505	0.0052804	1.800	0.974
100,000	4	335.19	175	1.915	0.008956	0.00421755	2.123	1.11
10,000	8	68.62	30.7	2.235	0.018922	0.0079	2.395	1.07
50,000	8	256.67	102	2.516	0.017044	0.0052804	3.228	1.28
100,000	8	473.67	175	2.707	0.017293	0.00421755	4.100	1.514

TABLE 4.3

F/H ratio Asymmetric Flow.

$S/\epsilon = 8.61$ $Pr = 10$

Re	P/ε	Nu_r	Nu_s [67]	H (Nu_r/Nu_s)	f_r	f_s	F (f_r/f_s)	F/H
10,000	2	179.79	89.4	2.010	0.009304	0.0079	1.178	0.586
50,000	2	703.55	360.0	1.954	0.007026	0.0052804	1.330	0.681
100,000	2	1320.63	668.0	1.977	0.006428	0.0042175	1,524	0.769
10,000	4	217.6	89.4	2.434	0.012825	0.0079	1.623	0.665
50,000	4	905.43	360.0	2.515	0.010267	0.0052804	1.944	0.771
100,000	4	1726.7	668.0	2.585	0.009708	0.0042175	2.302	0.890
10,000	8	296.27	89.4	3.314	0.02104	0.0079	2.663	0.804
50,000	8	1308.5	360.0	3.635	0.019299	0.0052804	3.655	1.004
100,000	8	2603.4	668.0	3.897	0.01993	0.0042175	4.726	1.213

TABLE 4.3 (continued)

$S/\epsilon = 13.82$ $Pr = 10$

Re	P/ϵ	Nu_r	Nu_s [67]	H (Nu_r/Nu_s)	f_r	f_s	F (f_r/f_s)	F/H
10,000	2	172.44	89.4	1.928	0.009122	0.0079	1.15	0.596
50,000	2	705.21	360.0	1.959	0.006892	0.0052804	1.30	0.664
100,000	2	1305.58	668.0	1.954	0.006302	0.0042175	1.49	0.763
10,000	4	214.39	89.4	2.398	0.0125	0.0079	1.58	0.659
50,000	4	891.93	360.0	2.478	0.009987	0.0052804	1.89	0.763
100,000	4	1699.4	668.0	2.544	0.009426	0.0042175	2.23	0.876
10,000	8	290.4	89.4	3.248	0.020241	0.0079	2.56	0.788
50,000	8	1276.7	360.0	3.546	0.018395	0.0052804	3.48	0.98
100,000	8	2529.9	668.0	3.787	0.018831	0.0042175	4.46	1.177

TABLE 4.3 (continued)

$S/\epsilon = 24.24$ $Pr = 10$

Re	P/ε	Nu_r	Nu_s [67]	H (Nu_r/Nu_s)	f_r	f_s	F (f_r/f_s)	F/H
10,000	2	169.02	89.40	1.891	0.008868	0.0079	1.12	0.592
50,000	2	684.85	360.0	1.902	0.00671	0.0052804	1.27	0.668
100,000	2	1285.5	668.0	1.924	0.006135	0.0042175	1.45	0.754
10,000	4	211.23	89.4	2.363	0.012065	0.0079	1.53	0.647
50,000	4	874.4	360.0	2.429	0.009636	0.0052804	1.82	0.749
100,000	4	1665.14	668.0	2.493	0.009081	0.0042175	2.15	0.862
10,000	8	273.94	89.4	3.064	0.019267	0.0079	2.44	0.796
50,000	8	1239.85	360.0	3.444	0.017389	0.0052804	3.29	0.955
100,000	8	2448.02	668.0	3.665	0.017676	0.0042175	4.19	1.144

TABLE 4.3 (continued)

$S/\epsilon = 29.45$ $Pr = 10$

Re	P/ε	Nu_r	Nu_s [67]	H (Nu_r/Nu_s)	f_r	f_s	F (f_r/f_s)	F/H
10,000	2	167.85	89.4	1.877	0.008763	0.0079	1.11	0.591
50,000	2	680.53	360.0	1.89	0.006638	0.0052804	1.26	0.666
100,000	2	1277.22	668.0	1.912	0.00607	0.0042175	1.44	0.753
10,000	4	209.52	89.4	2.344	0.011895	0.0079	1.51	0.644
50,000	4	867.45	360.0	2.41	0.009505	0.0052804	1.80	0.747
100,000	4	1651.62	668.0	2.472	0.008956	0.0042175	2.12	0.857
10,000	8	279.78	89.4	3.13	0.018922	0.0079	2.40	0.767
50,000	8	1226.18	360.0	3.406	0.017044	0.0052804	3.23	0.948
100,000	8	2419.02	668.0	3.621	0.017293	0.0042175	4.1	1.132

TABLE 4.4

F/H ratio asymmetric flow

$S/\varepsilon = 8.61$ $Pr = 30$

Re	P/ε	Nu_r	Nu_s [67]	H (Nu_r/Nu_s)	f_r	f_s	F (f_r/f_s)	F/H
10,000	2	233.43	127.0	1.838	0.009304	0.0079	1.18	0.642
50,000	2	931.54	532.0	1.751	0.007026	0.0052804	1.33	0.759
100,000	2	1783.92	1000.0	1.784	0.006428	0.0042175	1.52	0.852
10,000	4	284.31	127.0	2.239	0.012825	0.0079	1.62	0.724
50,000	4	1207.97	532.0	2.271	0.010267	0.0052804	1.94	0.854
100,000	4	2350.08	1000.0	2.350	0.009708	0.0042175	2.30	0.978
10,000	8	393.78	127.0	3.101	0.02104	0.0079	2.66	0.858
50,000	8	1765.88	532.0	3.319	0.019299	0.0052804	3.65	1.09
100,000	8	3585.32	1000.0	3.585	0.01993	0.0042175	4.73	1.319

TABLE 4.4 (continued)

$S/\varepsilon = 13.82$ $Pr = 30$

Re	P/ε	Nu_r	Nu_s [67]	H (Nu_r/Nu_s)	f_r	f_s	F (f_r/f_s)	F/H
10,000	2	223.36	127.0	1.759	0.009122	0.0079	1.15	0.654
50,000	2	927.0	532.0	1.743	0.006892	0.0052804	1.30	0.746
100,000	2	1764.55	1000.0	1.765	0.006302	0.0042175	1.49	0.844
10,000	4	280.27	127.0	2.207	0.0125	0.0079	1.58	0.716
50,000	4	1190.41	532.0	2.238	0.009987	0.0052804	1.89	0.844
100,000	4	2313.59	1000.0	2.314	0.009426	0.0042175	2.23	0.964
10,000	8	386.02	127.0	3.04	0.020241	0.0079	2.56	0.842
50,000	8	1723.12	532.0	3.239	0.018395	0.0052804	3.48	1.074
100,000	8	3483.86	1000.0	3.484	0.018831	0.0042175	4.48	1.285

TABLE 4.4 (continued)

$S/\varepsilon = 24:24$ $\quad$ $Pr = 30$

Re	P/ε	Nu_r	Nu_s [67]	H (Nu_r/Nu_s)	f_r	f_s	F (f_r/f_s)	F/H
10,000	2	219.60	127.0	1.729	0.008868	0.0079	1.15	0.665
50,000	2	908.37	532.0	1.707	0.00671	0.0052804	1.30	0.762
100,000	2	1739.23	1000.0	1.739	0.006135	0.0042175	1.49	0.859
10,000	4	279.12	127.0	2.198	0.012065	0.0079	1.58	0.719
50,000	4	1168.24	532.0	2.196	0.009636	0.0052804	1.89	0.860
100,000	4	2269.14	1000.0	2.269	0.009081	0.0042175	2.23	0.983
10,000	8	352.03	127.0	2.772	0.019267	0.0079	2.56	0.923
50,000	8	1674.58	532.0	3.148	0.017389	0.0052804	3.48	1.105
100,000	8	3373.09	1000.0	3.373	0.017676	0.0042175	4.48	1.330

TABLE 4.4 (continued)

$S/\epsilon = 29.45$ $Pr = 30$

Re	P/ε	Nu_r	Nu_s [67]	H (Nu_r/Nu_s)	f_r	f_s	F (f_r/f_s)	F/H
10,000	2	218.24	127.0	1.718	0.008763	0.0079	1.11	0.646
50,000	2	903.24	532.0	1.698	0.006638	0.0052804	1.26	0.742
100,000	2	1729.03	1000.0	1.729	0.00607	0.0042175	1.44	0.833
10,000	4	277.03	127.0	2.181	0.011895	0.0079	1.51	0.692
50,000	4	1159.64	532.0	2.18	0.009505	0.0052804	1.80	0.825
100,000	4	2251.93	1000.0	2.252	0.008956	0.0042175	2.12	0.941
10,000	8	372.5	127.0	2.933	0.018922	0.0079	2.40	0.818
50,000	8	1656.92	532.0	3.115	0.017044	0.0052804	3.21	0.995
100,000	8	3334.43	1000.0	3.334	0.017293	0.0042175	4.10	1.229

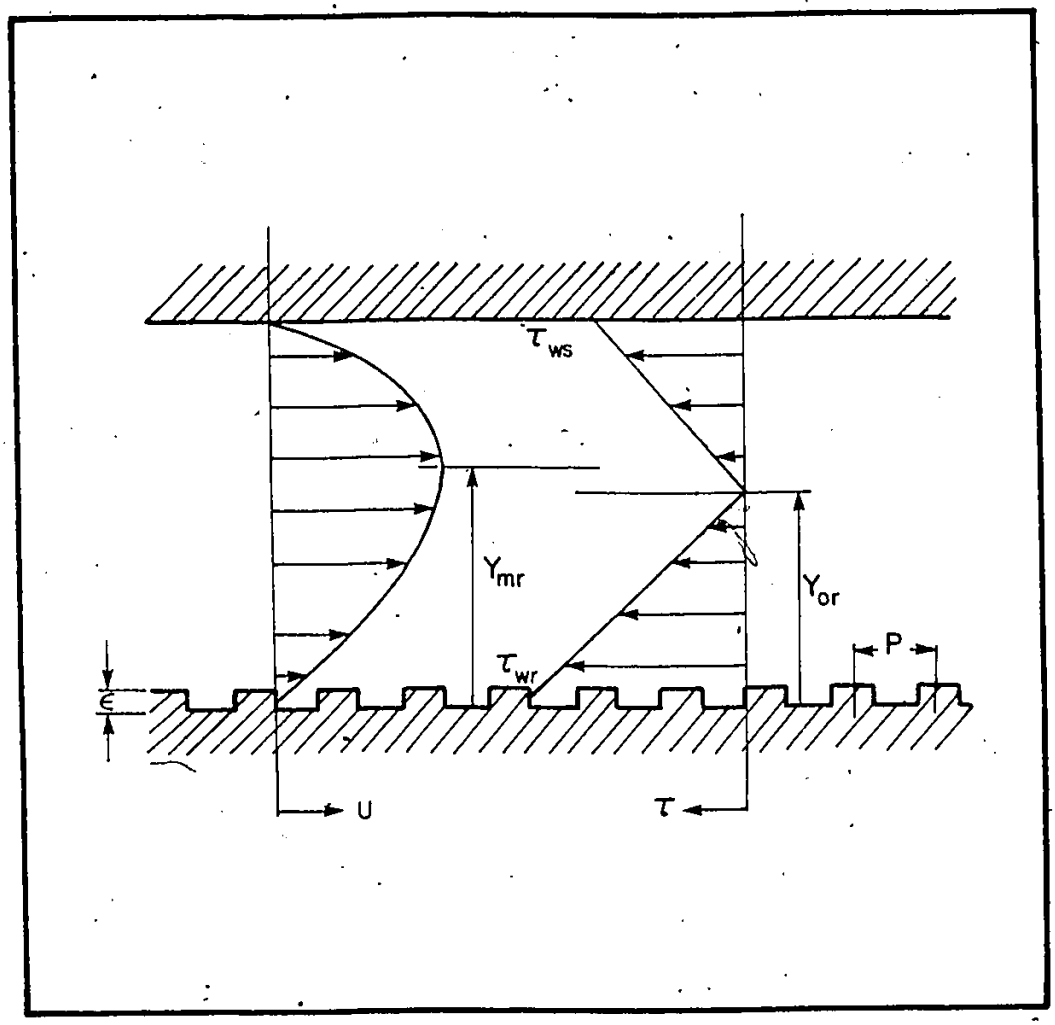

Fig. 3.1 Idealized Model

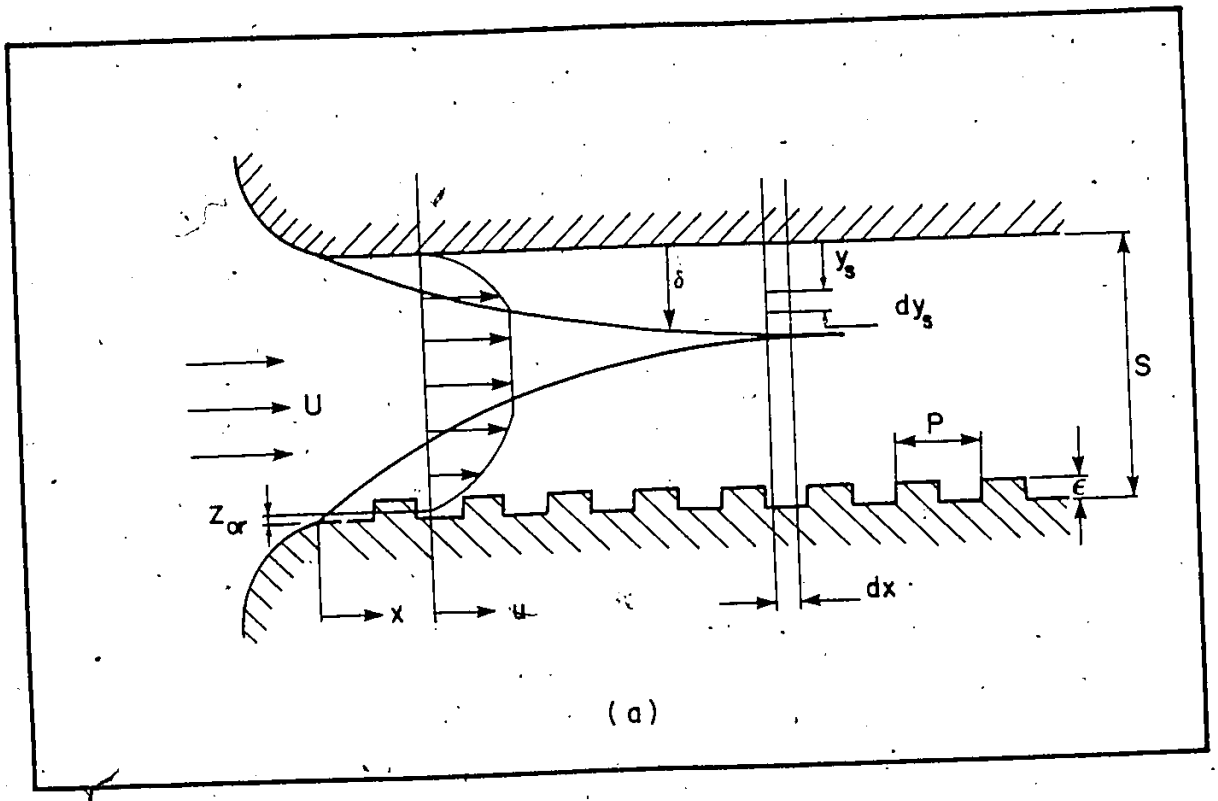

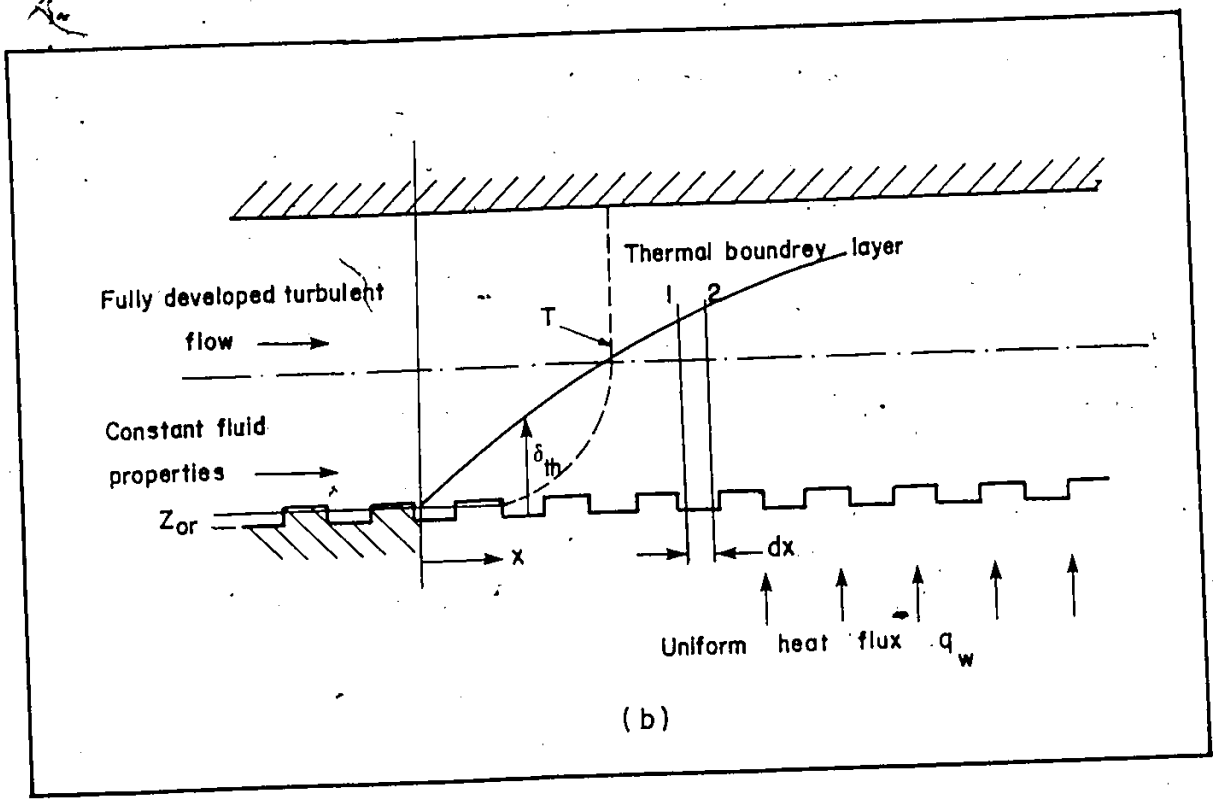

Fig. 3.2 Idealized Model.

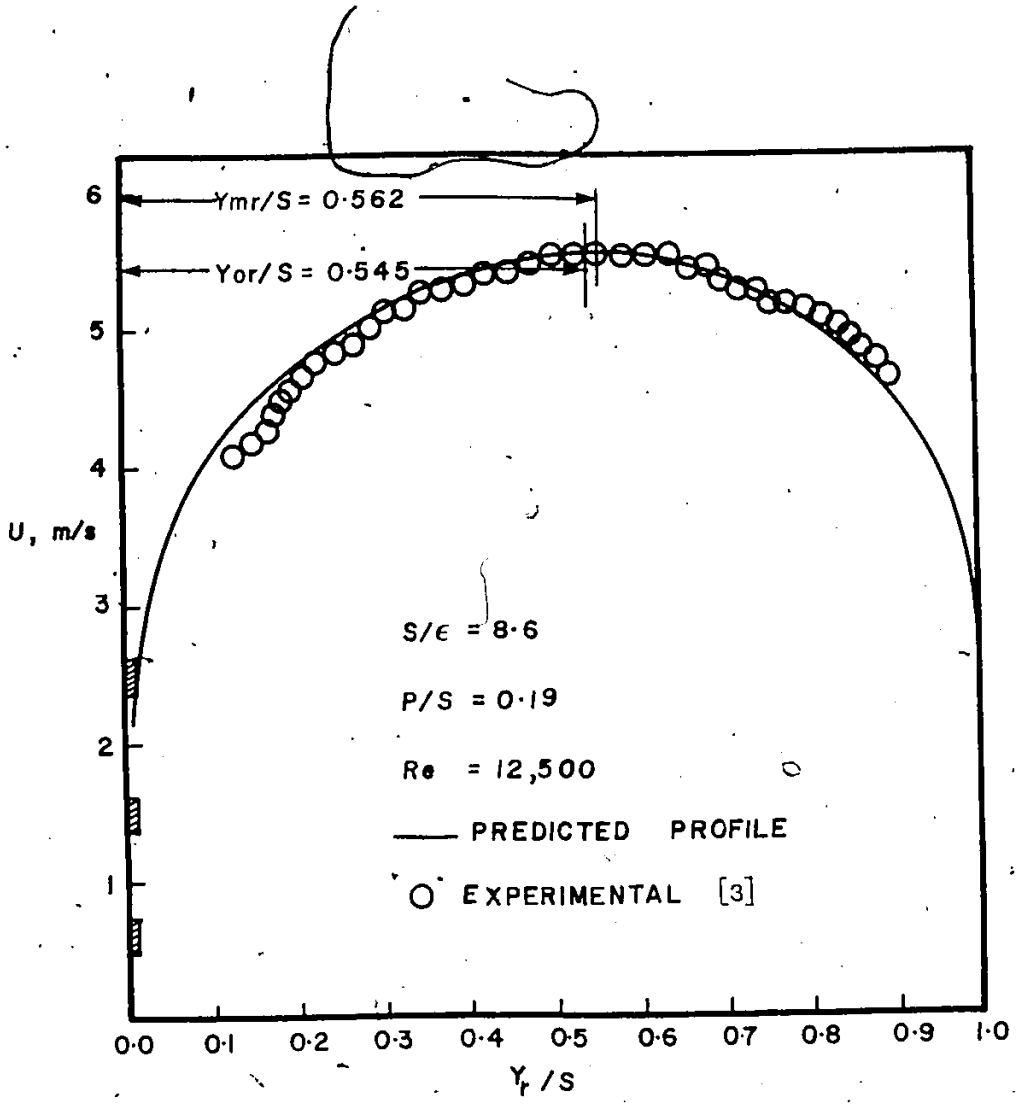

Fig. 4.1 Predicted Velocity Profile, Fully Developed Region

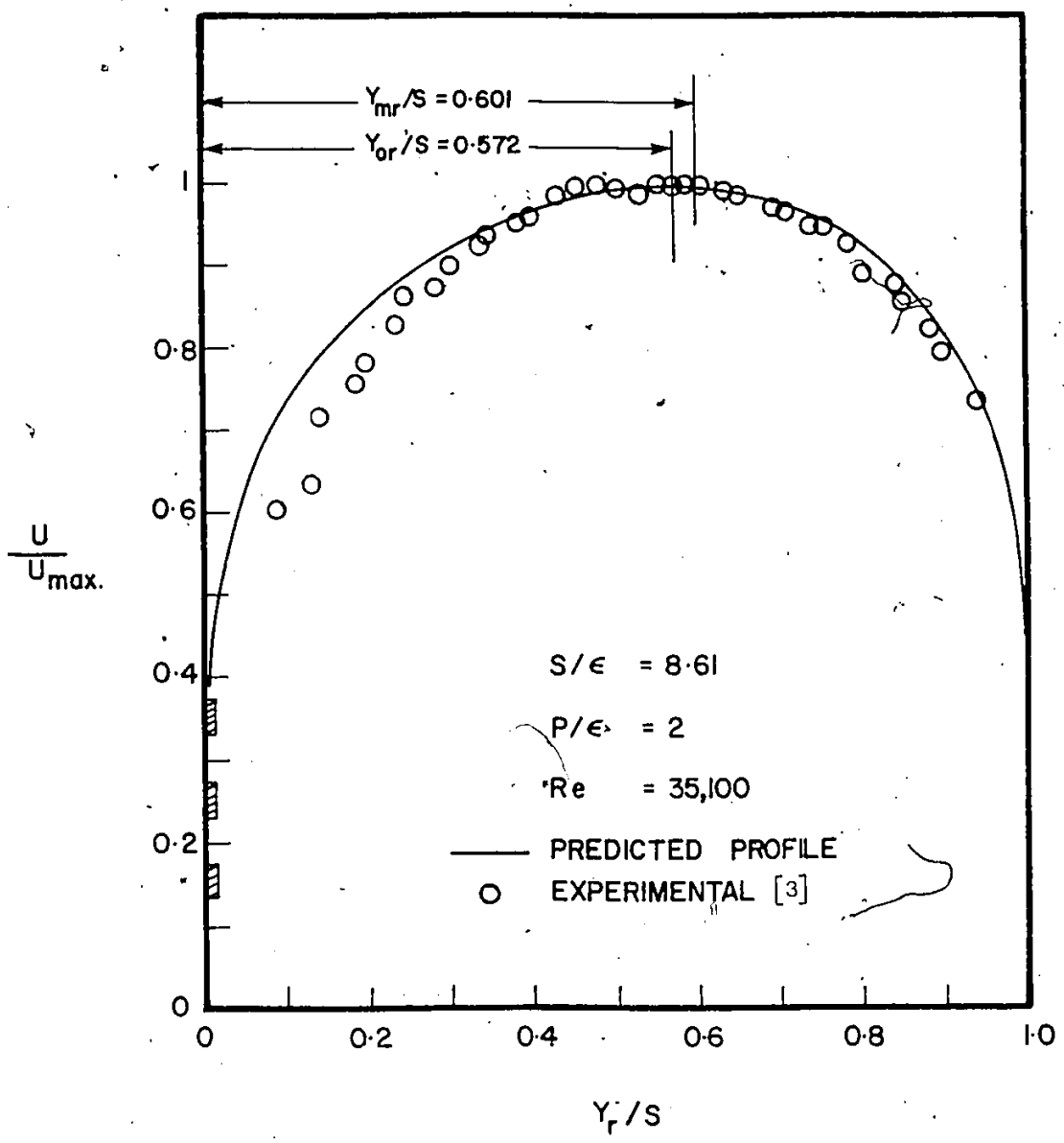

Fig. 4.2 Predicted Velocity Profile, Fully Developed Region

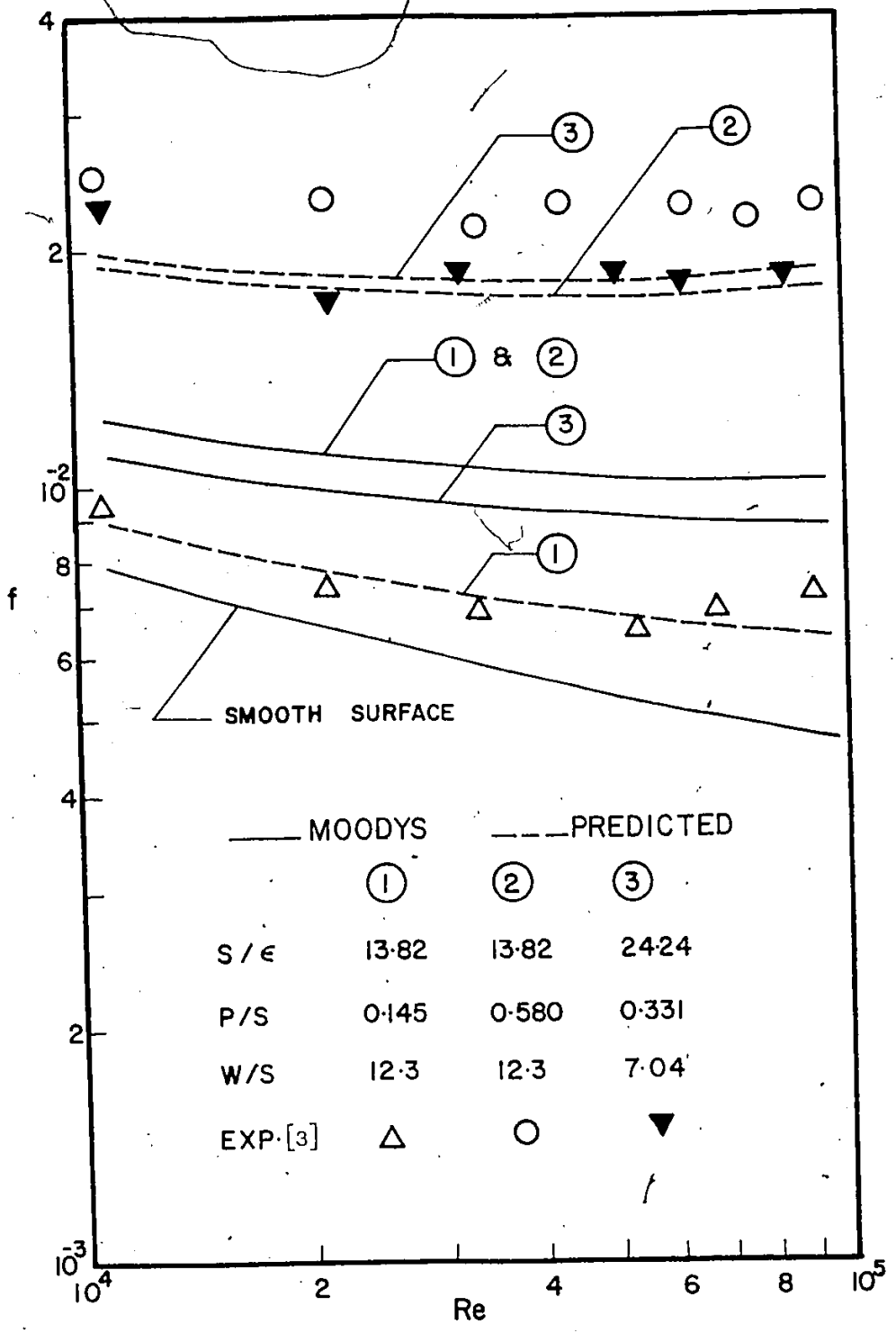

Fig. 4.3 Comparison of Experimental Results and Predicted Friction Factor

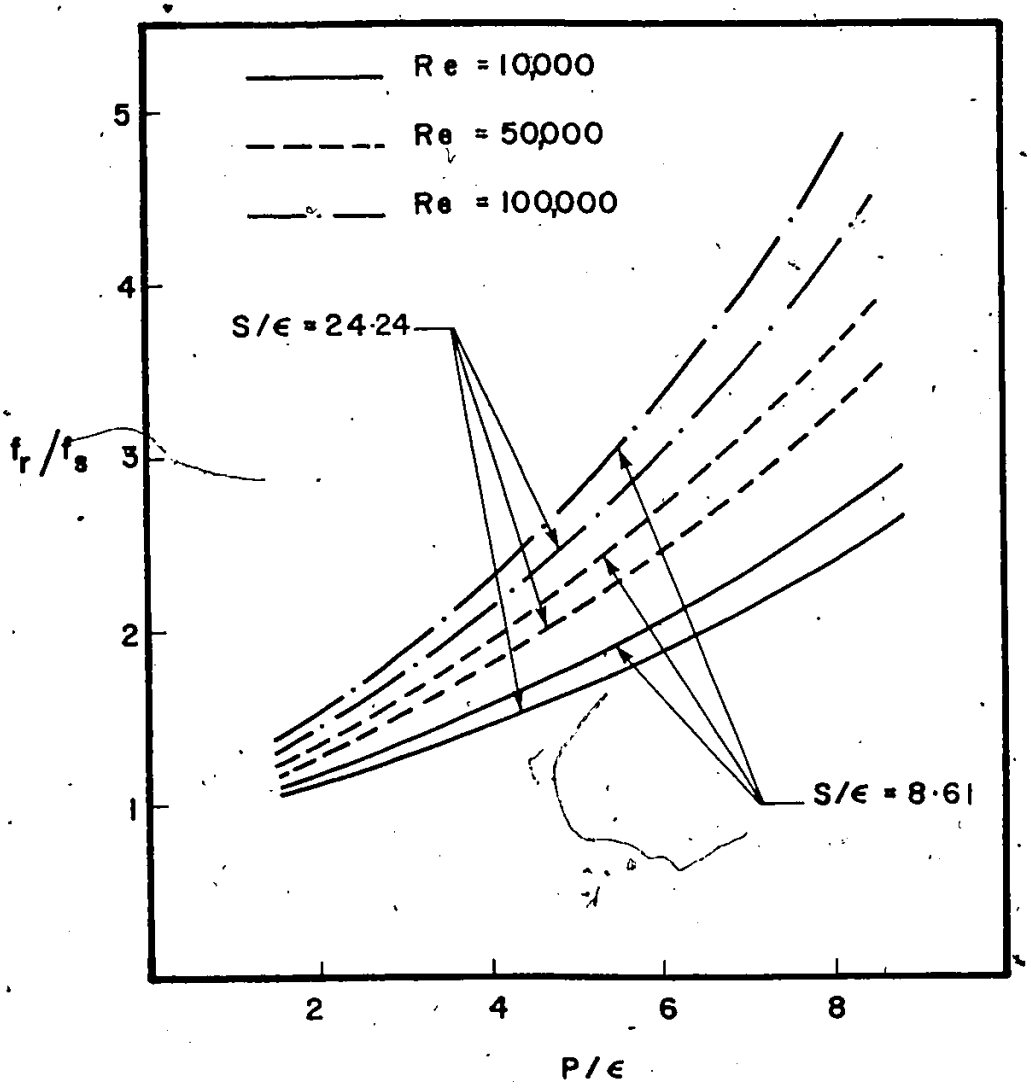

Fig. 4.4 Effect of Roughness Density on f_r/f_s

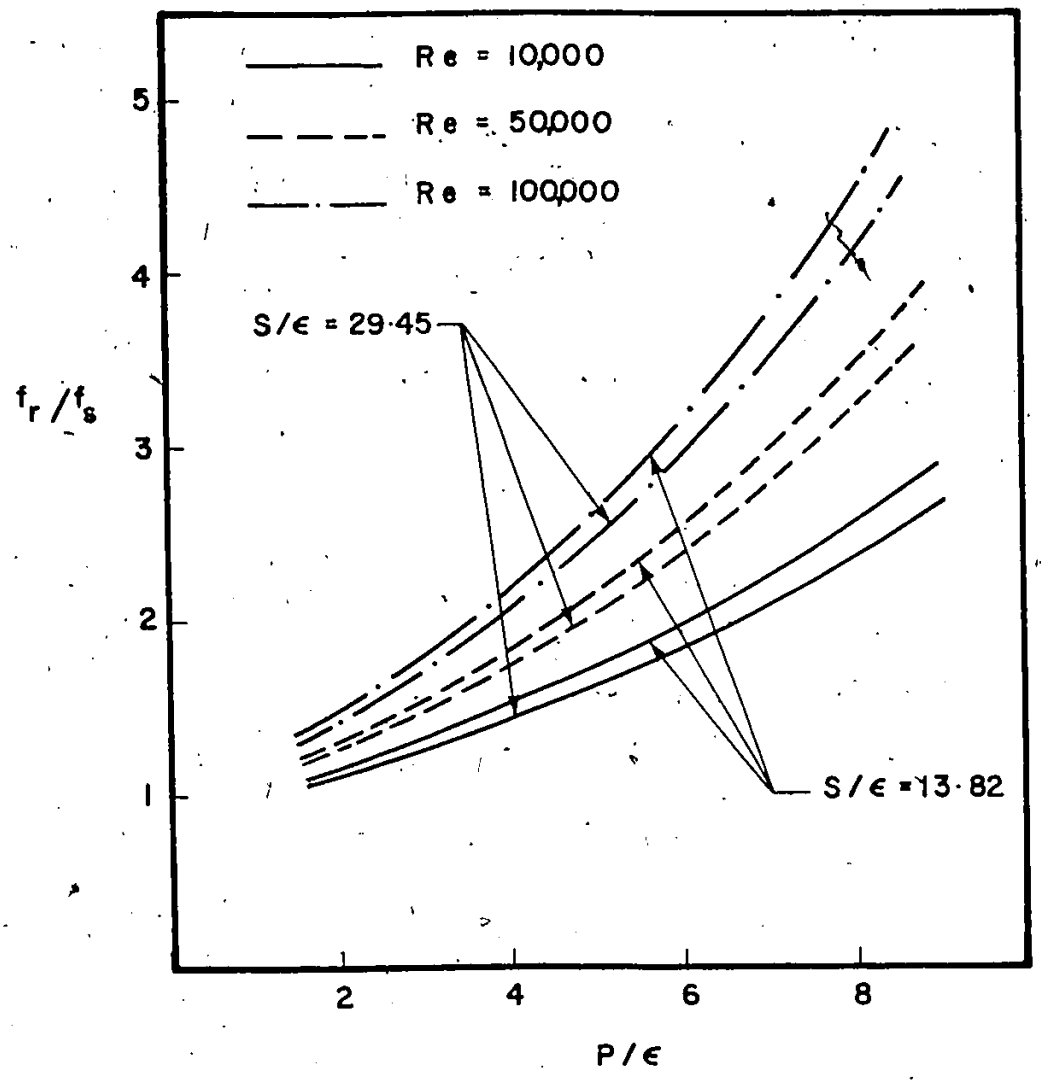

Fig. 4.5 Effect of Roughness Density on f_r/f_s

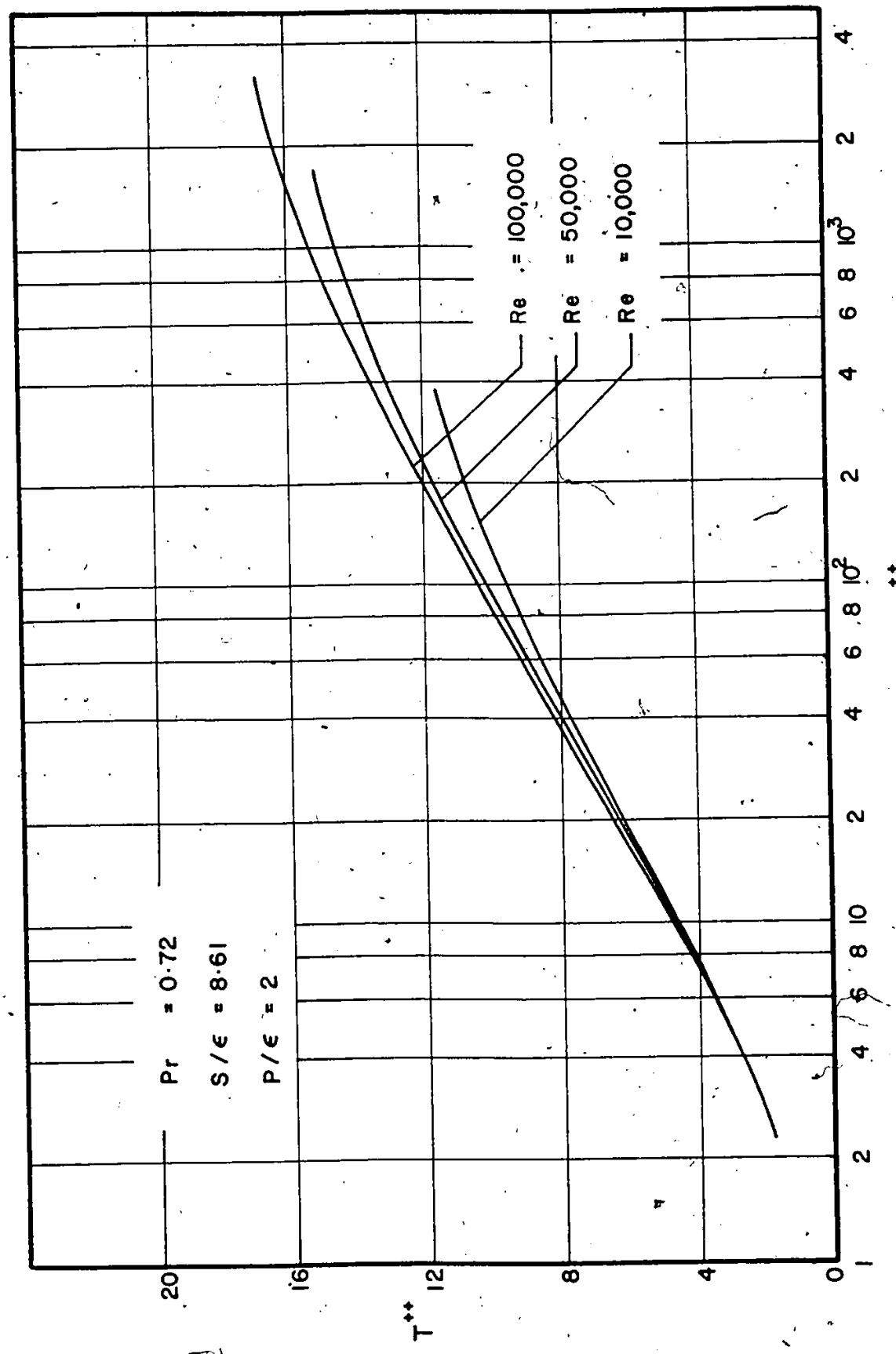

Fig. 4.5 Predicted Temperature Profiles

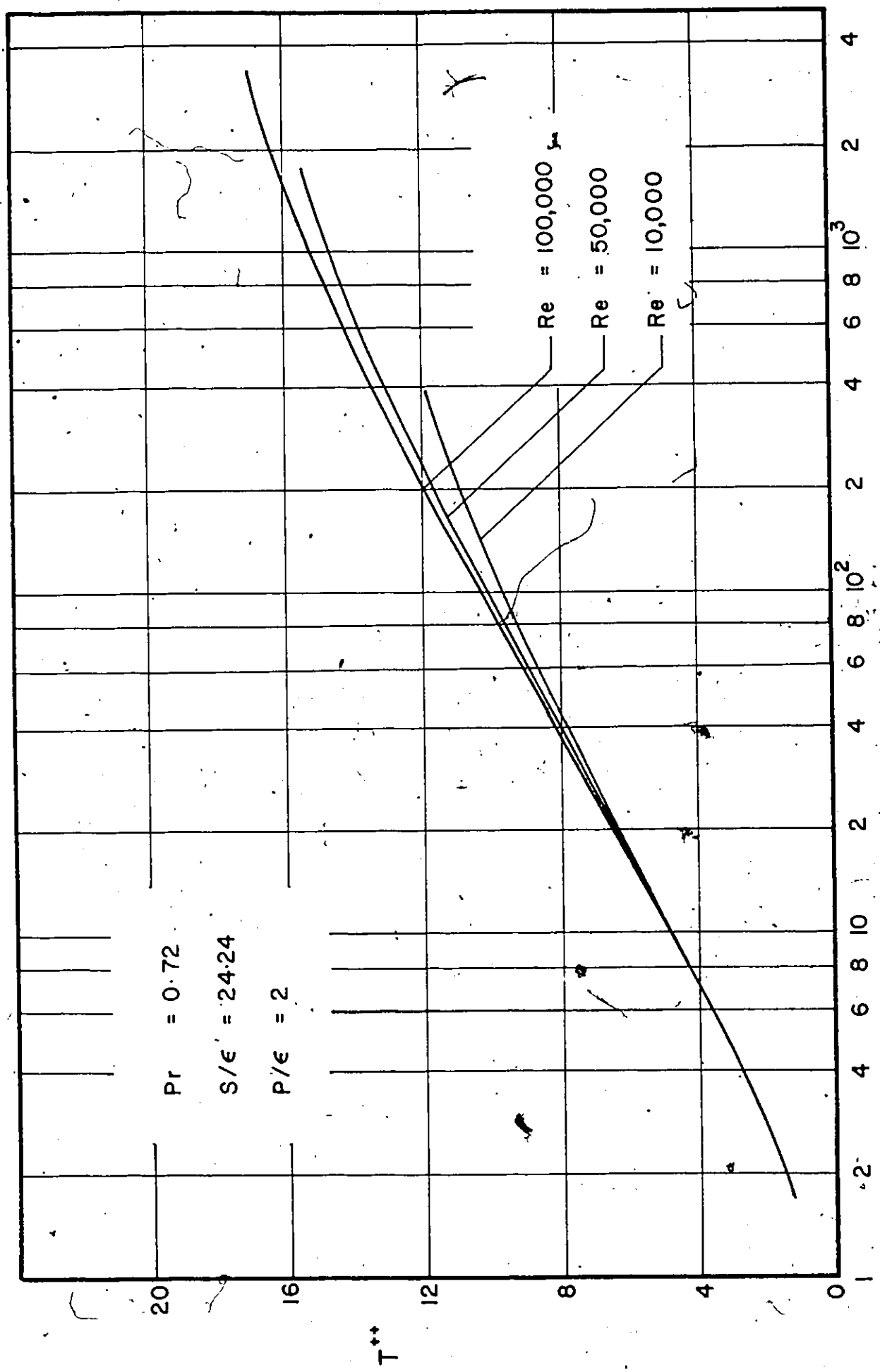

Fig. 4.7 Predicted Temperature Profile

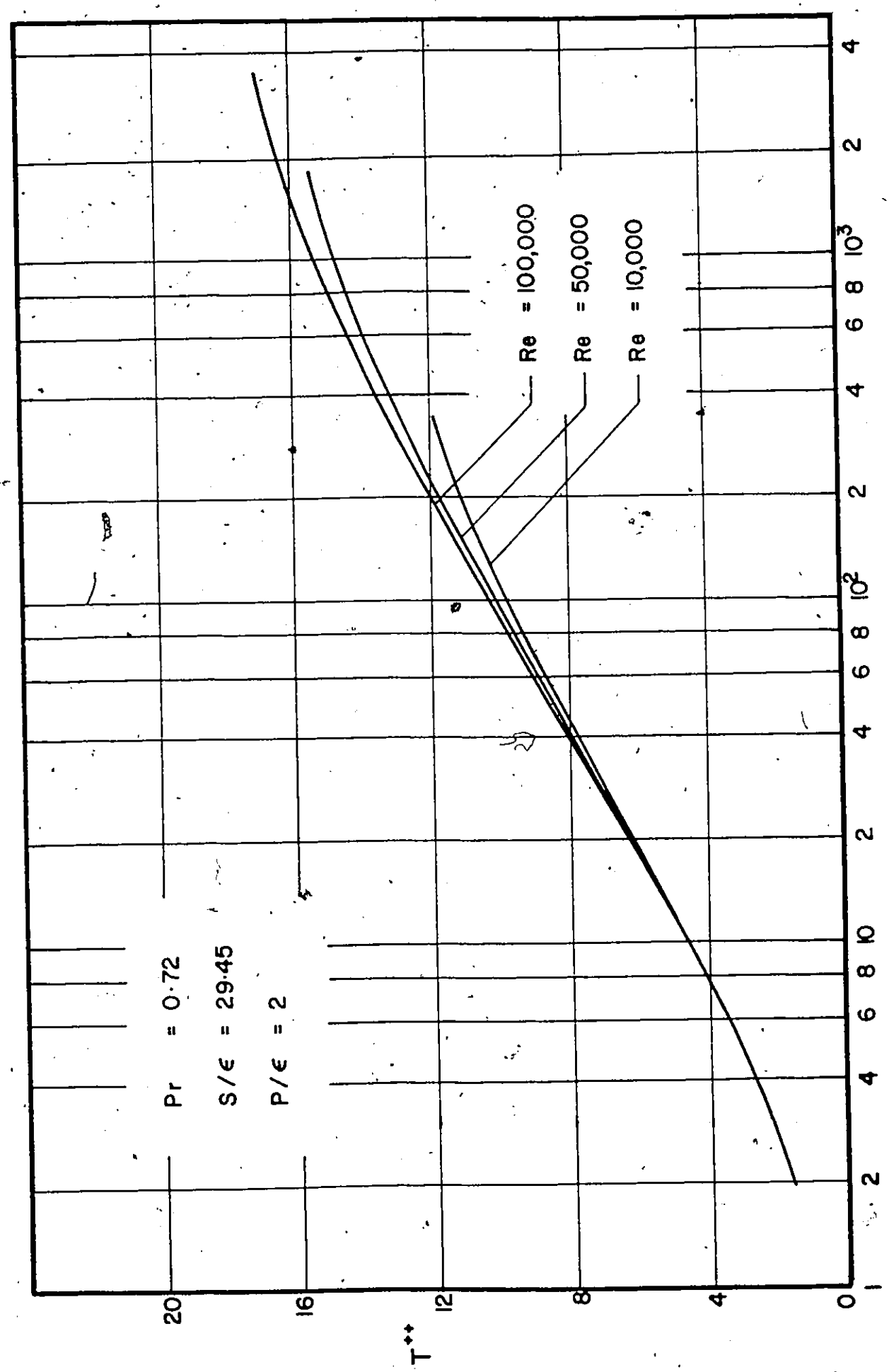

Fig. 4.8 Predicted Temperature Profiles

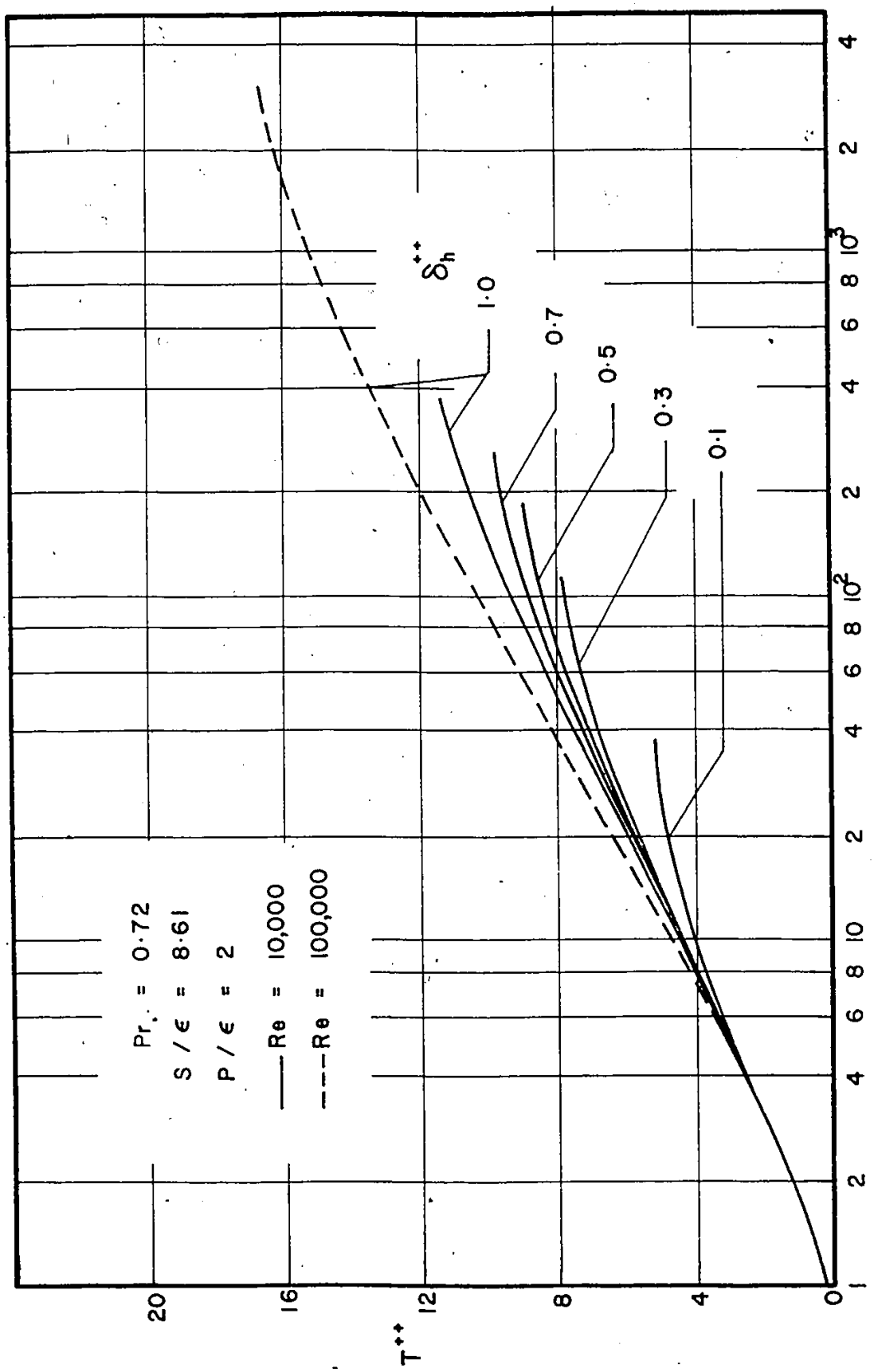

Fig. 4.10 Predicted Temperature Profiles, for Different Values of δ_{th}^{++}

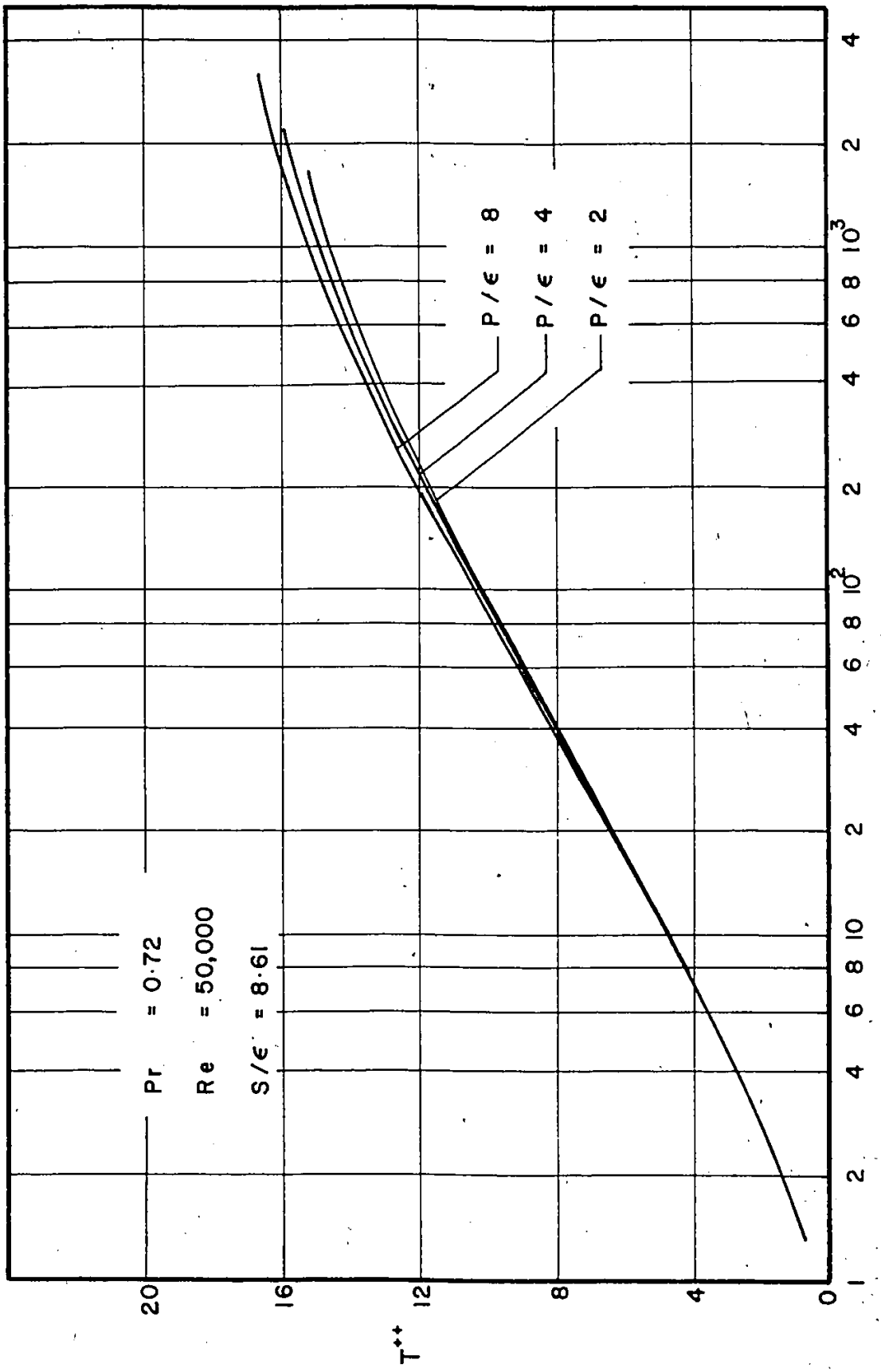

Fig. 4.9 Predicted Temperature Profiles, Effect of P/ε

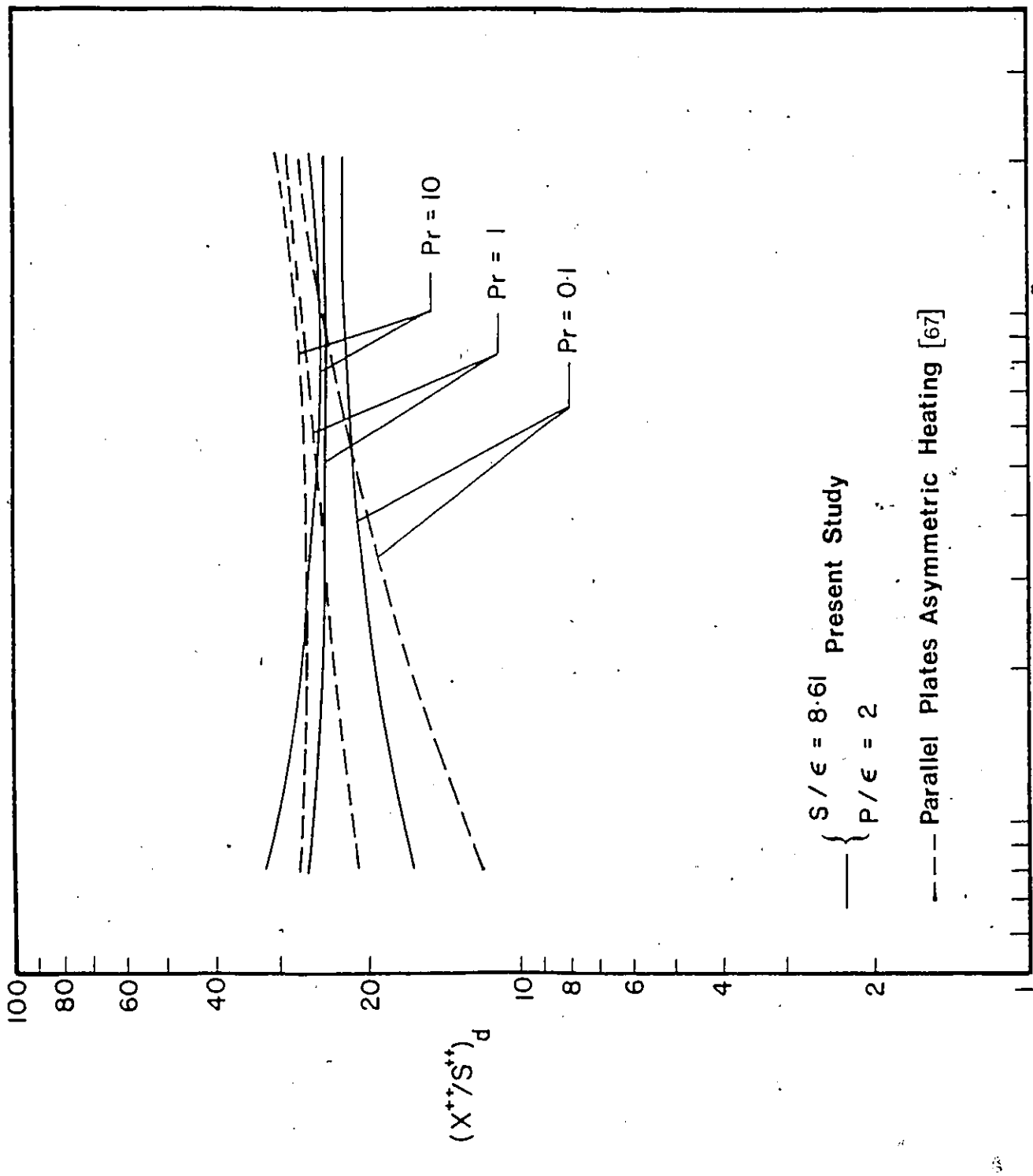

Fig. 4.11 Variation of Fully Developed Thermal Entrance Length vs. Re, Effect of Pr

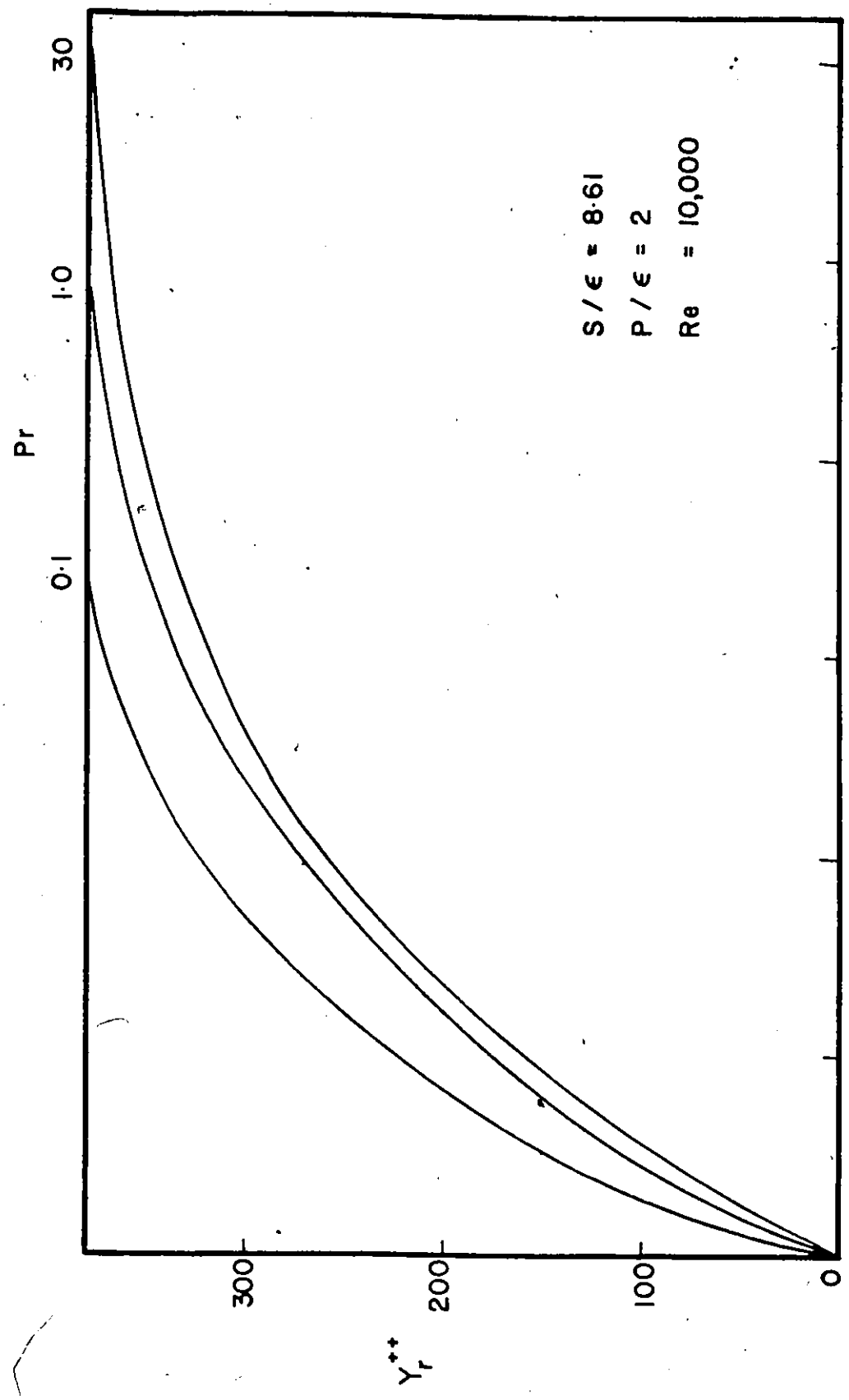

Fig. 4.12 Development of the Thermal Boundary Layer, Entrance Region, Effect of Pr

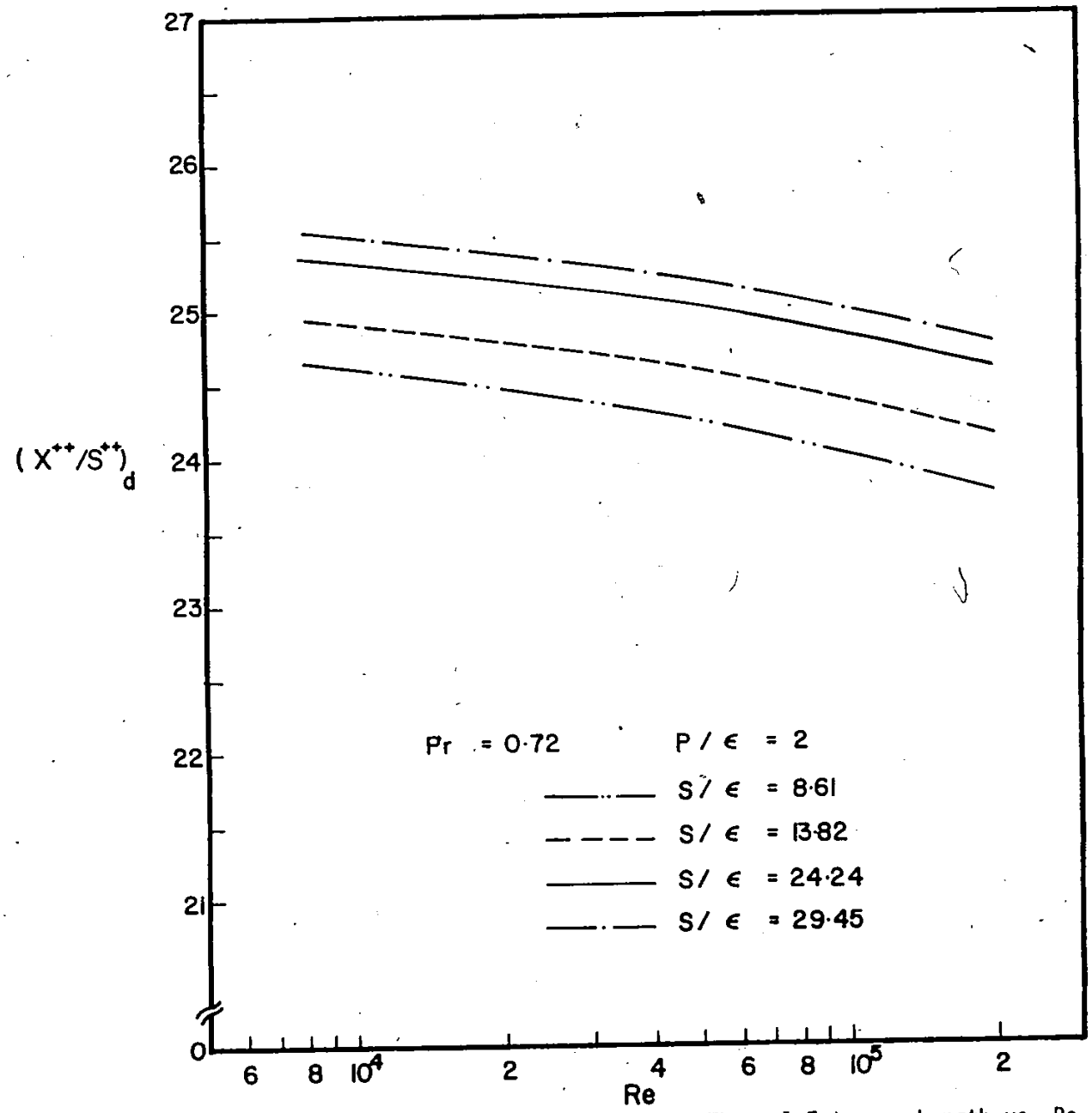

Fig. 4.13 Variation of Fully Developed Thermal Entrance Length vs. Re, Effect of s/ϵ

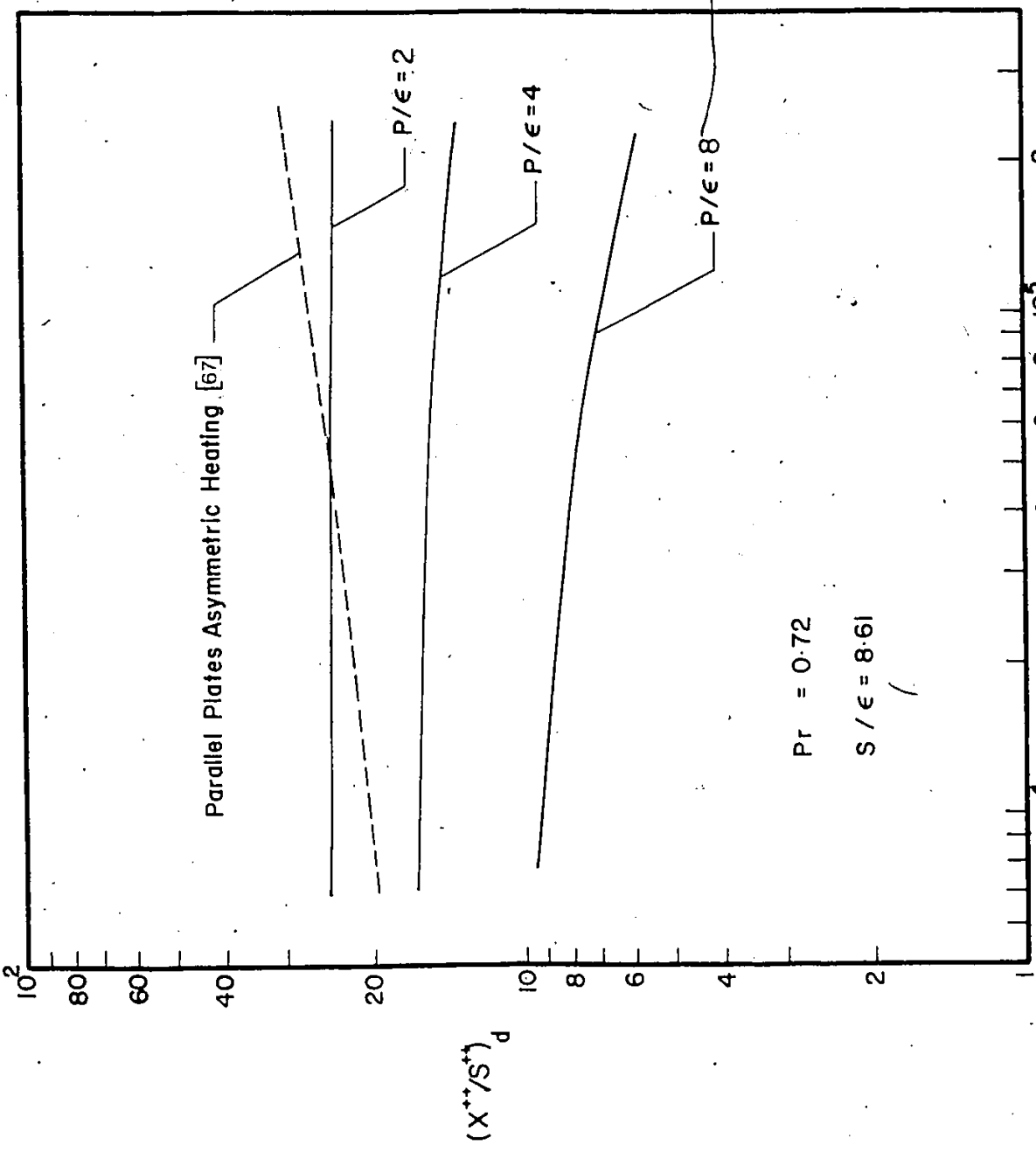

Fig. 4.14 Variation of Fully Developed Thermal Length vs. Re, Effect of P/ϵ

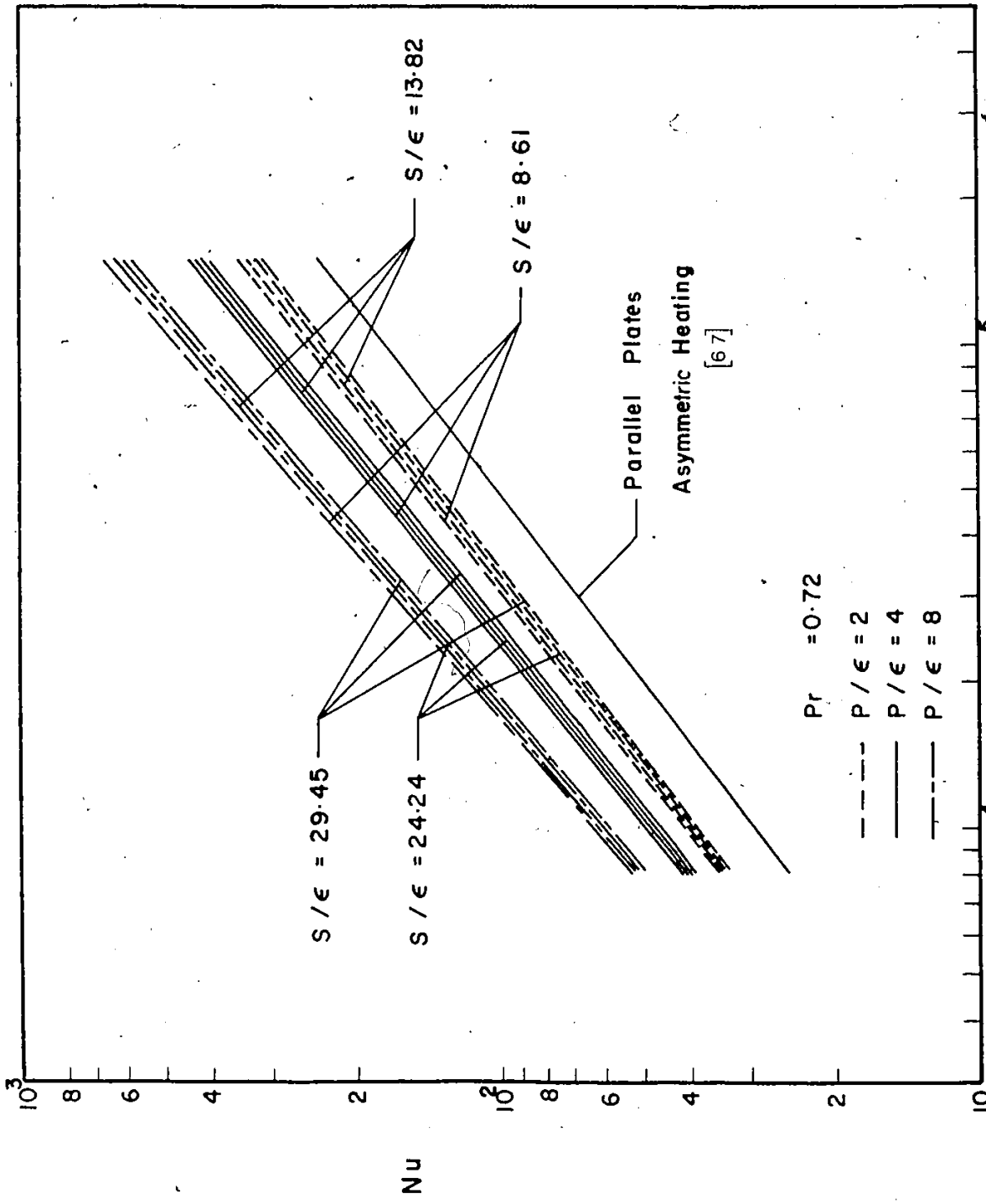

Fig. 4.15 Predicted Fully Developed Nusselt Numbers, Effect of S/ε, P/ε and Re

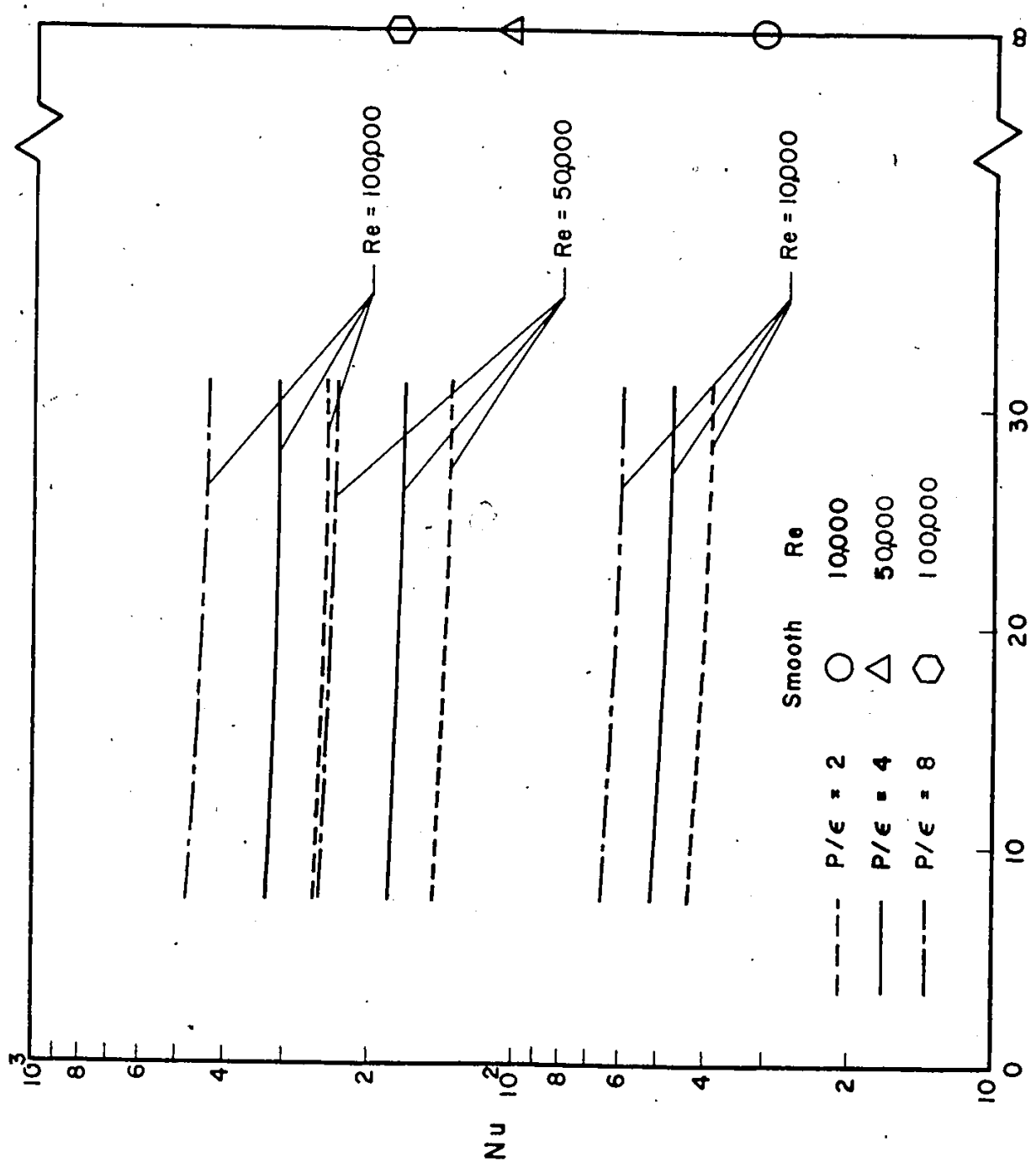

Fig. 4.16 Predicted Nusselt Numbers, Fully Developed Regions, Effect of S/ε

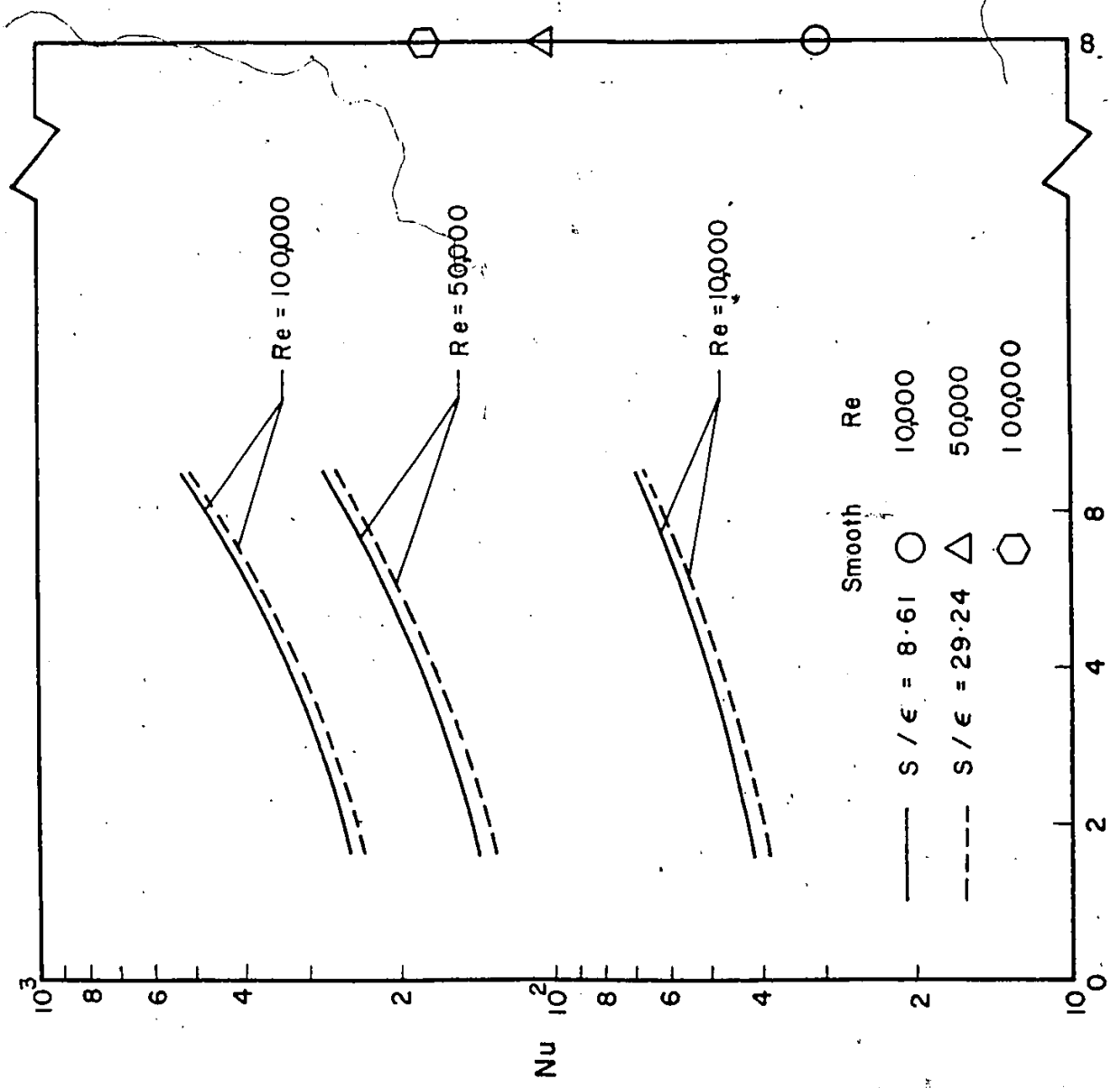

Fig. 4.17 Predicted Nusselt Numbers, Fully Developed Regions, Effect of P/ε

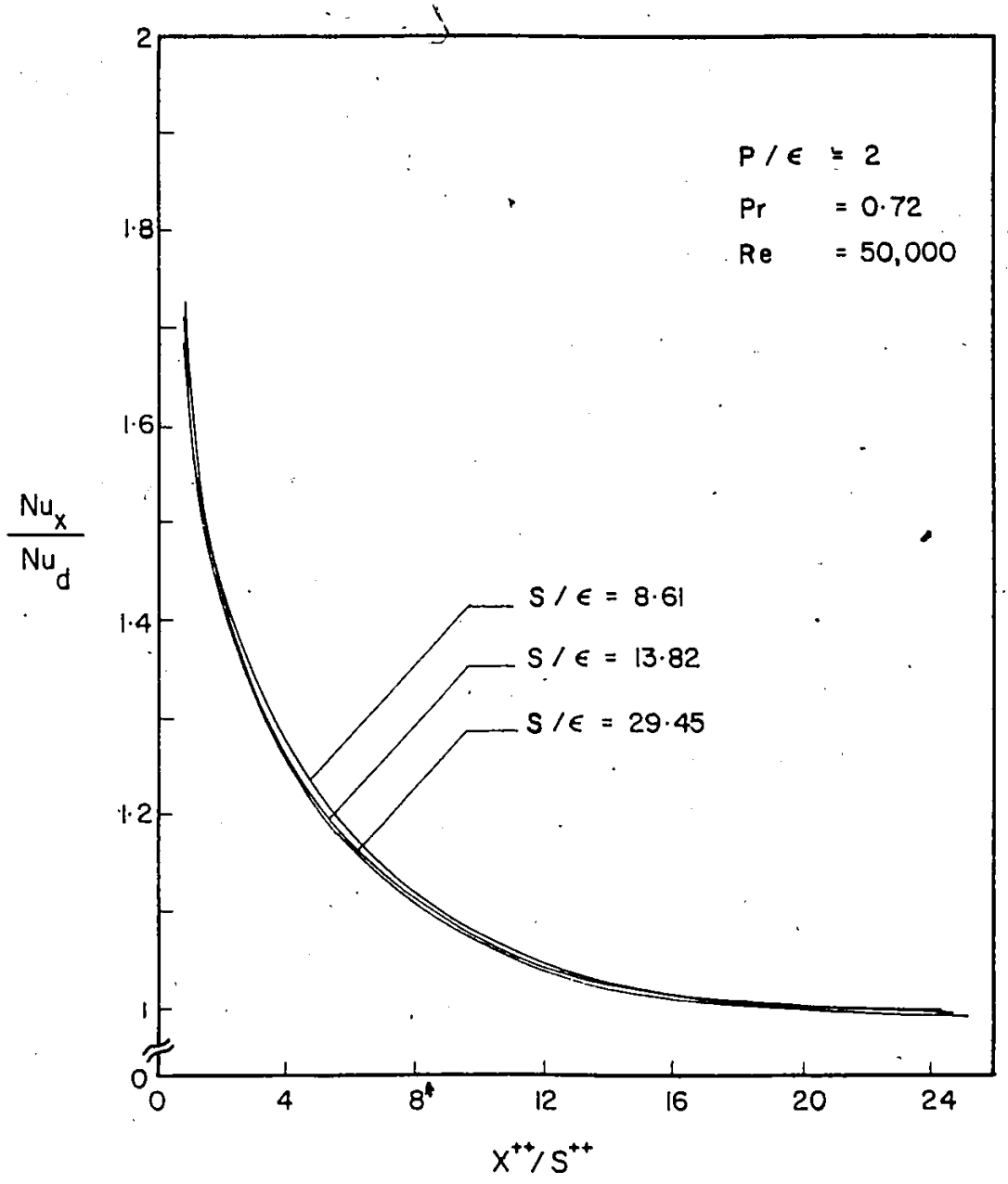

Fig. 4.18 Entrance Region Nusselt Numbers, Effect of S/ε

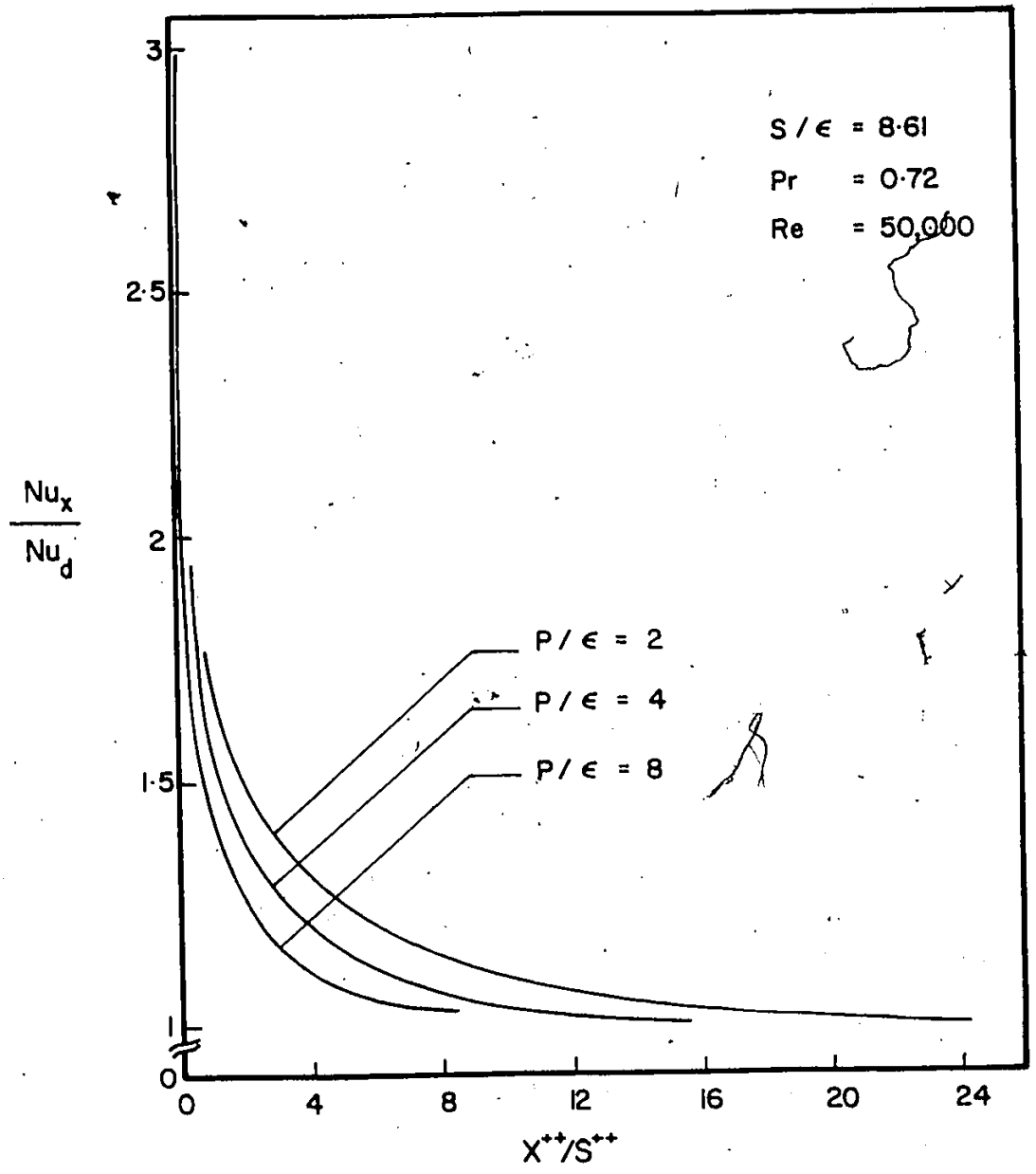

Fig. 4.19 Entrance Region Nusselt Numbers, Effect of P/ε

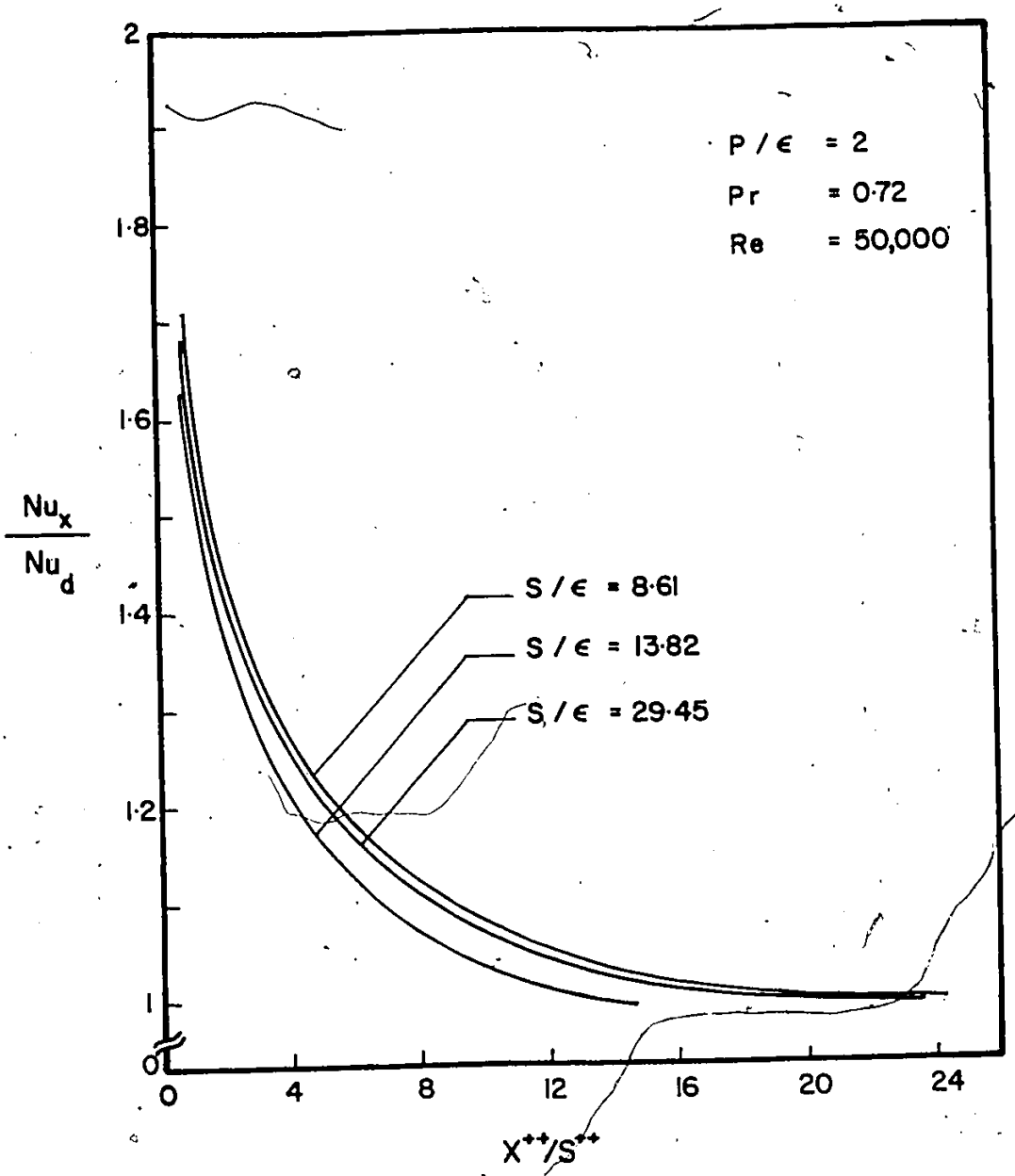

Fig. 4.20- Entrance Region Nusselt Numbers, Effect of Re.

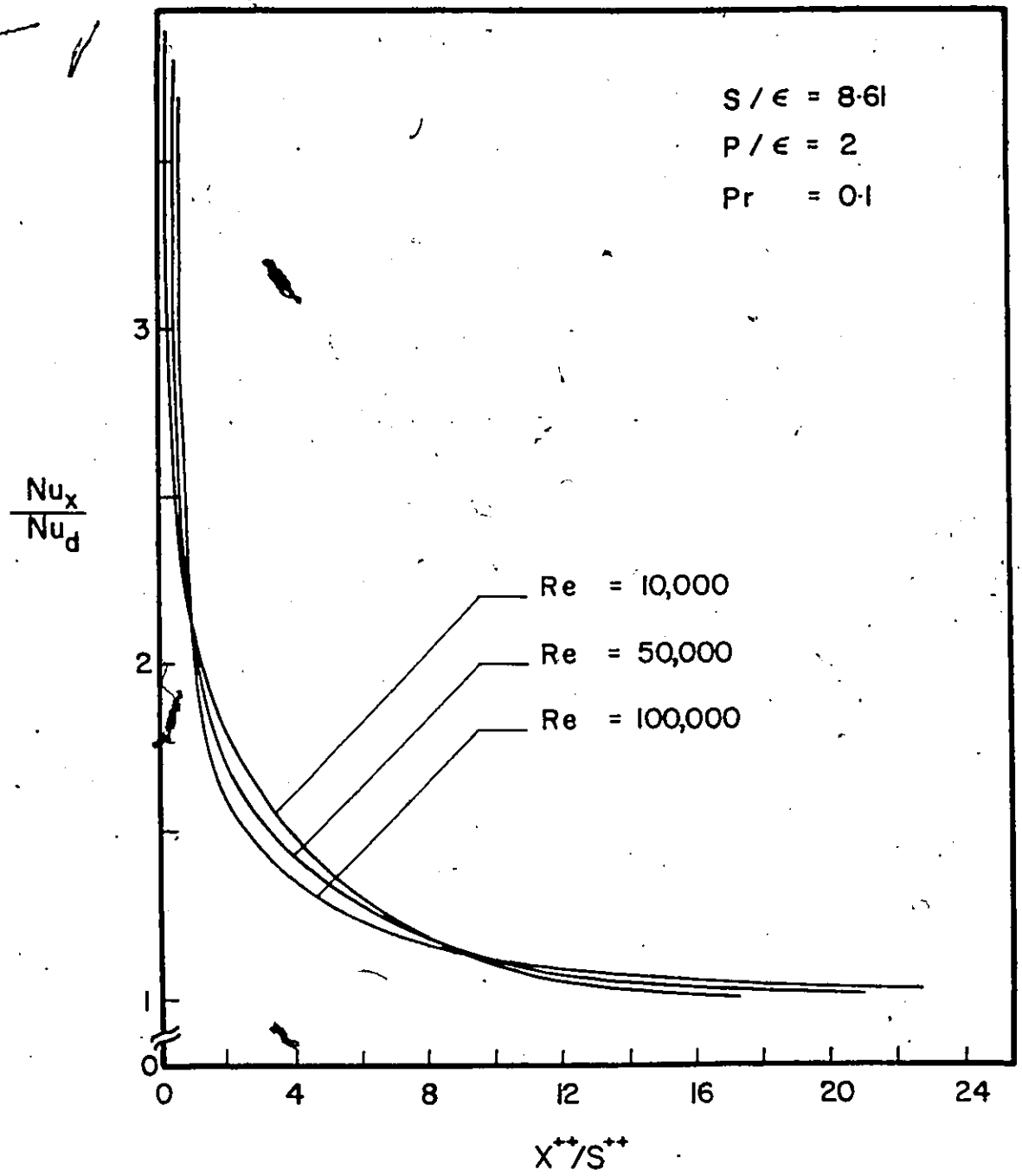

Fig. 4.21 Entrance Region Nusselt Numbers, Effect of Re

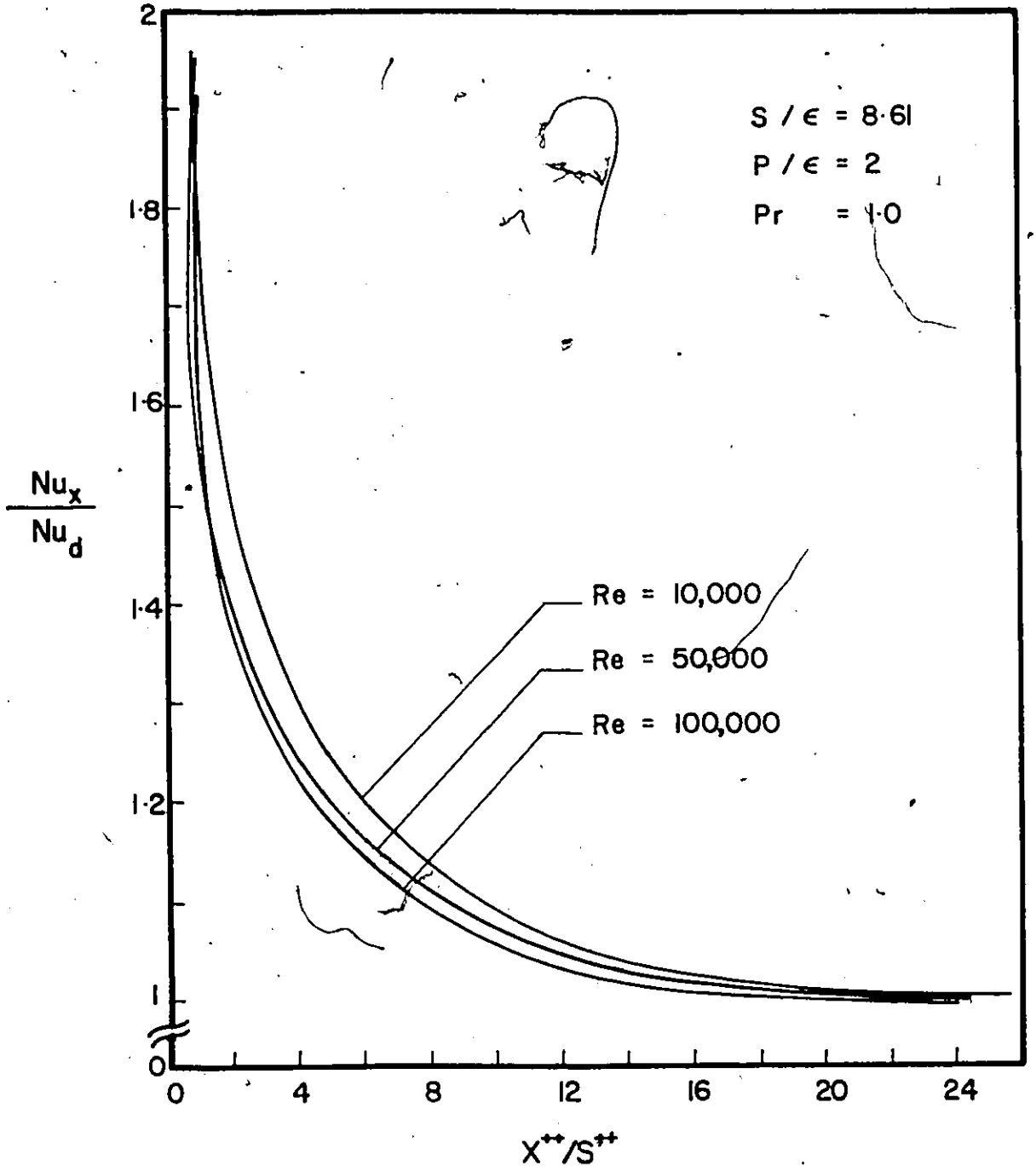

Fig. 4.22 Entrance Region Nusselt Numbers, Effect of Re

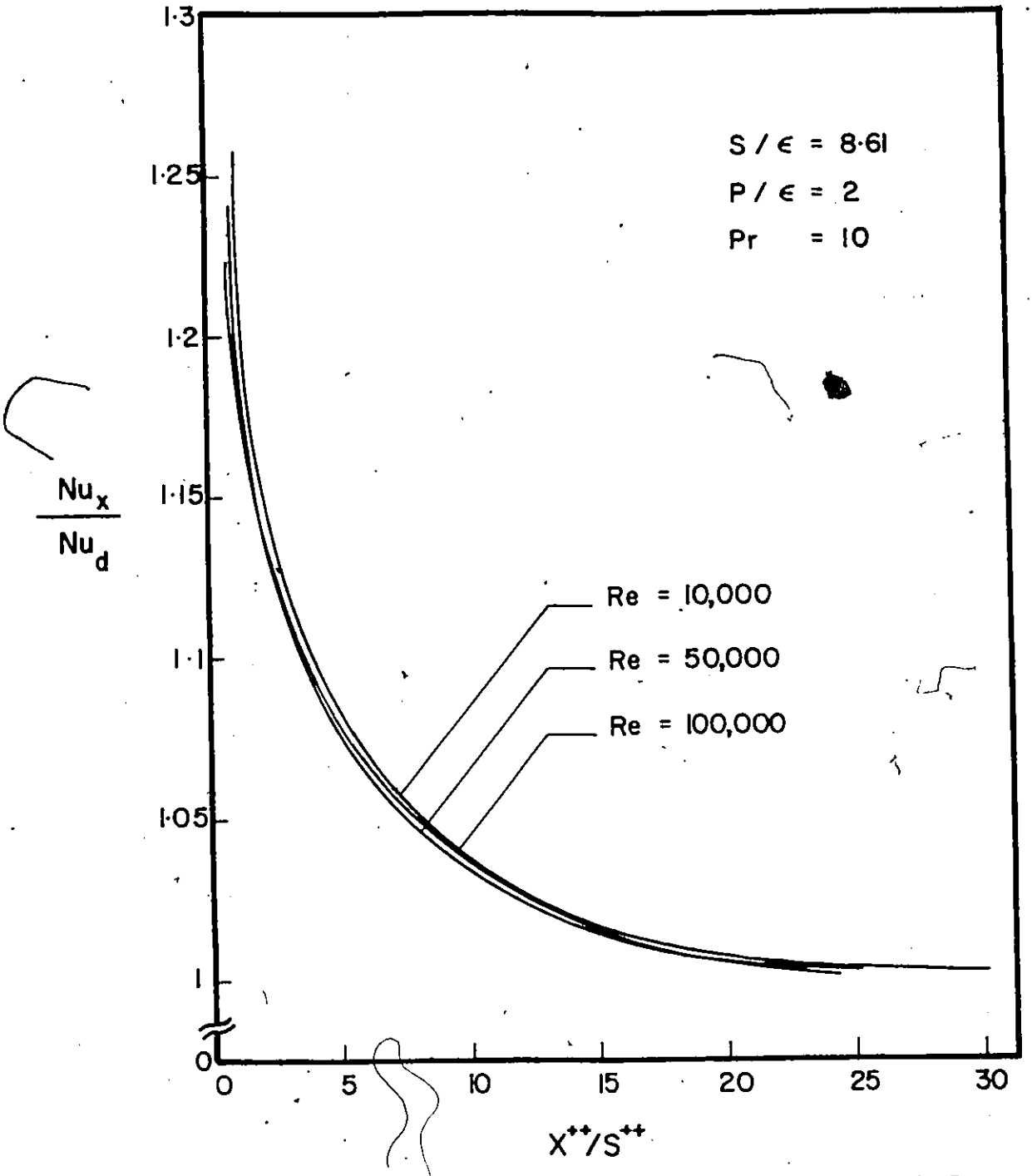

Fig. 4.23 Entrance Region Nusselt Numbers, Effect of Re

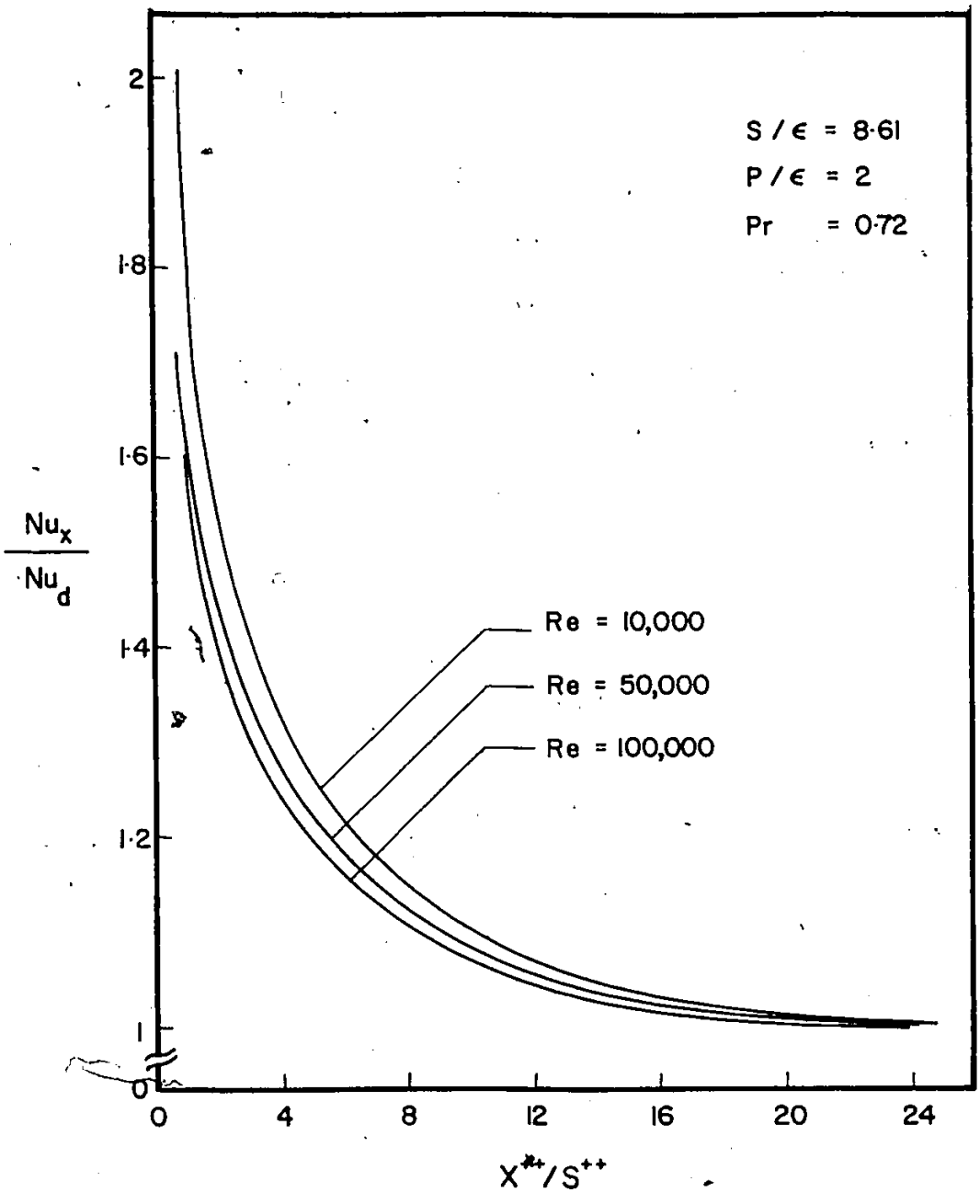

Fig. 4.24 Entrance Region Nusselt Numbers, Effect of Pr.

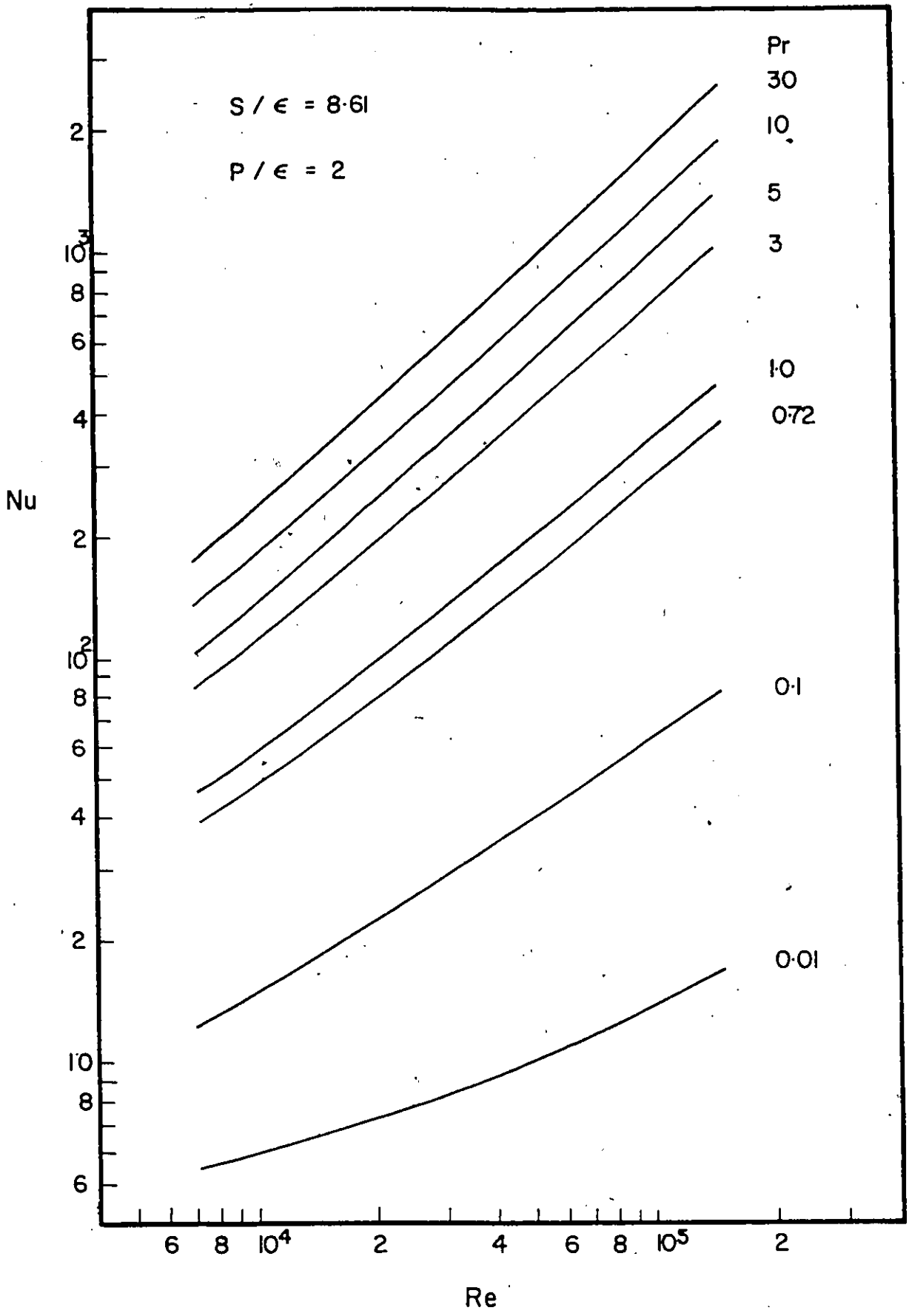

Fig. 4.25 Predicted Nusselt Numbers, Fully Developed Regions, Effect of Pr

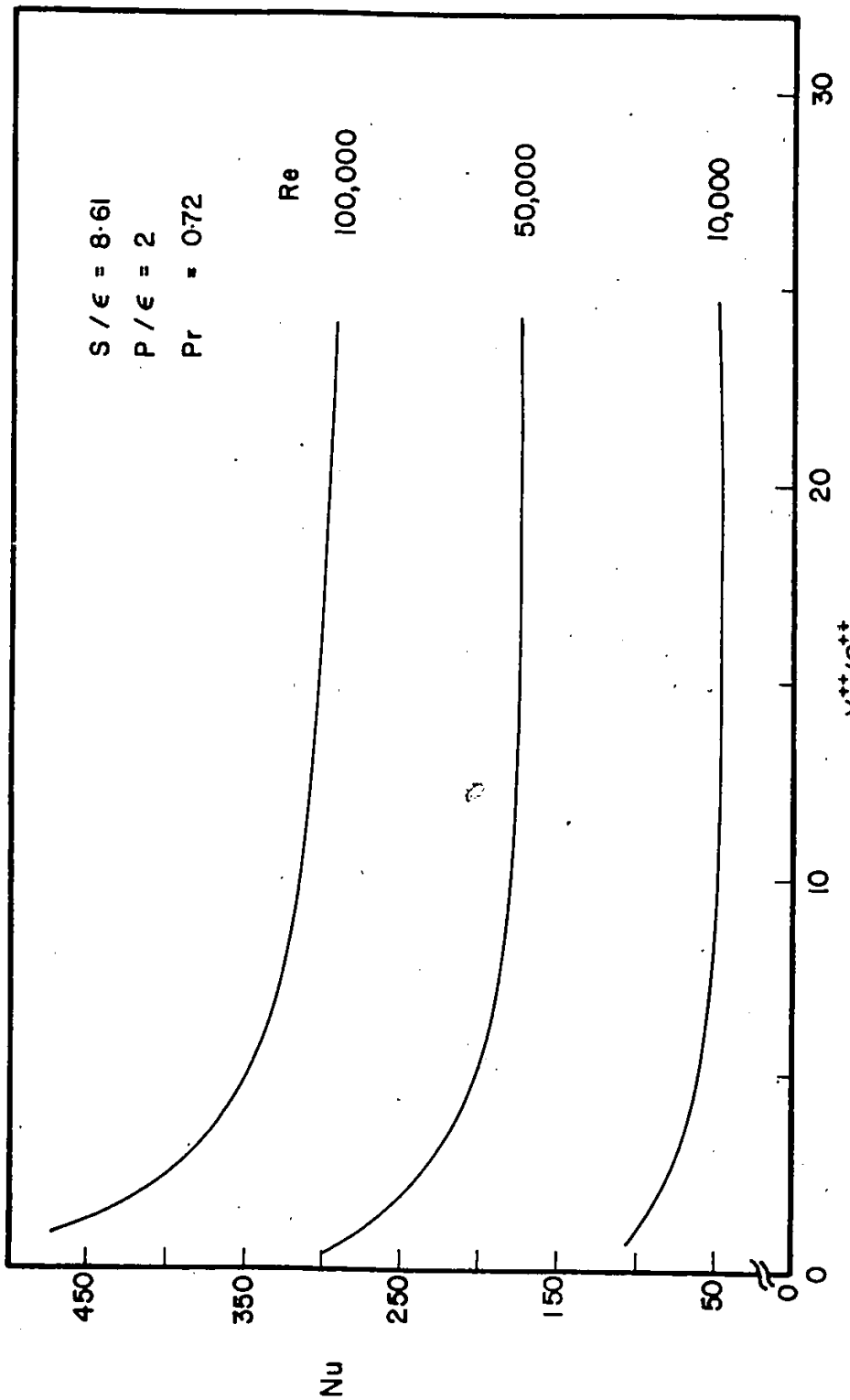

Fig. 4.26 Predicted Nusselt Numbers, Entrance Regions, Effect of Re

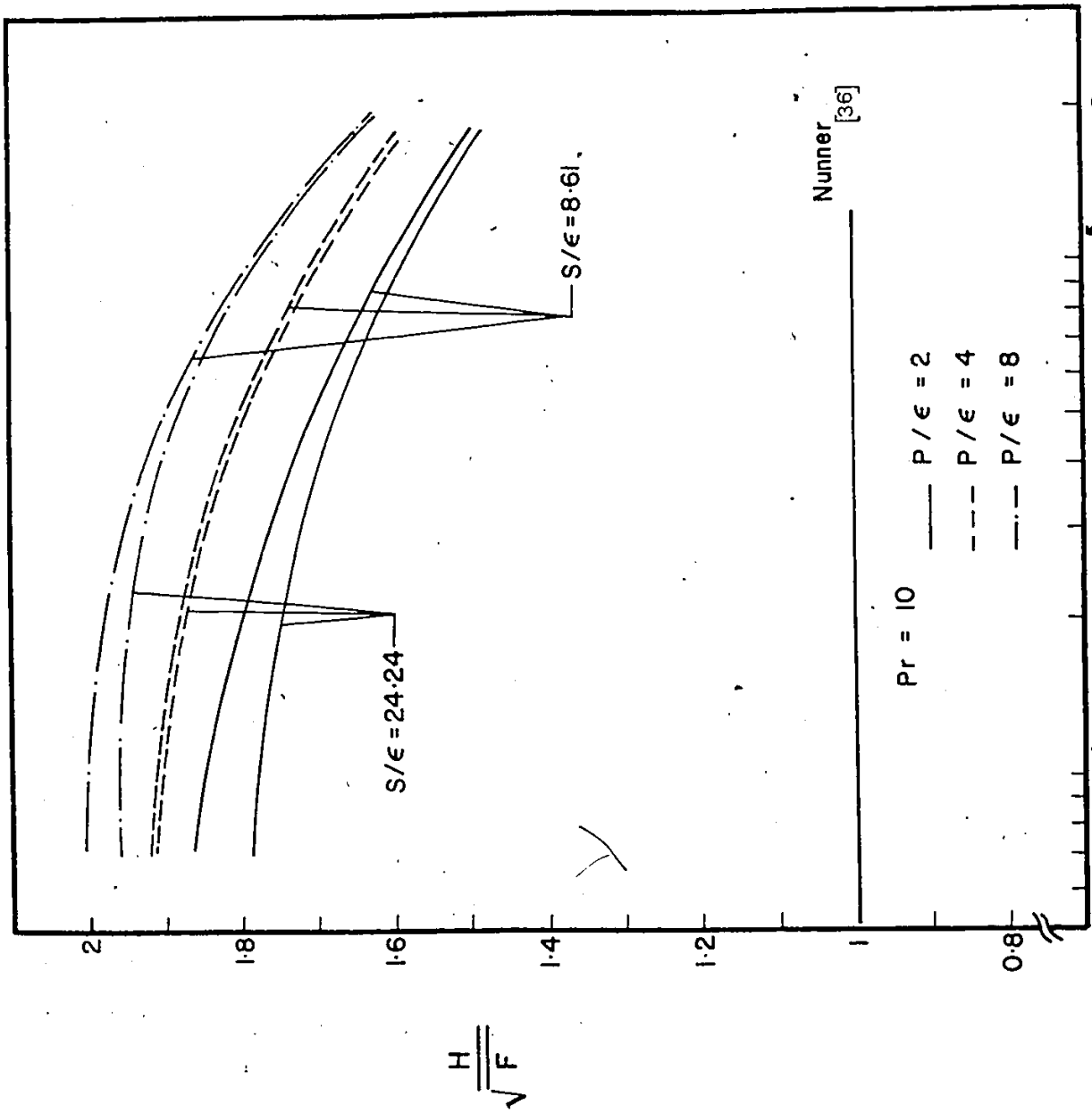

Fig. 4.27 $F/\sqrt{H}$ Ratio vs. Reynolds Number

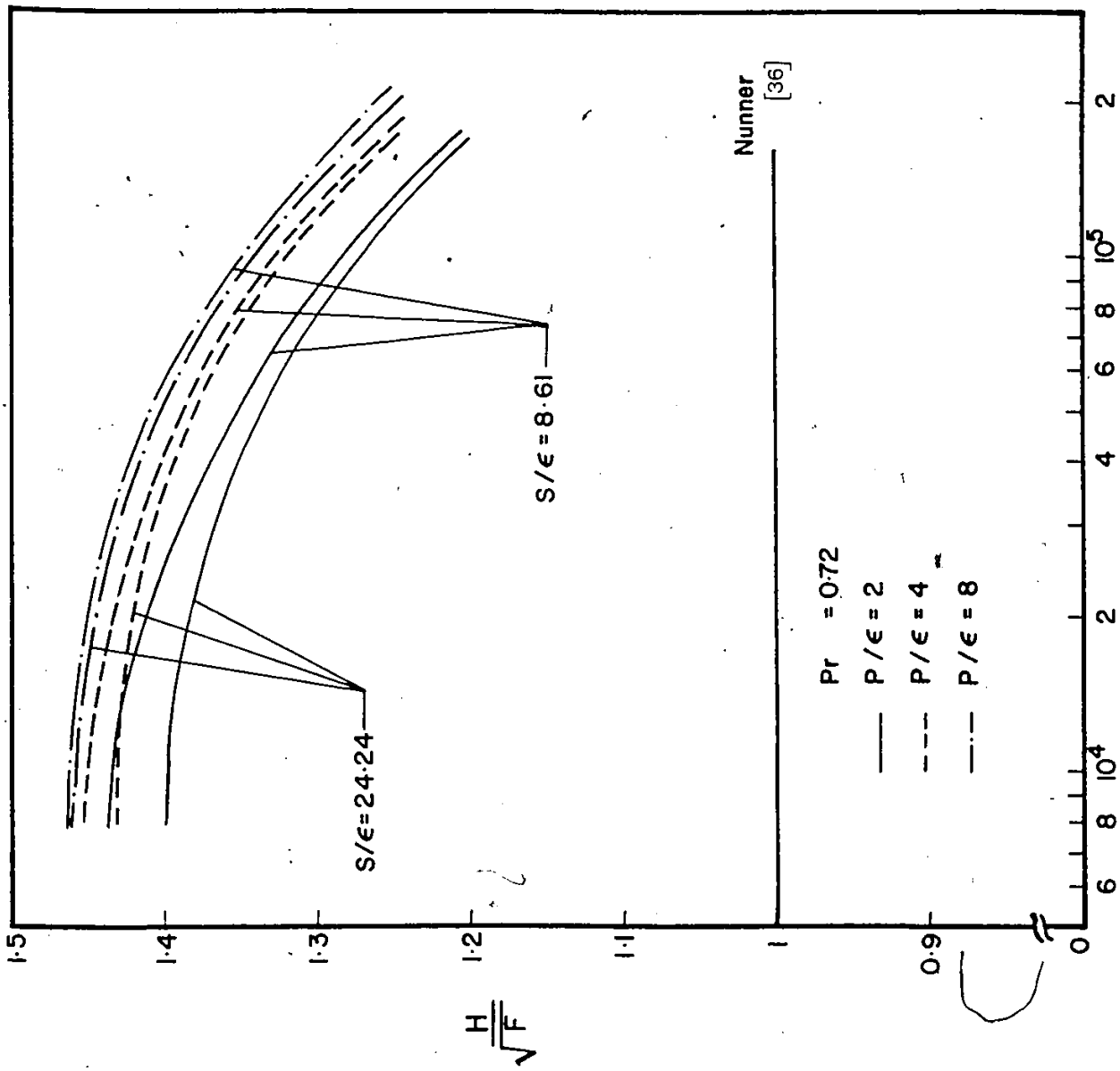

Fig. 4.28 $F/\sqrt{H}$ Ratio vs. Reynolds Number

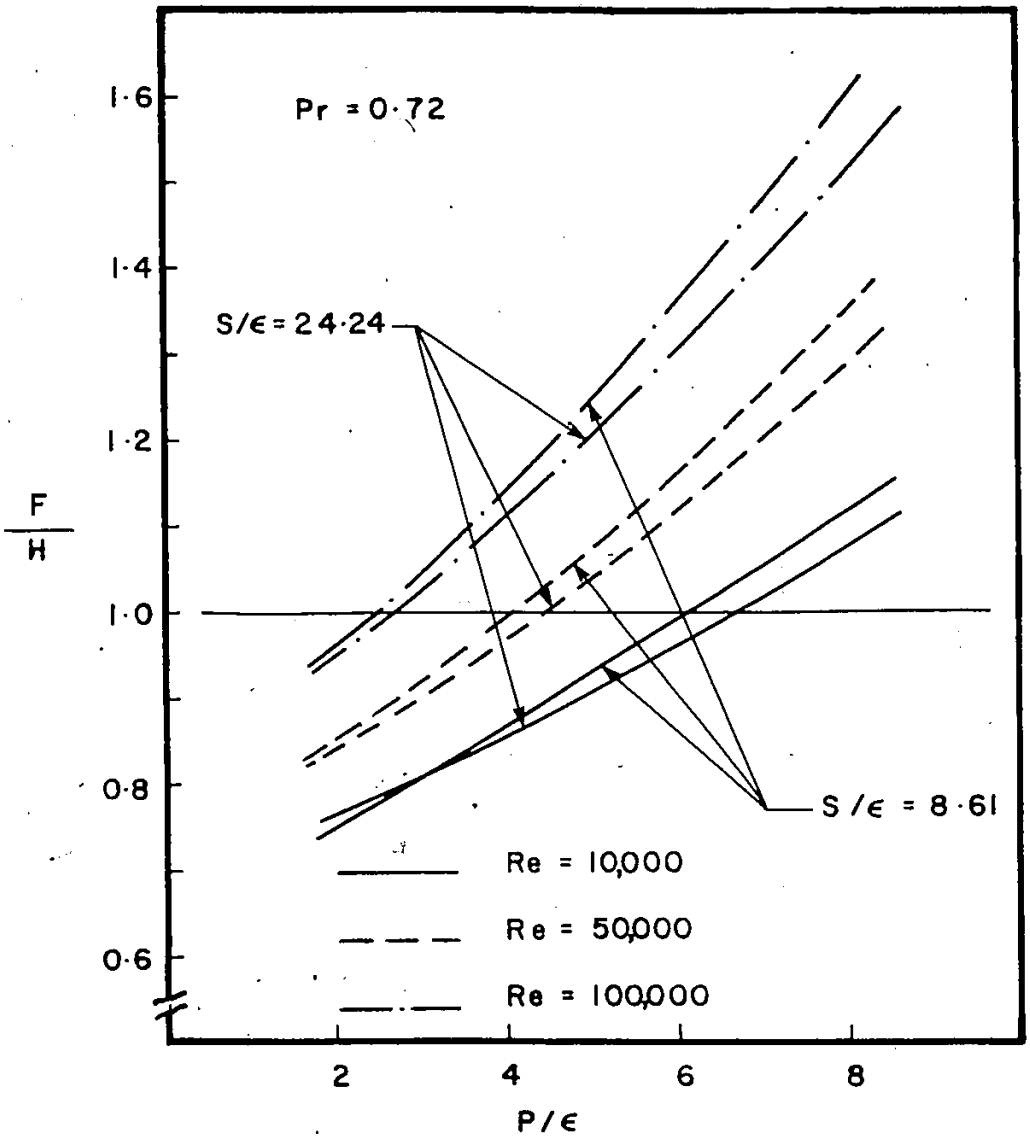

Fig. 4.29 F/H Ratio Asymmetric Flow

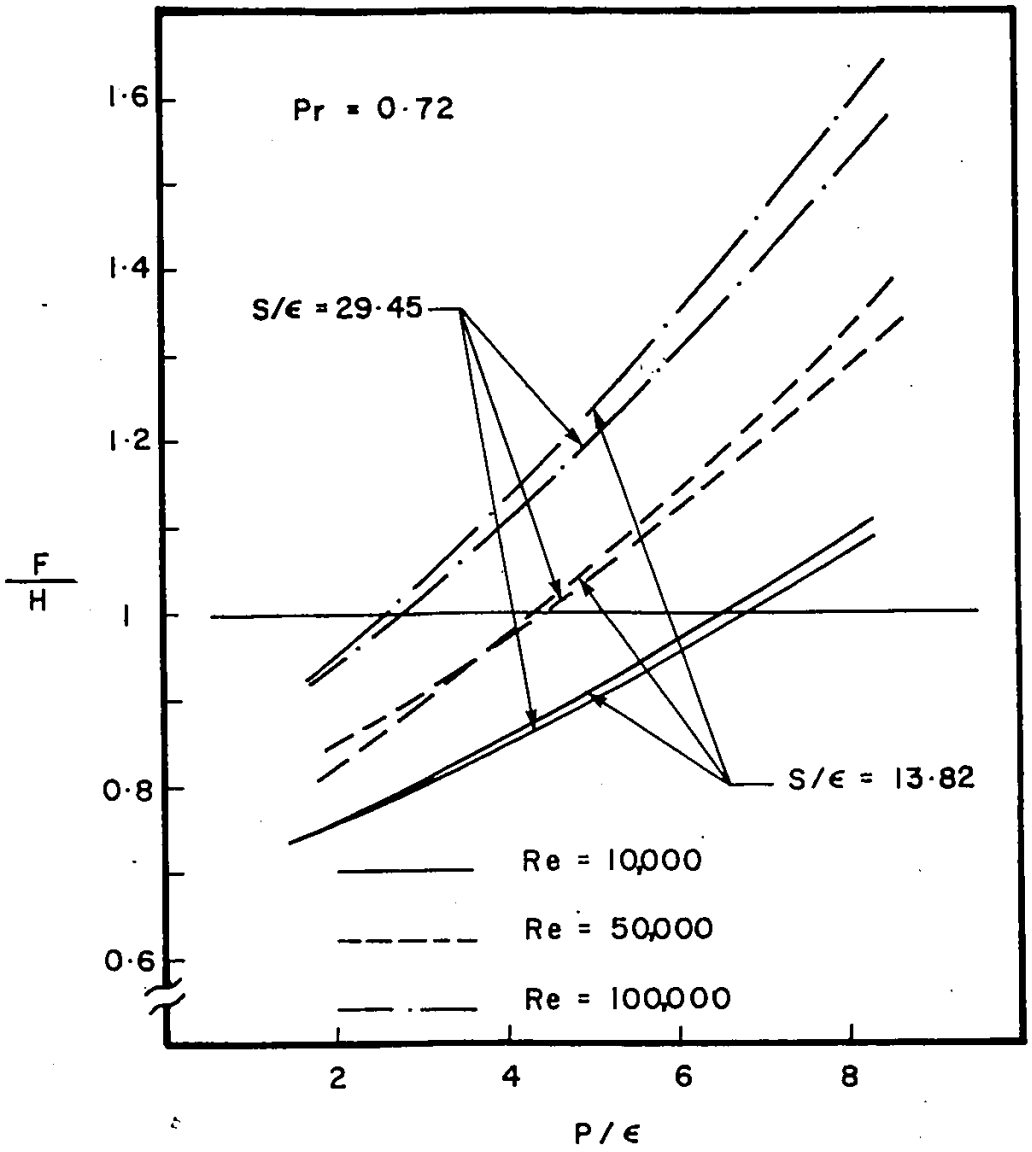

Fig. 4.30 F/H Ratio Asymmetric Flow

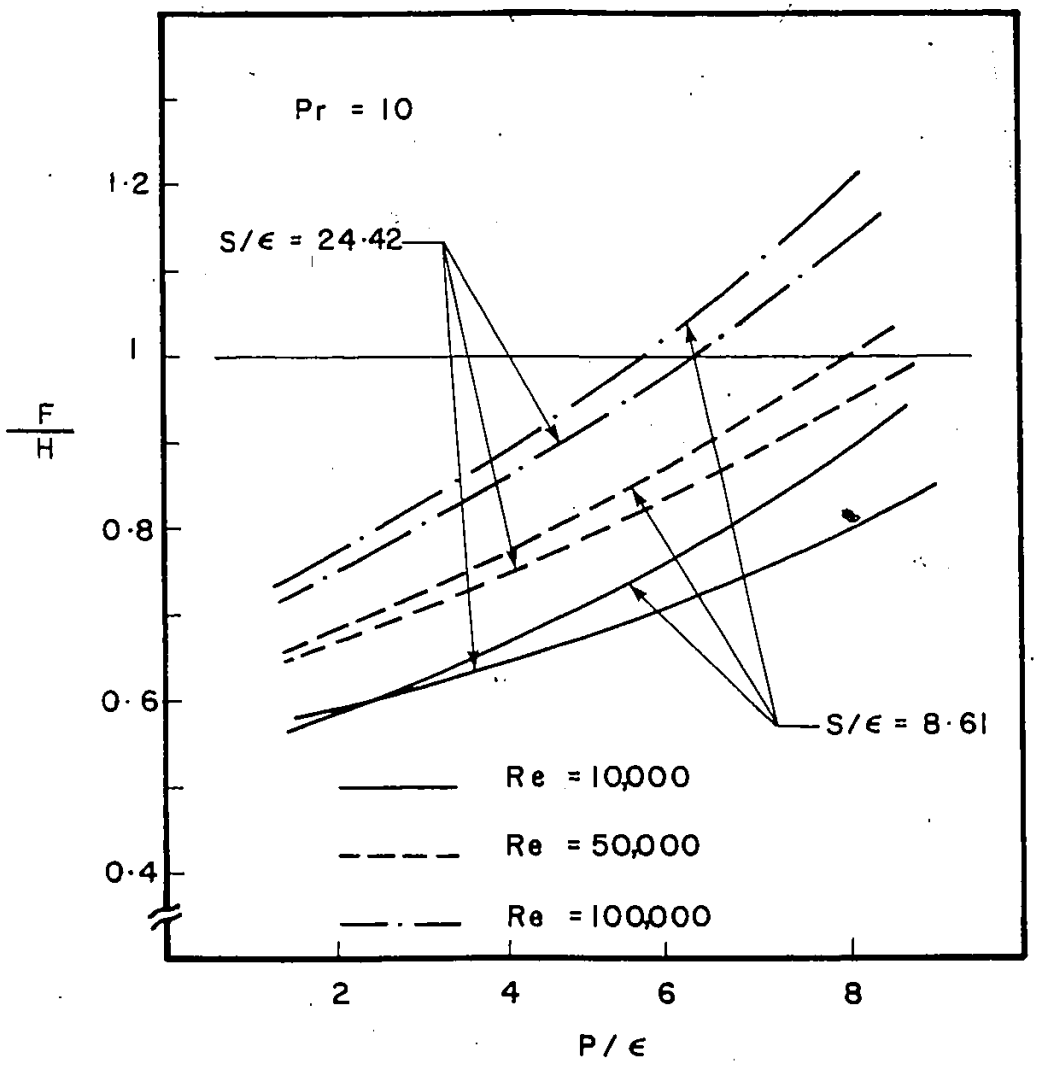

Fig. 4.31 F/H Ratio Asymmetric Flow

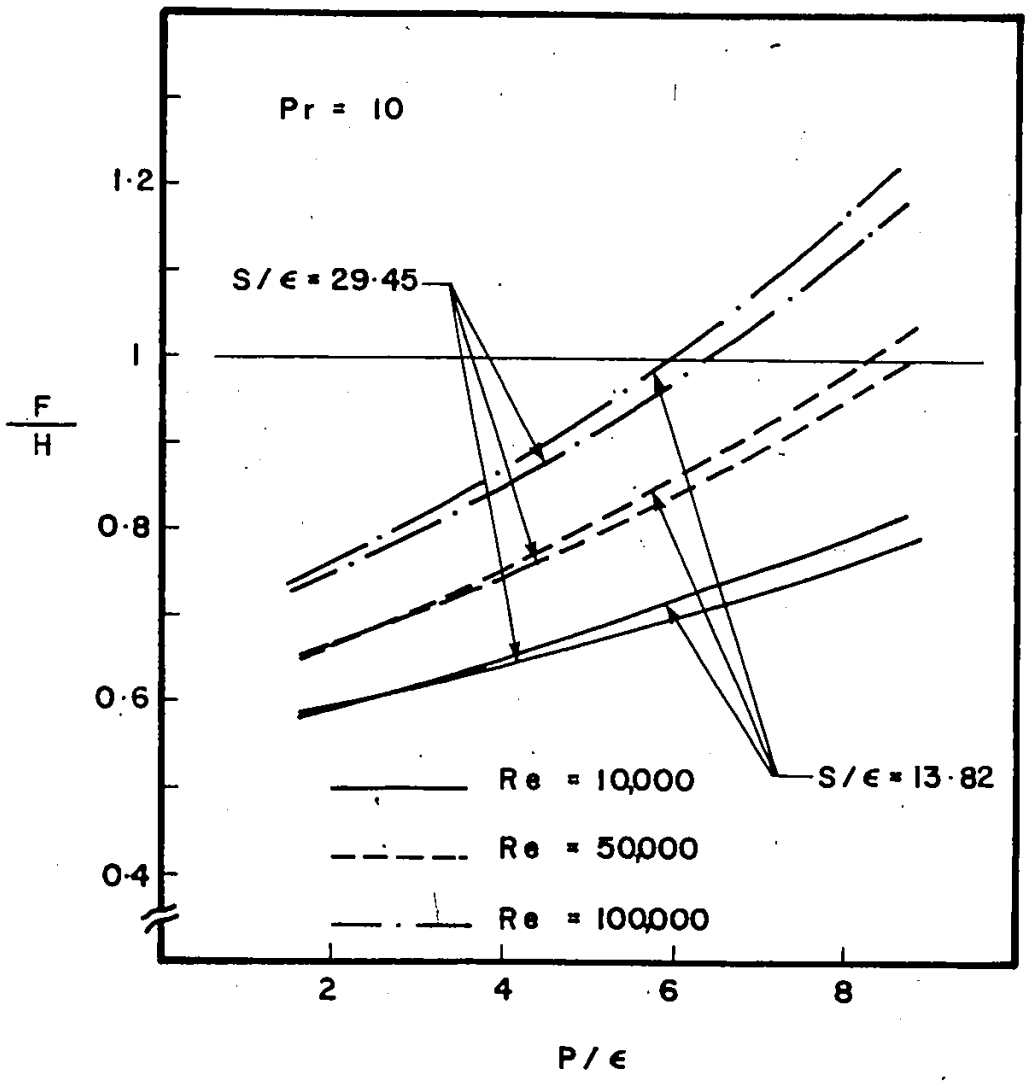

Fig. 4.32 F/H Ratio Asymmetric Flow

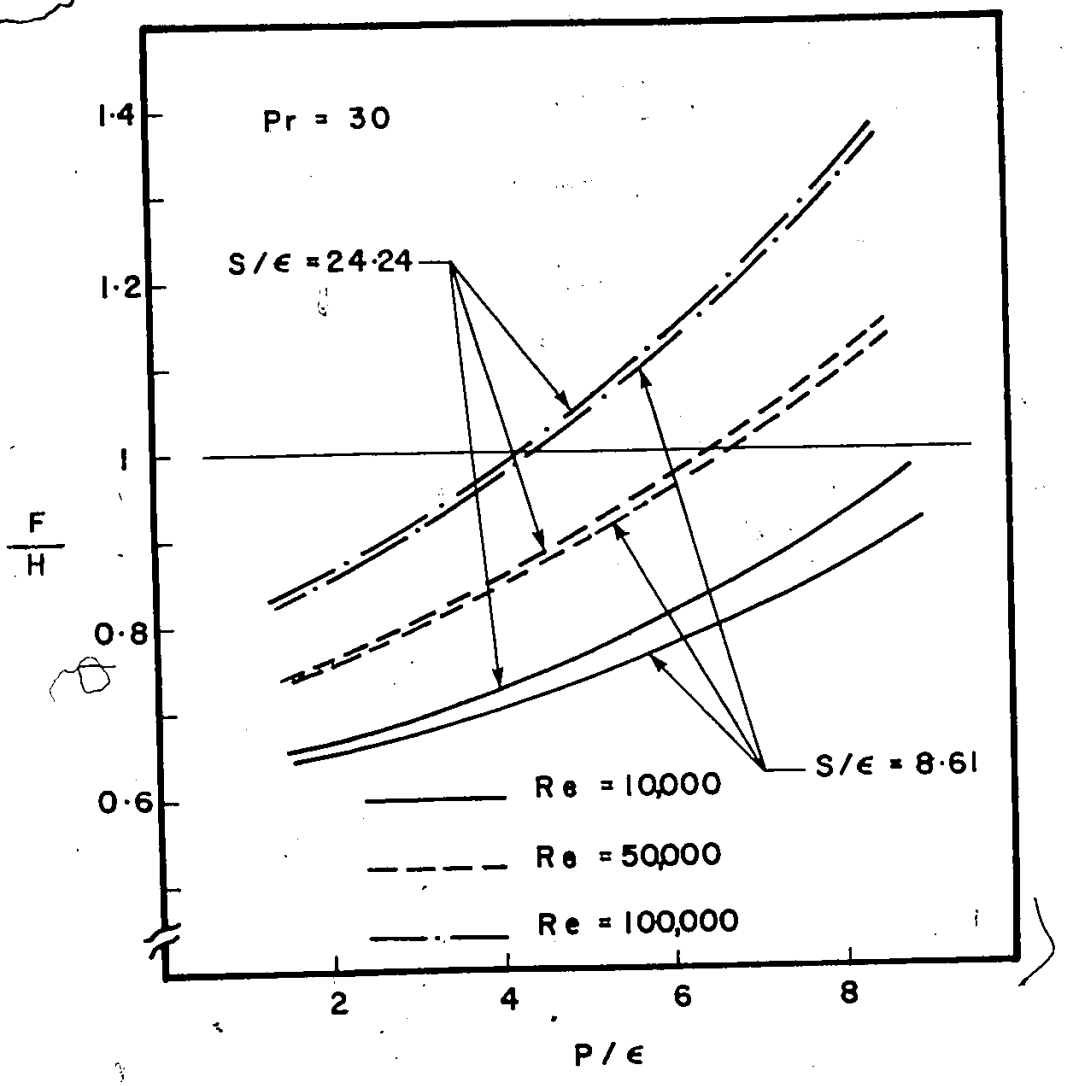

Fig. 4.33 F/H Ratio Asymmetric Flow

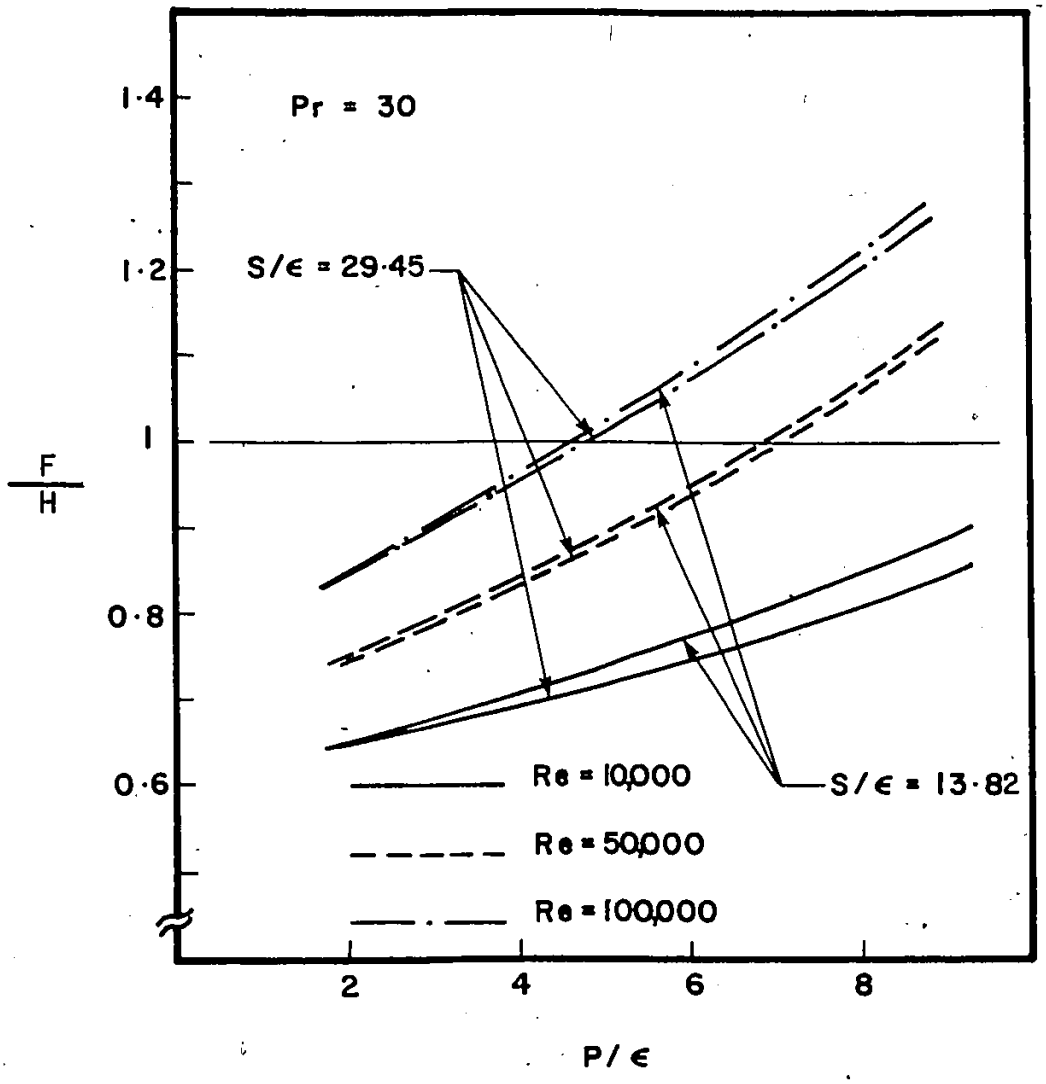

Fig. 4.34 F/H Ratio Asymmetric Flow

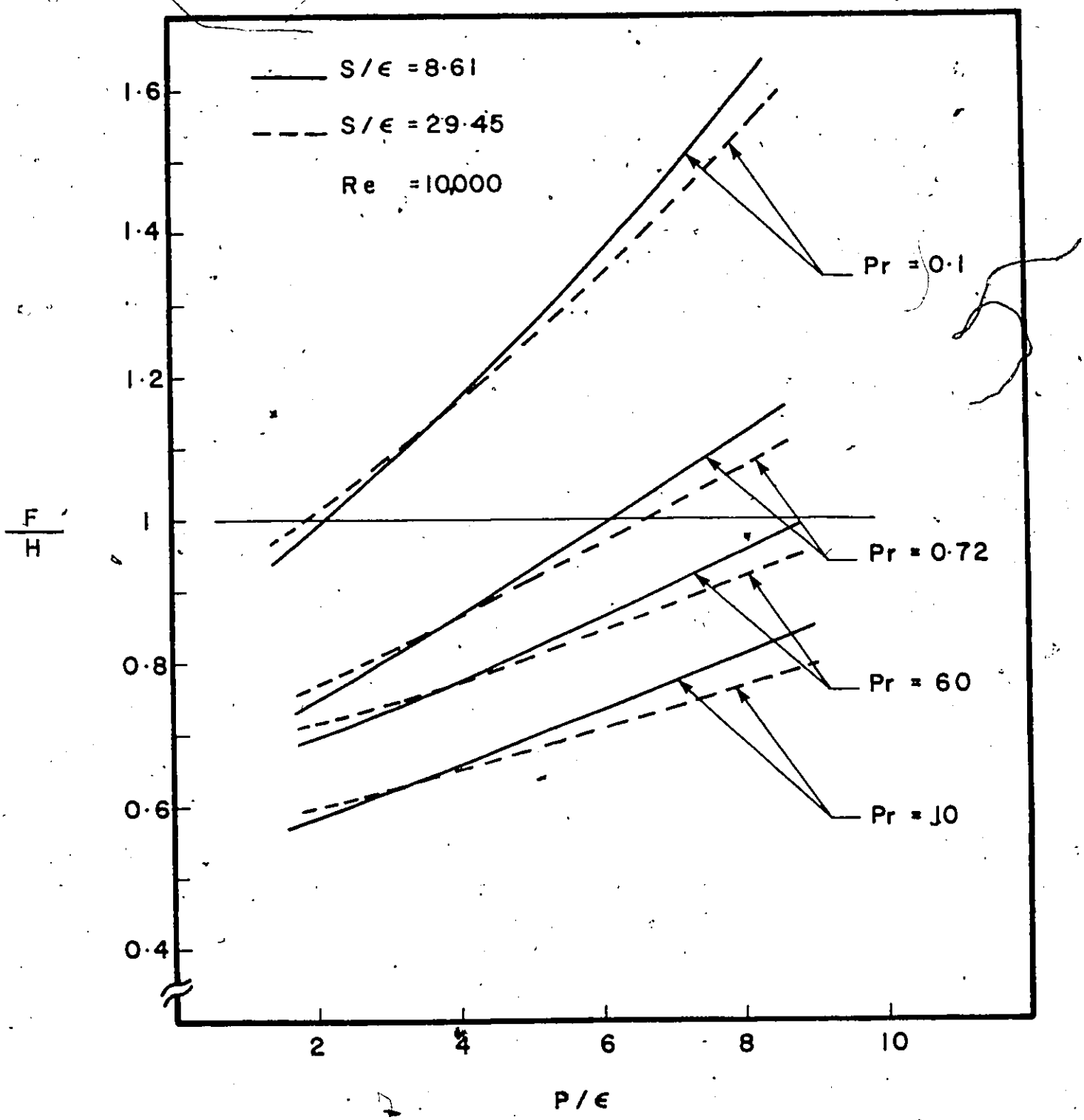

Fig. 4.35 F/H Ratio Asymmetric Flow, Effect of Pr.

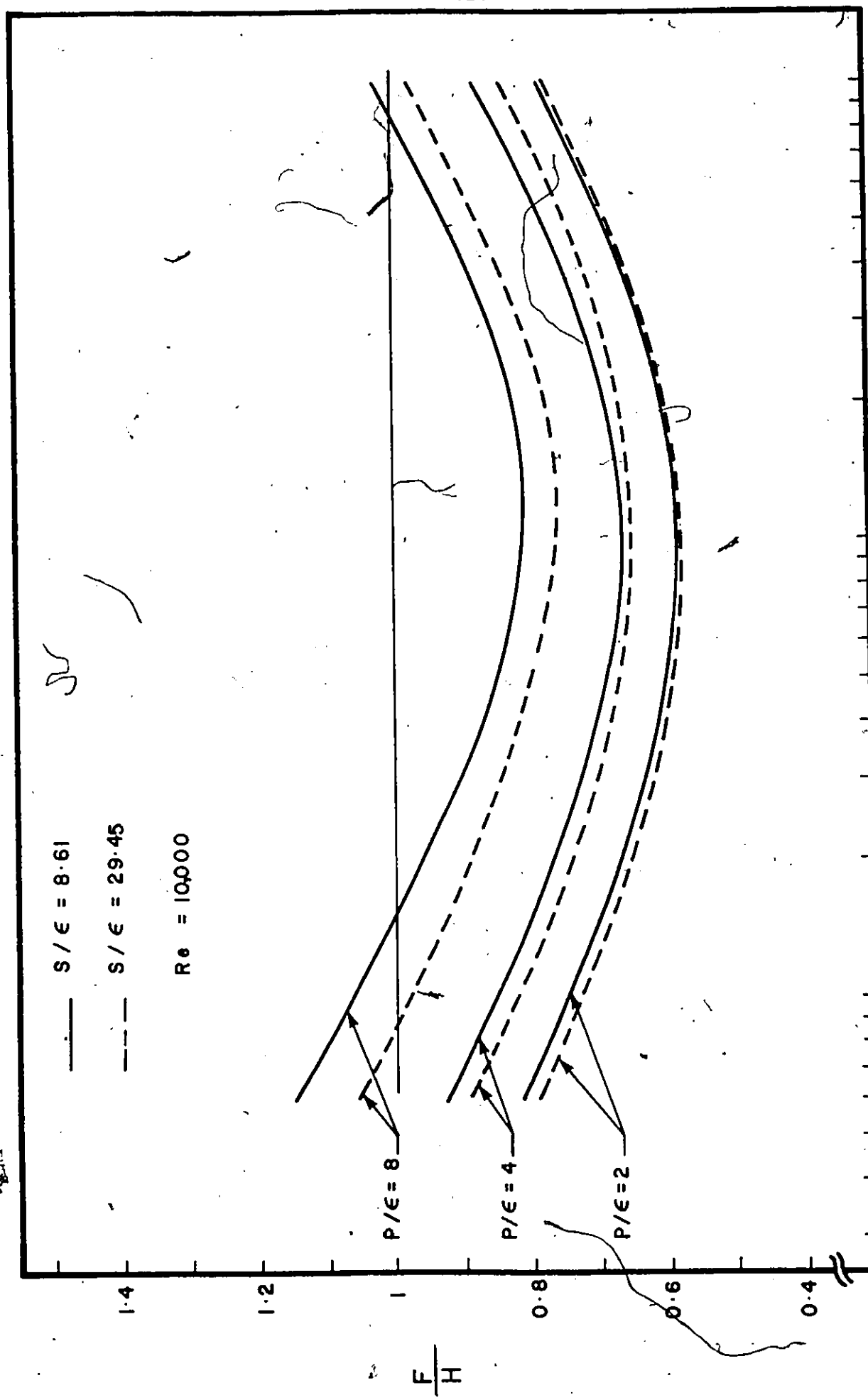

Fig. 4.36 F/H Ratio Asymmetric Flow, Effect of Pr

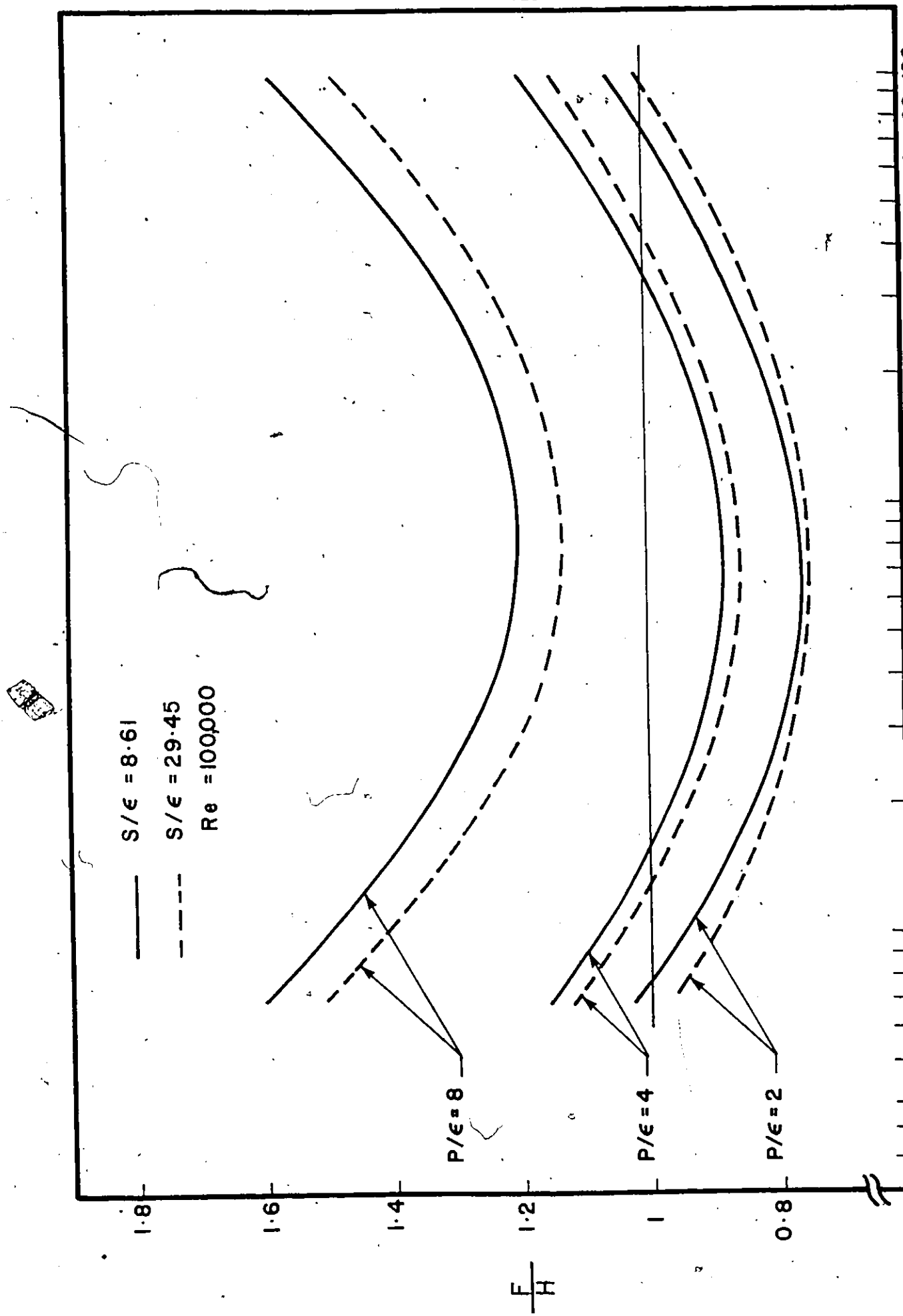

Fig. 4.37 F/H Ratio Asymmetric Flow, Effect of Pr

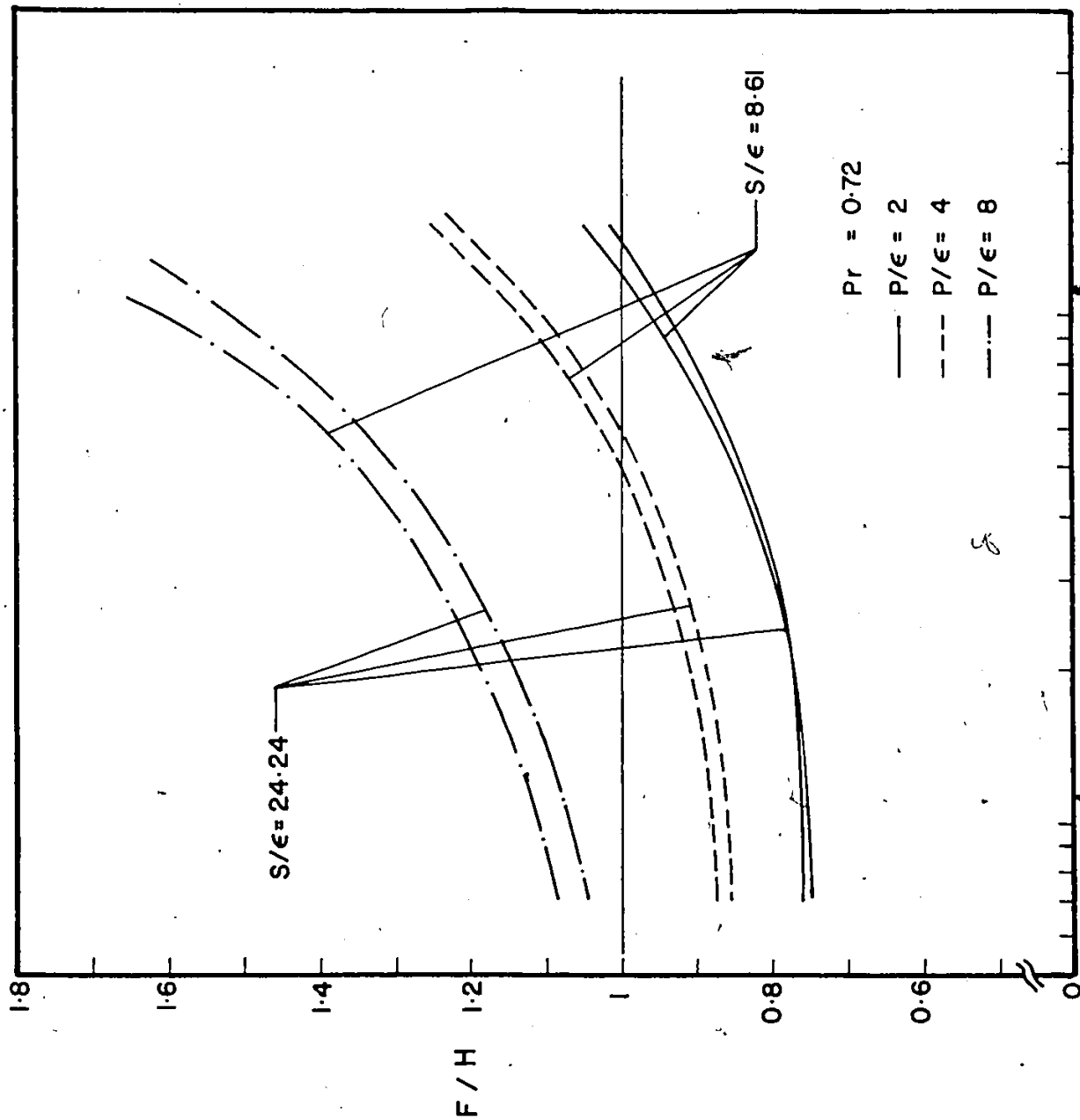

Fig. 4.38 F/H vs. Re

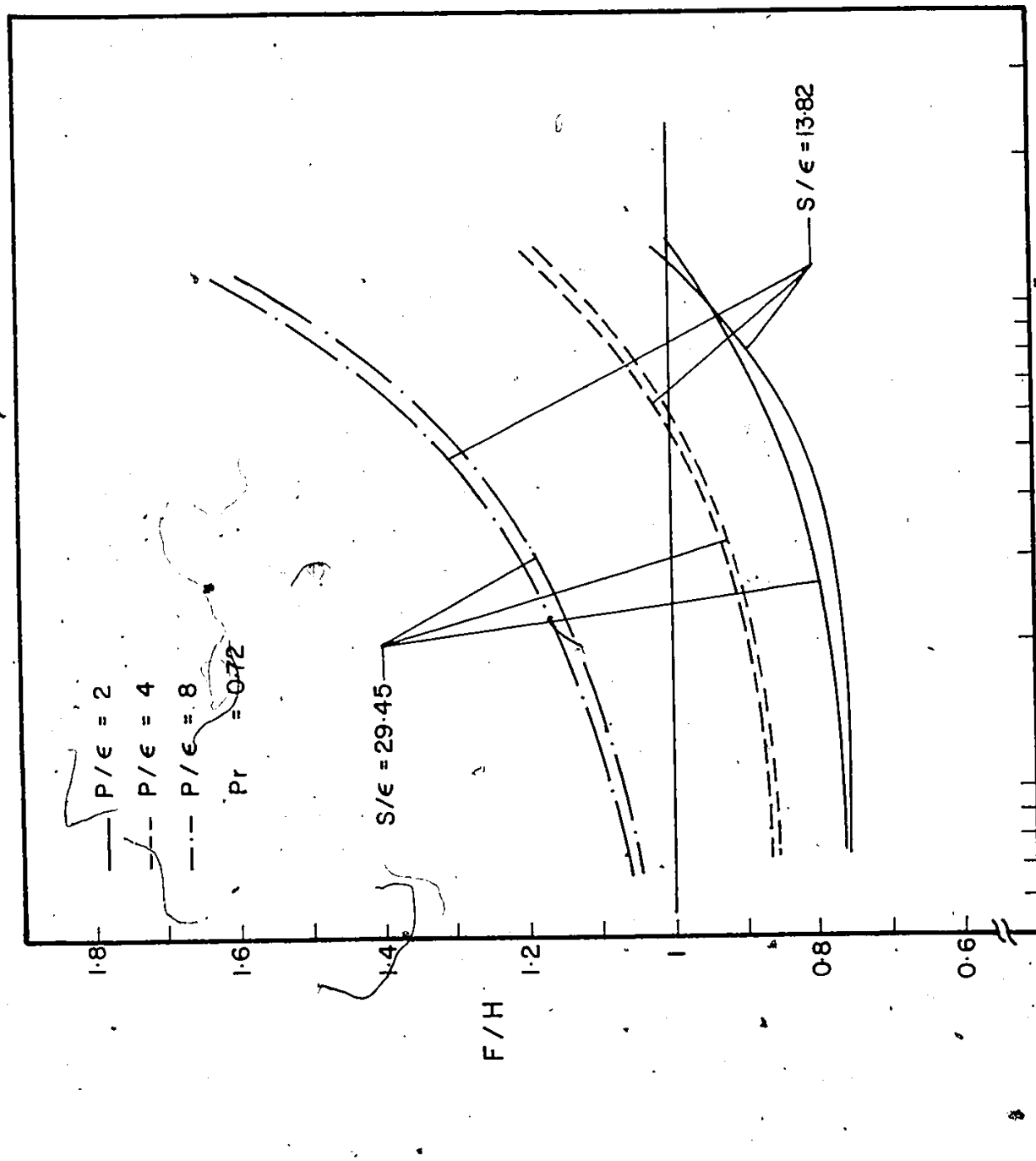

Fig. 4.39 F/H vs. Re

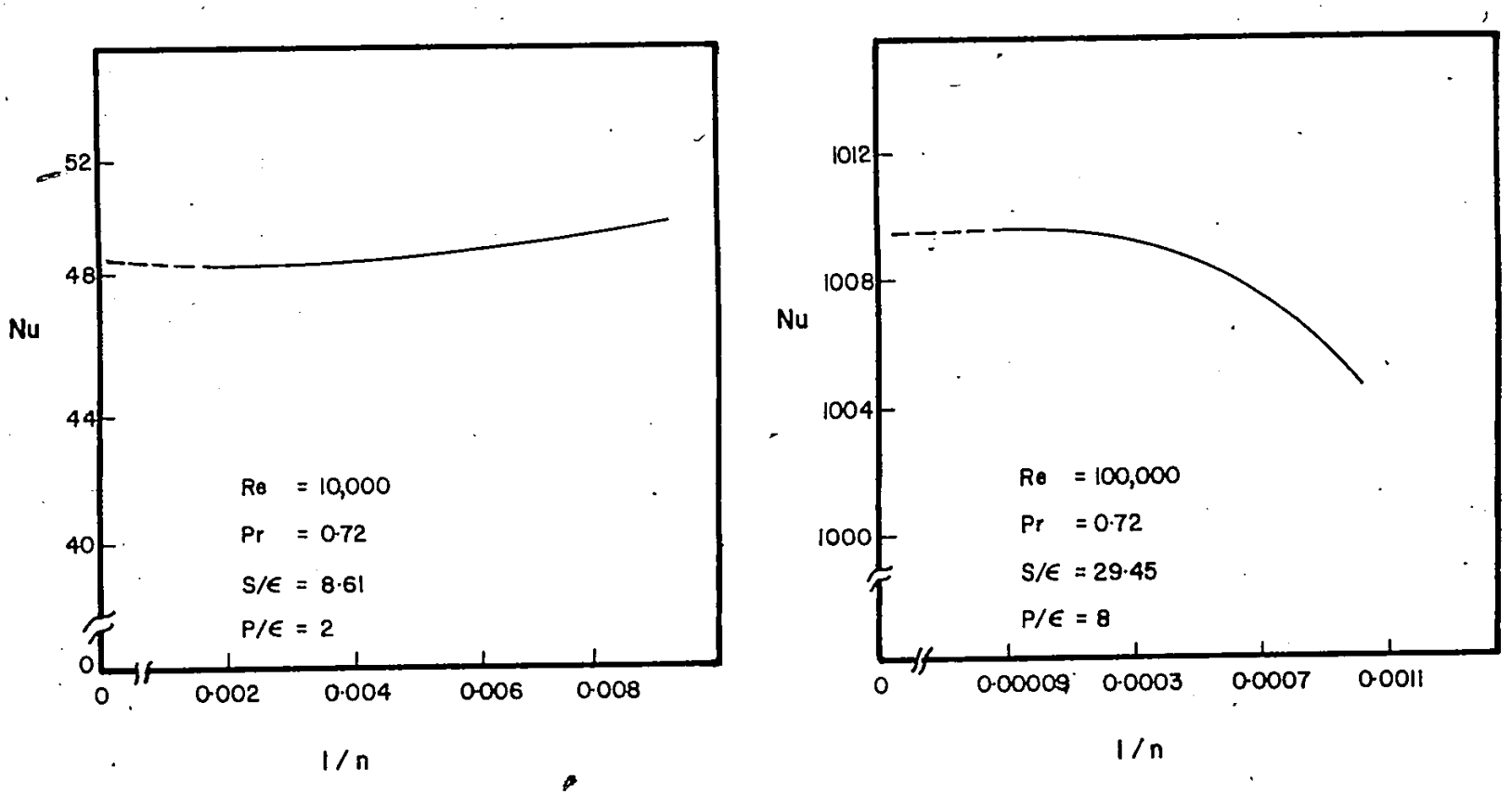

Fig. 4.40 Accuracy Check of Numerical Integration.